Holocentric plants of the genus *Rhynchospora* as a new model to study meiotic adaptations to chromosomal structural rearrangements

Inaugural-Dissertation

zur

Erlangung des Doktorgrades

der Mathematisch-Naturwissenschaftlichen Fakultät

der Universität zu Köln

vorgelegt von

Marco Castellani

aus Varese, Italia

Köln, 2023

Erklärung zur Dissertation

gemäß der Promotionsordnung vom 12. März 2020

„Hiermit versichere ich an Eides statt, dass ich die vorliegende Dissertation selbstständig und ohne die Benutzung anderer als der angegebenen Hilfsmittel und Literatur angefertigt habe. Alle Stellen, die wörtlich oder sinngemäß aus veröffentlichten und nicht veröffentlichten Werken dem Wortlaut oder dem Sinn nach entnommen wurden, sind als solche kenntlich gemacht. Ich versichere an Eides statt, dass diese Dissertation noch keiner anderen Fakultät oder Universität zur Prüfung vorgelegen hat; dass sie - abgesehen von unten angegebenen Teilpublikationen und eingebundenen Artikeln und Manuskripten - noch nicht veröffentlicht worden ist sowie, dass ich eine Veröffentlichung der Dissertation vor Abschluss der Promotion nicht ohne Genehmigung des Promotionsausschusses vornehmen werde. Die Bestimmungen dieser Ordnung sind mir bekannt. Darüber hinaus erkläre ich hiermit, dass ich die Ordnung zur Sicherung guter wissenschaftlicher Praxis und zum Umgang mit wissenschaftlichem Fehlverhalten der Universität zu Köln gelesen und sie bei der Durchführung der Dissertation zugrundeliegenden Arbeiten und der schriftlich verfassten Dissertation beachtet habe und verpflichte mich hiermit, die dort genannten Vorgaben bei allen wissenschaftlichen Tätigkeiten zu beachten und umzusetzen. Ich versichere, dass die eingereichte elektronische Fassung der eingereichten Druckfassung vollständig entspricht."

Date, Name und Unterschrift

28.4.2023

X _____
  Marco Castellani

MAX-PLANCK-GESELLSCHAFT

Max-Planck-Institut für
Pflanzenzüchtungsforschung

2

Die in dieser Arbeit beschriebenen Arbeiten wurden unter der Leitung von Dr. André Marques und Prof. Dr. Raphael Mercier am Max-Planck-Institut für Pflanzenzüchtungsforschung.

The work described in this thesis was conducted under the supervision of Dr. André Marques and Prof. Dr. Raphael Mercier at the Max Planck Institute for Plant Breeding Research and.

Erster Referent und Prüfer:	Prof. Dr. Raphael Mercier
Zweite Referentin und Prüferin:	Prof. Dr. Stanislav Kopriva
Beisitzerin/Schriftführerin:	Dr. Andre Marques
Vorsitzende der Prüfungskommission:	Prof. Dr. Ute Höcker

Contents

General Introduction

Climate change, world hunger and overpopulation are some of the biggest challenges the world is currently facing. Moreover, they are part of a multidimensional single scenario: as climate change continues to modify our planet, we might see a decrease of arable land and increase in extreme weather patterns, posing a threat to food security. This has a direct impact on regions with high population growth, where food security is already scarce. Considering additionally the unsustainability of intensive global food production and its contribution to greenhouse emissions and biodiversity loss, it´s clear that all these factors are interconnected (Cardinale et al., 2012; Prosekov & Ivanova, 2018; Wiebe et al., 2019).

Plants are the main source of staple food in the world and are also the main actors in carbon fixation, they are therefore key protagonists in controlling climate change. Plants are also an essential habitat-defining element balancing our ecosystem. Thus, how we grow plants and crops will, aside from the obvious implications for food security, also have a profound impact on the climate and biodiversity. The natural variability of species is considered an immense pool of genes and traits, and their understanding is key to generate new useful knowledge. For instance, natural populations can be more tolerant to abiotic and biotic stresses, or carry traits that combined together in hybrids, might achieve a higher seed number, or a faster growth. Classical breeding has exploited unrelated varieties to achieve traits of interest like dwarfism and higher grain production. However, only a limited number of crop species have been the focus of recent scientific and technological approaches, and they do not represent the extremely vast natural diversity of species that could generate useful knowledge for future applications (Castle et al., 2006; Pingali, 2012). The key to this natural variability is a process called meiotic recombination, the exchange of genomic material between homologous parental chromosomes. Meiotic recombination takes place during meiosis, a specialized cell division in which sexually reproducing organisms reduce the genomic complement of their gametes by half in preparation for fertilization.

Meiotic recombination takes place at the beginning of meiosis, in a stage called prophase I. To exchange DNA sequences, the strands of two homologous chromosomes must be fragmented. This specific process of physiologically induced DNA fragmentation is conserved in the vast majority of eukaryotes (Keeney et al., 1997). After the formation of double-strand breaks, the 3' ends that are left are targeted by recombinases that help the strands search and invade templates for repair. After invasion, the 3' end is extended by DNA synthesis, exposing sequences on the opposite strand that can anneal to the other 3' end of the original double strand

break. DNA synthesis at both ends generates a new structure called a double Holliday Junction (dHJ), forming a physical link between homologous chromosomes, named chiasma (Wyatt & West, 2014).

The resolutions of these structures are called crossovers (COs), which is the molecular event representing the outcome of meiotic recombination. Other outcomes are possible, like noncrossovers (NCOs). In this case, the invading strand is ejected and anneals to the single-strand 3´end of the original double-strand break (Allers & Lichten, 2001).

Crossovers can be divided into two main groups, called class I and class II. COs of the first group are considered to be sensitive to interference, which means that there are mechanisms that prevent two class I COs from happening in proximity of each other. Class II is insensitive to interference. Class I COs are the result of a pathway called ZMM, which involves a group of specialised proteins that are highly conserved among eukaryotes (Lambing et al., 2017; Mercier et al., 2015). Class I COs are the most common, studied and important type of COs.

Centromeres are structures, located on regions of the chromosomes, that allow proper chromosome segregation during mitosis and meiosis. Centromeres have a profound effect on plant breeding and crop improvement, as it is known that meiotic recombination is suppressed at centromeres in most eukaryotes. This represents a great limitation for crop improvement, as many possibly useful traits might be in regions not subject to recombination and thus might not be available for breeding purposes.

Additionally, the mechanisms behind how recombination is regulated and prevented from happening at centromeres are still unclear. In most model organisms centromeres are single entities localized on specific regions on the chromosomes. This configuration is called monocentric. However, another type of configuration can be found in nature, but is less studied. In fact, some organisms harbour multiple centromeric determinants distributed over their whole chromosomal length. This configuration is called holocentric.

The Cyperaceae comprise a vast, diverse family of plants, with a cosmopolitan distribution in all habitats (Spalink et al., 2016). Despite the presence of this family worldwide, knowledge about it is limited. Few genomes are available and molecular insights are scarce. This family is also known to be mainly formed by holocentric species (Melters et al., 2012). Understanding if and how meiotic recombination is achieved in holocentric plants will generate new knowledge that in the future might unlock new traits in elite crops, previously unavailable to breeding, that could help humanity face global climatic, economic and social challenges.

Recent studies have reported new knowledge about important meiotic, chromosome and genome adaptions found in species of the Cyperaceae family and in particular the genus *Rhynchospora* (Marques et al., 2015, 2016a). With the recent publication of the first reference genomes for several *Rhynchospora* species, we could already perform a comprehensive analysis of their unique genome features and trace the evolutionary history of their karyotypes and how these have been determined by chromosome fusions (Hofstatter et al., 2021, 2022). This new resource paves the way for future research utilising *Rhynchospora* as a model genus to study adaptations to holocentricity in plants.

With this work, my intention is to shed light on the underexplored topic of holocentricity in plants. Using cutting edge techniques, I examine the conservation of meiotic recombination together with other species-specific adaptations like achiasmy and polyploidy in holocentrics. My results reveal new insights into how plant meiotic recombination is regulated when small centromere units are found distributed chromosome-wide, challenging the classic dogma of suppression of recombination at centromeres.

Chapter 1: Meiotic recombination dynamics in plants with repeat-based holocentromeres shed light on the primary conserved drivers of crossover patterning

Authors:

Marco Castellani[#], Meng Zhang[#], Gokilavani Thangavel, Yennifer Mata Sucre, José A. Campoy, Thomas Lux, Magdalena Marek, Bruno Huettel, Hequan Sun, Klaus F. X. Mayer, Korbinian Schneeberger, André Marques*

#equal contribution

*corresponding author: amarques@mpipz.mpg.de

Abstract

Meiotic recombination is a conserved pathway among eukaryotes and subject to tight regulation. A combination of large-scale (epi)genetic and structural chromosome features is presumed to influence the overall recombination patterning. Here, we studied how recombination is regulated and distributed in *Rhynchospora breviuscula*, a species with repeat-based holocentromeres. Combining immunocytochemistry, chromatin analysis, and crossover calling from high-throughput single-gamete sequencing from thousands of pollen grains, we found that the uniform distribution of centromeric-units and (epi)genetic features does not affect the broad-scale crossover distribution. Remarkably, we found evidence for a miniature centromere effect indicating an evolutionary conserved crossover control across repeat-based holocentromeres. We further show that the telomere-led pairing seems to be the primary force determining the observed U-shaped recombination landscape. Our results suggest that the common shared U-shaped crossover distribution of eukaryotes is independent of chromosome compartmentalization and centromere organization. We propose that centromere and (epi)genetic properties only affect local crossover formation.

Key words: meiotic recombination, holocentric chromosomes, single-cell sequencing, centromere effect, epigenetics

Introduction

Meiosis is a specialized cell division at the base of gene reshuffling, biological diversity and evolution. During meiosis, homologous chromosomes undergo meiotic recombination, in which genomic material is exchanged between the fragmented strands of two homologous chromosomes. This process of physiologically induced DNA fragmentation and the proteins involved, are highly conserved in the vast majority of eukaryotes (Keeney, 2008; Keeney et al., 1997). The resolution of this fragmentation is called a crossover (CO). This result is thought to be the most common outcome, but other outcomes are possible, like noncrossovers (NCOs) or other alternative recombination pathways (Allers & Lichten, 2001).

Crossovers can be divided into two main groups: class I and class II, although the existence of other alternative crossover pathways cannot be excluded (Lambing et al., 2017; Mercier et al., 2015). COs of the first group are the most common and considered to be sensitive to interference, which means that there are mechanisms that prevent two class I COs from occurring in close proximity to each other. Class I COs are the result of a pathway called ZMM, which includes, among other proteins, the key proteins ZIP1 and HEI10, which are involved in synaptonemal complex assembly and CO designation, respectively (Chelysheva et al., 2012; Durand et al., 2022; Higgins et al., 2005; K. Wang et al., 2012; M. Wang et al., 2010).

The global distribution of COs is typically associated and correlated with the distribution of genetic and epigenetic features (Lian et al., 2022; Zelkowski et al., 2019). In most eukaryotes there is a positive correlation between gene and euchromatin density, and higher frequencies of COs (Brazier & Glémin, 2022; Mézard et al., 2015). In contrast, lower CO frequencies typically correlate with heterochromatic regions, including (peri)centromeres (Lambie & Roeder, 1986; Topp & Dawe, 2006). In monocentric species, where centromeres are single defined structural entities and are typically repeat-based, centromeric regions display low recombination. This phenomenon is called "centromere effect" (Talbert & Henikoff, 2010). However, monocentricity is not the only centromeric organization present in eukaryotes. Holocentric species, for instance, harbour multiple centromeric determinants over the whole length of their chromosomes (Kursel & Malik, 2016; Schubert et al., 2020). Thus, it would be interesting to understand how COs are regulated in species with repeat-based holocentromeres.

Holocentricity has evolved independently multiple times in nematodes, insects and plants (Marcial Escudero et al., 2016; Melters et al., 2012). In the holocentric animal models *Caenorhabditis elegans* and *Bombyx mori,* holocentromeres do not associate with specific sequences (Senaratne et al., 2021; Steiner & Henikoff, 2014). By contrast, holocentric plants of the *Rhynchospora* genus (beak-sedges) display repeat-based holocentromeres in both mitosis and meiosis (Marques et al., 2015, 2016a). Recently, we sequenced the genomes of three beak-sedges (*R. breviuscula*, *R. pubera* and *R. tenuis*) and determined that each chromosome harbours multiple short arrays (~20 kb each) of the specific *Tyba* tandem repeat, evenly spaced (every 400–500 kb) along the entire chromosomal length, and specifically associated with centromeric histone H3 protein CENH3 (Hofstatter et al., 2022). This particular chromosome organization is associated with a remarkable uniform distribution of genes, repeats, and epigenetic features, contrasting to the compartmentalized chromosome organization of close monocentric relatives (Hofstatter et al., 2022). Thus, beak-sedges offer an excellent model to study the mechanisms of CO formation along repeat-based holocentromeres.

Regardless of the centromere and chromosome organization, most studied eukaryotes show a typical U-shaped distribution of COs, which is usually explained by structural chromosome features (telomere and centromere effects) and correlation with (epi)genetic factors (Brazier & Glémin, 2022; Haenel et al., 2018; Saito & Colaiácovo, 2017; Yelina et al., 2015; Zelkowski et al., 2019). Therefore, it is very intriguing to understand the main factors influencing the meiotic recombination patterning in *Rhynchospora*, where the uniform distribution of (epi)genetic features and "absence" of conventional centromeres presents a unique case among eukaryotes. Meiosis in holocentric plants has been mainly studied with respect to their intriguing "inverted meiosis", more than for the potential implications regarding recombination (Cabral et al., 2014; Heckmann et al., 2014; Hofstatter et al., 2021; Melters et al., 2012). Moreover, chromosomes in *Rhynchospora* maintain their repeat-based holocentromere organization during meiosis (Marques et al., 2016a), which challenges the idea of recombination suppression at and near centromeres. However, no direct evidence for meiotic recombination frequency and distribution have been reported for any holocentric plant yet. If and how plant holocentromeres interact or interfere with meiotic recombination is still unknown.

Here, we use *Rhynchospora breviuscula* as a model to study meiotic recombination dynamics in the absence of both a localized centromere and compartmentalized chromosome organisation, features that potentially mask underlying factors affecting the distribution of COs. Using a combination of immunocytochemistry, chromatin and DNA analysis, and an adapted CO-calling pipeline from single-cell transcriptome deep sequencing (RNA-seq) of pollen nuclei, we develop the first comprehensive overview of meiotic recombination dynamics and distribution for a species with repeat-based holocentromeres. We further show that despite this unique chromosome organization, COs show a biased distribution towards the distal regions of chromosomes. Surprisingly, this U-shaped recombination landscape did not correlate with any genetic and epigenetic feature analysed at broad-scale. Furthermore, we observed that despite the transition to holocentricity, the relative proximity of repeat-based centromeric units does not affect recombination events. However, these were suppressed inside centromeric units, indicating an evolutionary conserved miniature centromere effect. Our data point to a major influence of the pairing and synapsis dynamics starting from chromosomal ends in determining the broad-scale recombination landscape and indicate that centromere and (epi)genetic effects only play a local role in CO patterning.

Results

Molecular dynamics of prophase I are conserved in *R. breviuscula*

We performed cytological studies on inflorescences of *R. breviuscula*, which provided an overview of a conserved prophase I progression in this species. All the main prophase I stages were found, i.e., leptotene, zygotene, pachytene, diplotene, diakinesis (Figure 1a-e). In contrast to the holocentric animal *C. elegans* (Saito & Colaiácovo, 2017), which forms only a single chiasma per bivalent, we observed the presence of five bivalents connected by one or two chiasmata in *R. breviuscula* (Figure 1e). Moreover, we confirmed the holocentric nature of the *R. breviuscula* chromosomes in mitosis and meiosis by immunostaining with antibodies against CENH3 (Figure 1f-h).

Conservation level of pairing and synapsis

During the first stages of prophase I (leptotene and zygotene), homologous pairing and assembly of the synaptonemal complex (SC) take place. ASY1 is a structural component of the chromosome axis, thus making it an excellent marker for unpaired chromosomes at leptotene and zygotene. It is also essential for proper recombination (Armstrong et al., 2002; Lambing, Kuo, et al., 2020). ZYP1 is the transverse filament of the proteinaceous zipper-like structure called the SC that connects two homologous chromosomes. Its function however goes beyond

14

its role as a structural protein as it is also involved in recombination and CO interference (Barakate et al., 2014; Capilla-Pérez et al., 2021; Higgins et al., 2005; M. Wang et al., 2010). We investigated the immunolocalization of ASY1 and ZYP1 as indicators of a conserved and functional machinery for pairing and SC assembly. We could observe that in early prophase I stages, corresponding with leptotene, the linear signal of ASY1 is present on the entire length of unpaired chromosomes (Figure 2a). As the pairing starts and progresses through zygotene, the SC starts to be assembled and ZYP1 is gradually loaded onto synapsed chromosomes. As ZYP1 is loaded, two ASY1 linear signals can be followed until they converge, lose intensity and the ZYP1 linear signal becomes clear and intense (Figure 2b-c). As meiosis progresses into pachytene, represented by complete synapsis and pairing, the linear ZYP1 signal is present on the whole length of the chromosomes (Figure 2d). The signal of ZYP1 is localized in the groove between paired homologous chromosomes. Interestingly, the combined behaviour of ASY1 and ZYP1 is consistent with what is observed in monocentric models, hinting at a conserved pairing and synapsis in *R. breviuscula*. Moreover, consistent with the holocentric nature of *R.*
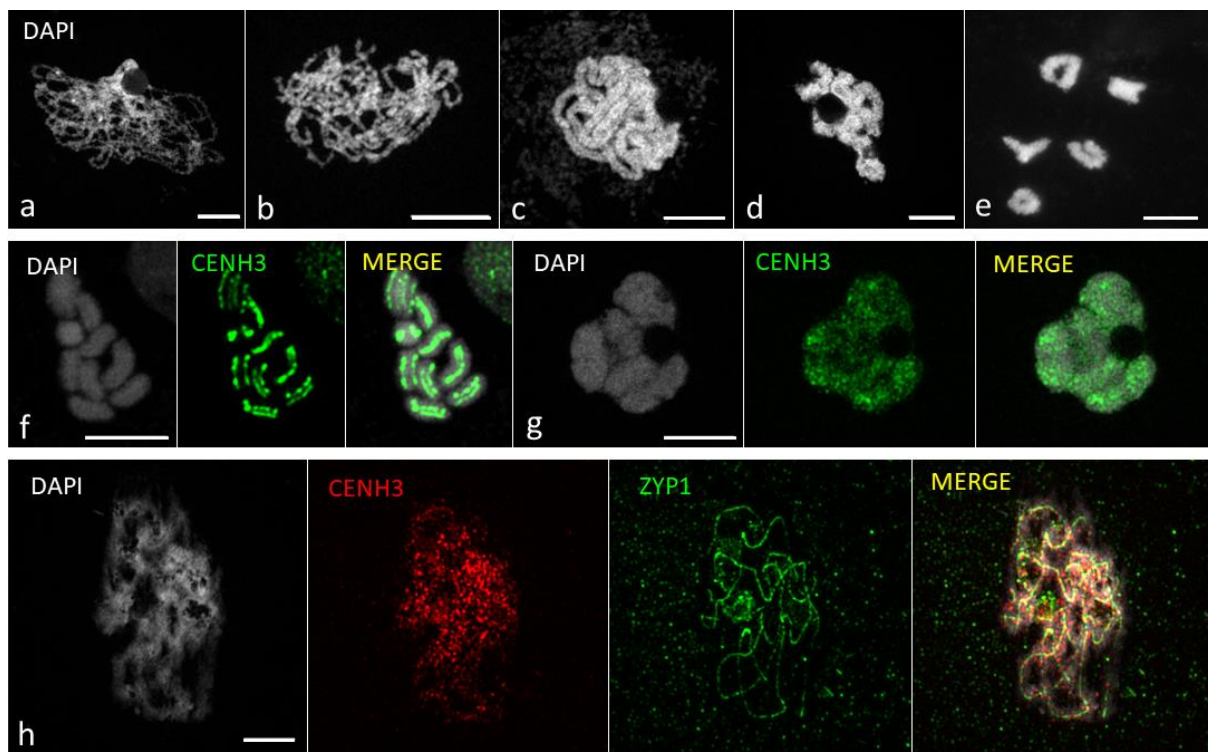
Figure 1

Chromosome spreads and immunolocalization in male *R. breviuscula* meiocytes. (a-e) Meiotic stages are displayed including leptotene (a), zygotene (b), pachytene (c), diplotene (d) and diakinesis (e). (f-g) Immunolocalization was performed against centromeric protein CENH3, which appears as lines during mitosis (f) and as cluster-holocentromeres in meiosis (g). (h) Immunolocalization of ZYP1 and CENH3 during pachytene showing the presence of active centromeric chromatin along the entire length of synapsed chromosomes. Maximum projection is shown, and DNA is counterstained with DAPI. Scale bar = 5 μm (a-g), 10 μm (h).

breviuscula meiotic chromosomes, CENH3 was found localized along the entire synapsed chromosomes (Figure 1h).

Next, we asked whether the meiosis-specific alfa-kleisin REC8 is also conserved in *R. breviuscula*. REC8 is responsible for sister chromatid cohesion and important for chromosome segregation and recombination (Lambing, Tock, et al., 2020) and it is also an established marker for meiotic cytological studies. Indeed, we observed a conserved linear signal on unpaired
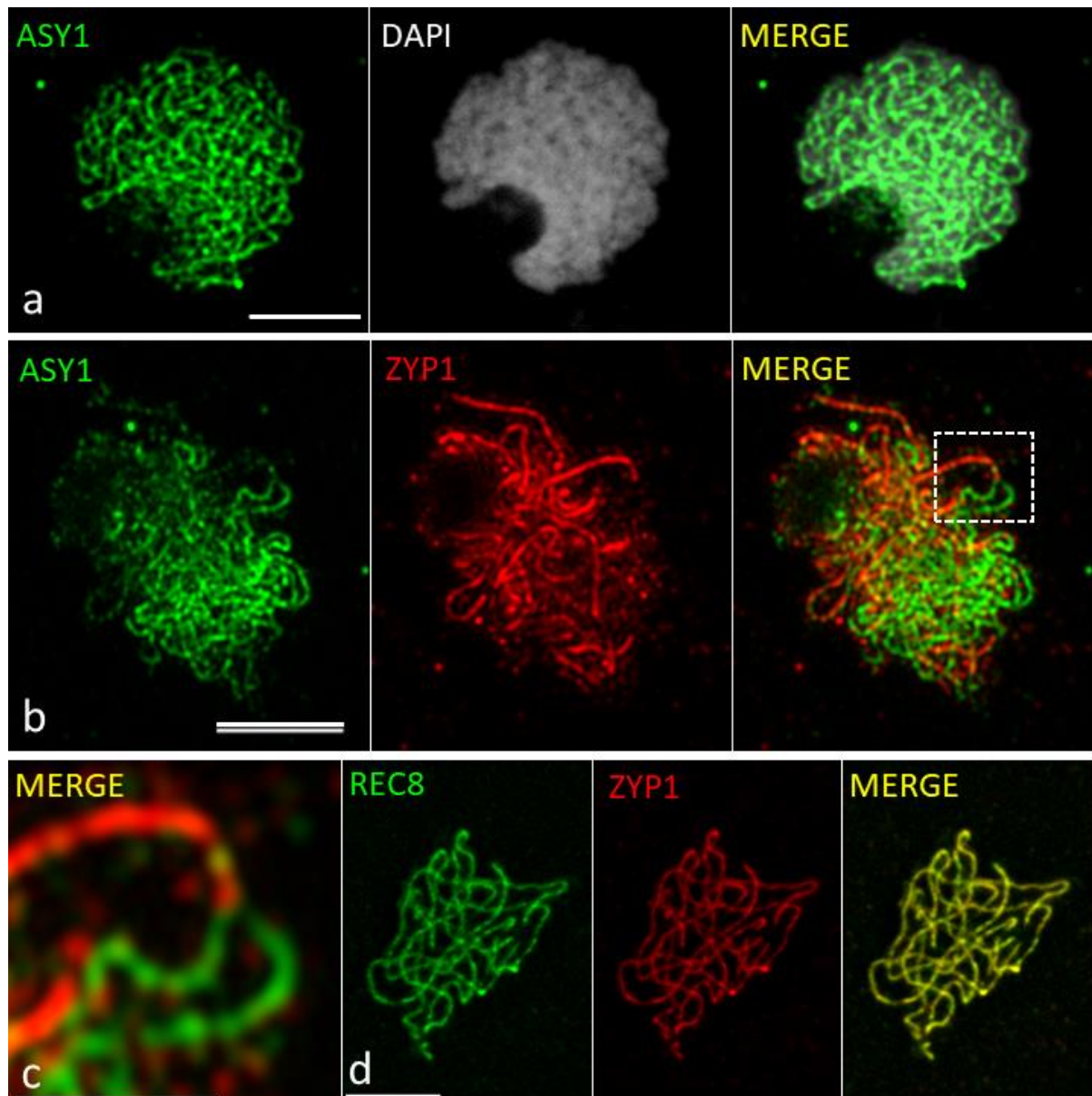
Figure 2

Immunolocalization of ASY1, REC8, ZYP1 from leptotene to pachytene. **(a)** ASY1 (green) appears as a linear signal on unpaired chromosomes. **(b)** Synapsis is visualized as the loading of ZYP1 (red), as ASY1 (green) signal disappears. **(c)** Detail of two unpaired chromosomes, represented by ASY1 (green) coming together to synapse, loss of the ASY1 signal and loading of ZYP1 (red). **(d)** Full colocalization of cohesin protein REC8 (green) and ZYP1 (red) at pachytene. Maximum projection is shown, and chromosomes are stained with DAPI. Scale bar = 5 μm (**a, b, d).** Scale bar = 2 μm **(c).**

chromosomes. This signal becomes more intense when pairing takes place as the two linear signals come together. At pachytene, REC8 colocalizes with ZYP1 as a continuous linear signal along the entire chromosomal length (Figure 2d). Thus, pairing and synapsis in the holocentric plant *R. breviuscula* are conserved like in other monocentric models.
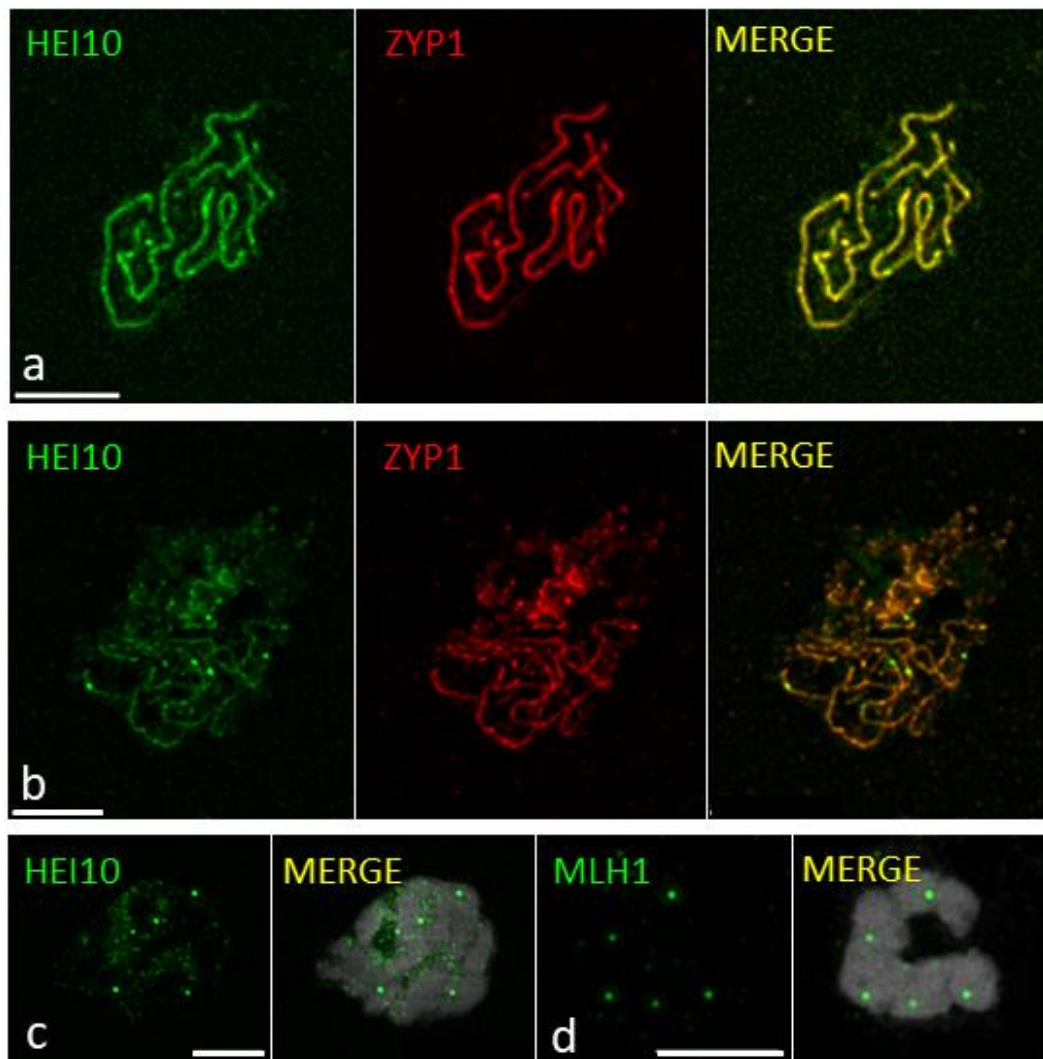
Figure 3

Immunolocalization of HEI10, ZYP1 and MLH1 in late prophase I. **(a)** HEI10 (green) is first displayed as many closely spaced foci, appearing as lines, at pachytene, and they co-localise with ZYP1 (red). **(b)** In late pachytene, the linear signal of HEI10 still colocalises with ZYP1, but becomes weaker, except for a few high-intensity foci. **(c)** At diplotene and diakinesis, HEI10 only appears as foci on bivalents and there is no linear signal anymore. **(d)** MLH1 (green) appears in late prophase I stages as foci, representing chiasmata on bivalents. Maximum projection is shown, and chromosomes are stained with DAPI. Scale bars = 5 μm.

Meiotic recombination and class I CO pathway

ASY1, ZYP1 and REC8 are useful markers for assessing the progression of meiosis in the first stages of prophase I and the functioning of the meiotic recombination machinery. However, other markers are required to study later stages of prophase I, where recombination intermediates are processed into final crossovers. HEI10 is a E3 ubiquitin ligase characterized in mammals, yeast (*Saccharomyces cerevisiae*) and plants. HEI10 appears in the middle of the ZMM pathway, after pairing, but before the resolution of COs. It is proposed that HEI10 interacts with both early and late recombination proteins, and acts by stabilizing recombination sites and promoting their maturation into class I COs (Chelysheva et al., 2012; Serra et al., 2018; K. Wang et al., 2012). When pairing and synapsis start, HEI10 is gradually loaded as a linear signal constituted by many closely spaced foci (Figure 3a). At pachytene, when synapsis is complete, the HEI10 linear signal starts to disappear. However, a few foci, putatively class I CO sites, increase in intensity (Figure 3b). At diplotene and diakinesis only high-intensity foci remain (Figure 3c). This phenomenon, recently described as "coarsening" (Morgan et al., 2021; Stauffer et al., 2019; L. Zhang et al., 2021) is observed in *Rhynchospora breviuscula* and is consistent with observations in other model organisms. Another established marker for meiotic recombination is the mismatch repair protein MLH1. Its role is essential in meiosis and it is believed to have a meiosis-specific resolvase activity in processing dHJs into final class I COs. MLH1 interacts with MSH4 and MSH5 in a dHJs resolution pathway, thus marking specifically class I COs in distantly related species (Lhuissier et al., 2007). In *R. breviuscula*, MLH1 appears as bright foci on bivalents at diplotene and diakinesis (Figure 3d, Figure 4, Supplementary Figure 1). We always observed a minimum of five foci, one per each bivalent, and a maximum of eight foci, which is consistent with the formation of two COs in some bivalents. The mean number of foci detected with MLH1 was 6.27 (n=83) (Figure 4, Figure 7c).

Phased genome assembly of *R. breviuscula* as a prerequisite for CO identification by gamete-sequencing

Determining whether recombination in *R. breviuscula* is affected by the genome-wide distribution of holocentromeres requires the detection of CO events in a large number of recombinant individuals. However, *R. breviuscula* is an outbred wild species with high levels of self-incompatibility, which hampers the standard detection of COs, typically involving the time-consuming generation of segregating offspring. As gametes already carry the outcome of meiotic recombination, and they can be obtained in large numbers in a relatively inexpensive manner from pollen grains, we adapted a strategy based on the gamete-binning method

described Campoy et al. (2020) (See below). To identify COs from a single *R. breviuscula* individual, the genome of the given organism must be heterozygous and a phased chromosome-level reference genome must be available. The recent available nonphased genome of *R. breviuscula* was reported to be 1% heterozygous (Hofstatter et al., 2022) suggesting the feasibility of phasing the genome. We took advantage of the recent development of the assembler software Hifiasm (Cheng et al., 2021), which enables the accurate phasing of both haplotypes from primary assembled contigs using a combination of HiFi reads and Hi-C (See Materials & Methods; Figure 5a-b). Further Hi-C scaffolding of each set of haplotype-phased contigs led to high-quality haplotype-phased chromosome-level genome assemblies (Figure 5c; Supplementary Table 1). We performed a synteny analysis and detected the structural variants between the two haplotypes, revealing a high degree of synteny between the haplotypes with only few inversions, translocations and duplications (Figure 5d; Supplementary Table 2).

To genotype the haploid gamete genomes and determine which haplotype a genomic segment is derived from, genome-wide markers are needed to distinguish the two haplotypes. By aligning the ~26 Gb Illumina whole-genome short reads of *R. breviuscula* with the haplotype 1 phased genome (from the reference genome, rhyBreHap1), we detected 820,601 haplotype-specific single nucleotide polymorphisms (SNPs, ~1 SNP/449 bp) and used them as markers for genotyping (Figure 6b; Supplementary Figure 4; Supplementary Figure 6A).

Single-cell RNA sequencing of pollen nuclei allows high-throughput identification of genome-wide COs

We identified genome-wide CO events by conducting 10X Genomics single-cell RNA sequencing (scRNA-seq) on the nuclei extracted from pollen grains of *R. breviuscula* and *R. tenuis*. The addition of gametes from *R. tenuis* was done for multiplexing purposes, and they will be analysed in another study. We extracted pollen nuclei for 10X scRNA-seq library preparation and sequencing (Figure 6; described in Materials & Methods). We pre-processed the resulting scRNA sequences by correcting barcodes, demultiplexing, and removing cells with a low number of reads. We obtained viable sequence data for 8,001 sorted nuclei for downstream analyses. We mapped the deduplicated DNA reads from these viable 8,001 nuclei to both the *R. breviuscula* and *R. tenuis* genomes, and removed the nuclei of *R. tenuis* based on the alignment rates (Supplementary Figure 5, see Materials & Methods). Finally, we obtained individual sequence data for 4,392 *R. breviuscula* pollen nuclei.

We called SNPs from the *R. breviuscula* alignments and compared them to the 820,601 markers defined from the reference genome. The intersection between the SNPs in every nucleus and markers on the reference genome defined the set of genotyping markers in these pollen samples. After removing doublets and correcting the sequences (Supplementary Figure 5, see Materials & Methods), we obtained a final set of 1,641 pollen samples with at least 400 markers (~1 marker/Mb). These markers (median resolution ~1 marker/542 kb) covered almost the entire length of all five chromosomes (Supplementary Figure 6B), guaranteeing a genome-wide CO detection. We detected 4,047 COs in the 1,641 pollen nuclei by inspecting genotype conversions, as indicated in Figure 6c-d (Supplementary Figure 7). Overall, we delineated a complete and detailed pipeline to detect COs in an economical way by high-throughput scRNA sequencing of gametes from a single heterozygous individual (Figure 6).

R. breviuscula

$W_{Mann-Whitney} = 1043.50$, $p = 2.29e-04$, $\hat{r}^{rank}_{biserial} = -0.39$, $CI_{95\%}$ [-0.55, -0.19], $n_{obs} = 124$
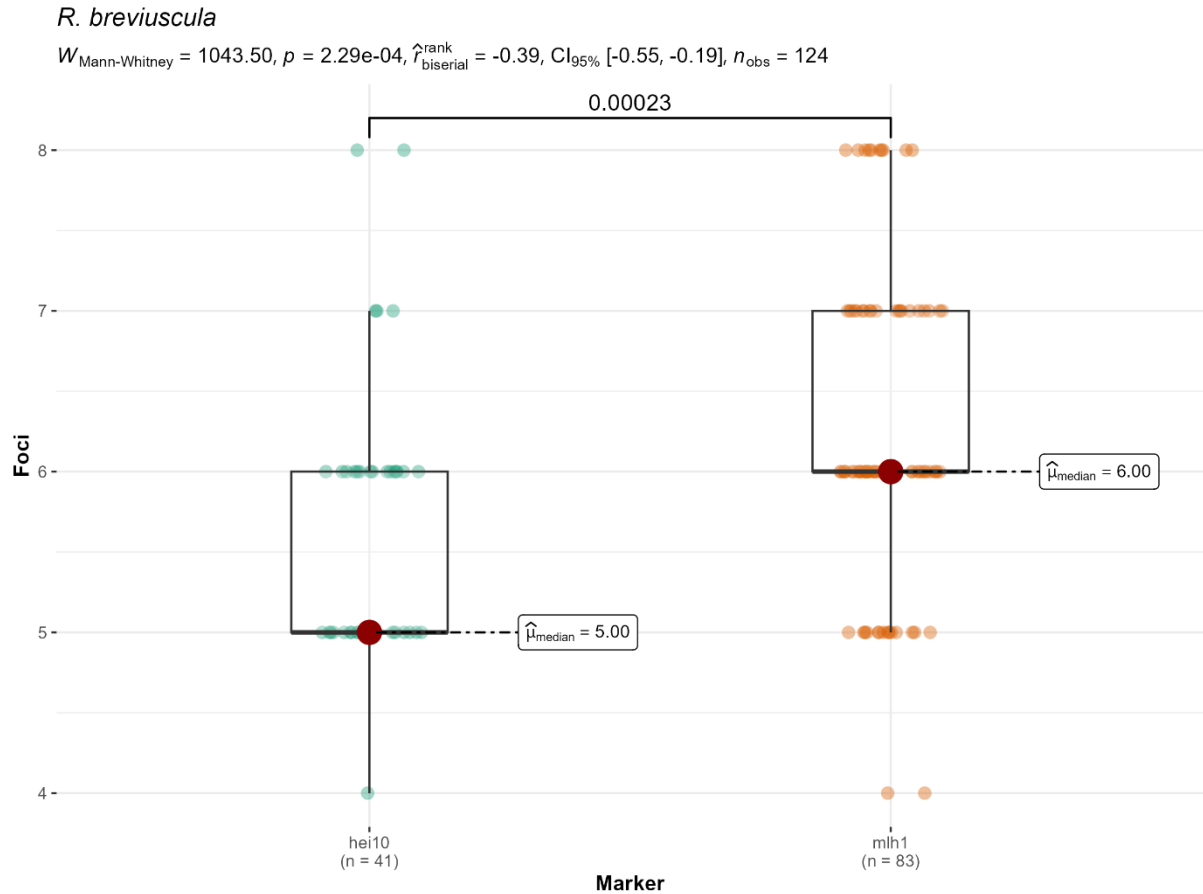
Figure 4

Foci counting for HEI10 (**left**) and MLH1 (**right**) based on immunostaining of *R. breviuscula*. Both markers fit into an expected model for CO assurance, which implies a minimum of 5 foci. The relatively narrow window with a maximum of 7-8 foci also supports the presence of CO interference. Foci counting for the two markers are significantly different (p=00023). This could be due to a technical bias due to the low robustness of our HEI10 antibodies, or a biological meaning considering the different functions of HEI10 and MLH1. The plot was realised in R using the package ggstatsplot (Indrajeet Patil 2021).

CO Mapping reveals a U-shaped recombination landscape

Counting the occurrence of COs in chromosome-wide genomic intervals across all pollen nuclei, we computed CO rates along chromosomes and established the first linkage map for *R. breviuscula* with a total length of 246.6 cM (Figure 7a-b). The overall location interval of COs (median ~1.5 Mb and mean ~2.24 Mb resolution) allowed us to analyse the distribution and frequency of meiotic recombination events in a species with repeat-based holocentromeres for the first time. The landscape contained large regions of high- and low-recombination frequencies, i.e., recombination domains. Most regions with high recombination rates were located at distal chromosomal regions, while central chromosomal regions showed lower recombination rates. Unexpectedly, the recombination landscape of holocentric *R. breviuscula*

resembled a U-shaped distribution of COs, which is commonly present in monocentric models (Figure 7a-b). Remarkably, chromosomes 1 and 2 each had only one high-CO domain at one chromosomal end. The other three chromosomes harboured two high-recombination domains at both ends, revealing that CO rates have an uneven distribution (Figure 7a), distinct from the almost uniform centromere distribution (See below; Hofstatter et al. 2022).

We compared CO numbers estimated from DNA sequencing and the number of MLH1 foci observed by cytology. To have a precise estimation of CO number and not bias the result by the low number of markers, we only counted those COs from pollen nuclei with more than 2000 markers (n = 81). On average, we detected around three COs per haploid gamete, or 0.6 COs per chromatid (Figure 7c-d). As gametes only have one chromatid from each recombined chromosome, the number of expected COs should be approximately half of the detected number of MLH1 foci. Furthermore, all chromosomes had exactly one CO in half of these gametes (n = 81), while double COs appeared in only 5% of the 81 gametes considered (Figure 7d). Chromosome 3 showed the highest frequency of double COs (9%, Figure 7d), which confers it the longest genetic length among all *R. breviuscula* chromosomes (55 cM; Figure 7b). This is especially remarkable considering that chromosome 1 (53 cM) is physically longer than chromosome 3 (by 20 Mb).

We also tested whether CO interference occurred in *R. breviuscula*. We used a Chi-square goodness-of-fit test to investigate whether the CO number on each chromosome follows a Poisson distribution, which revealed a significant discrepancy between observed and expected CO numbers (Supplementary Figure 9a). This proved that the CO numbers were not randomly distributed but under-dispersed based on the negative alpha values from dispersion tests, indicating the existence of a positive CO interference. We also computed the coefficient of coincidence (CoC) of COs across the genome, which measures the observed double COs frequency over their expected frequency. The CoC curve of all chromosomes showed that the coefficients are below 1 for genomic intervals with distances less than around 60 Mb w (Figure 7e; Supplementary Figure 9b), suggesting that the frequency of double COs is lower than expected. This result supports the conclusion that there is substantial CO interference in *R. breviuscula*.
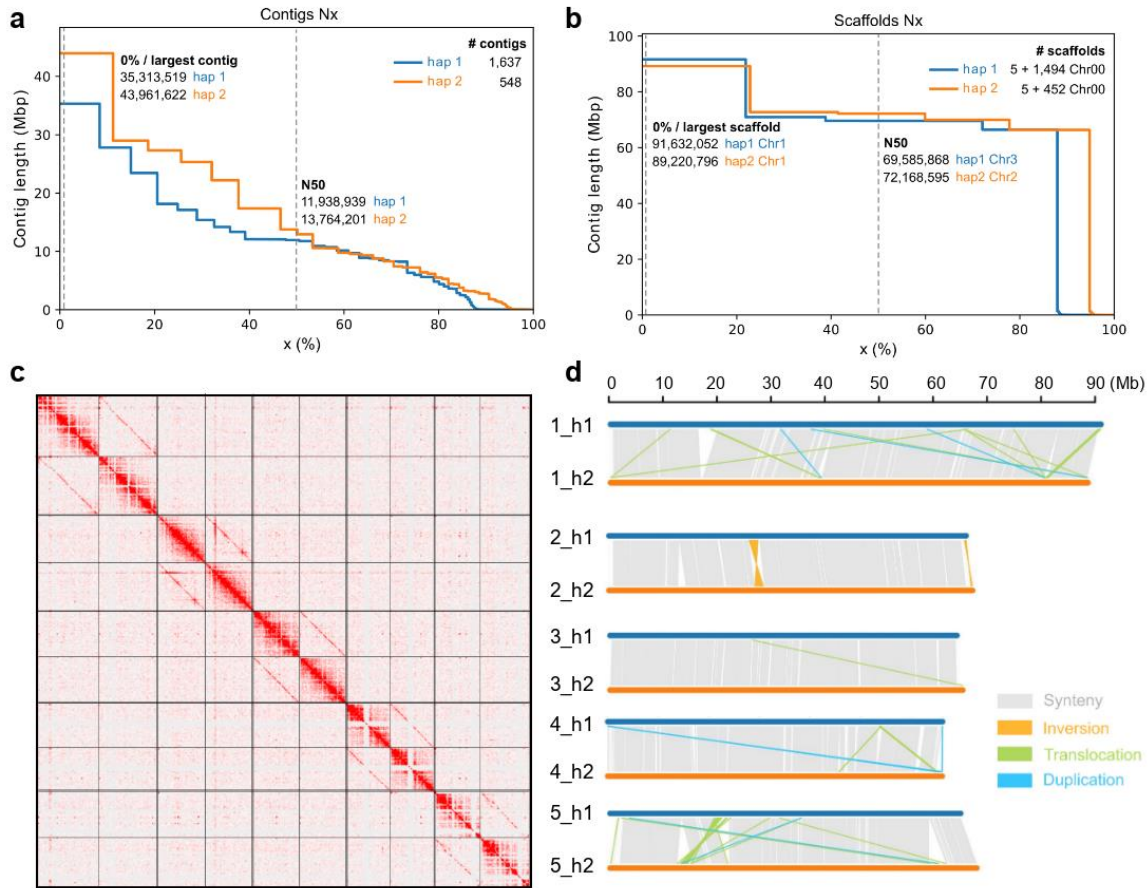
Figure 5

Phasing and structural variations of the *R. breviuscula* heterozygous genome. (**a-b**) Assembly statistics of phased contigs (**a**) and scaffolds (**b**) in haplotype 1 and haplotype 2. (**c**) Hi-C scaffolding of the five haplotype-phased pseudochromosomes. Homozygous regions between haplotypes are seen as clear regions depleted of signals on the Hi-C map. (**d**) Synteny comparison and structural variations (> 10 kb) identified between the two haploid assemblies. Note the overall high synteny found between the two haplotypes. Synteny blocks were computed with SyRI (Goel and Schneeberger 2022).

Broad-scale recombination landscape is independent of holocentromere distribution and (epi)genetic features

We compared the broad-scale recombination landscape with all known (epi)genetic features to determine whether any specific feature would explain the CO distribution of *R. breviuscula*. A chromosome-wide comparison of the recombination landscape of *R. breviuscula* revealed no apparent correlation between the uniform holocentromere distribution and other genomic (gene, TEs, SNPs densities or GC content) and epigenomic features (such as H3K4me3, H3K27me3, H3K9me2 or DNA methylation). In fact, no (epi)genomic feature showed strong correlation with CO distribution, as they are all uniformly distributed along the chromosomes of *R. breviuscula* (Figure 8a). We re-iterated the statistical analysis and confirmed the absence of any correlation between CO frequencies and the (epi)genomic features considered (Figure 8b).

These results indicate that, at broad-scale, meiotic recombination occurs independently of chromosome-wide holocentromere distribution and (epi)genetic features.
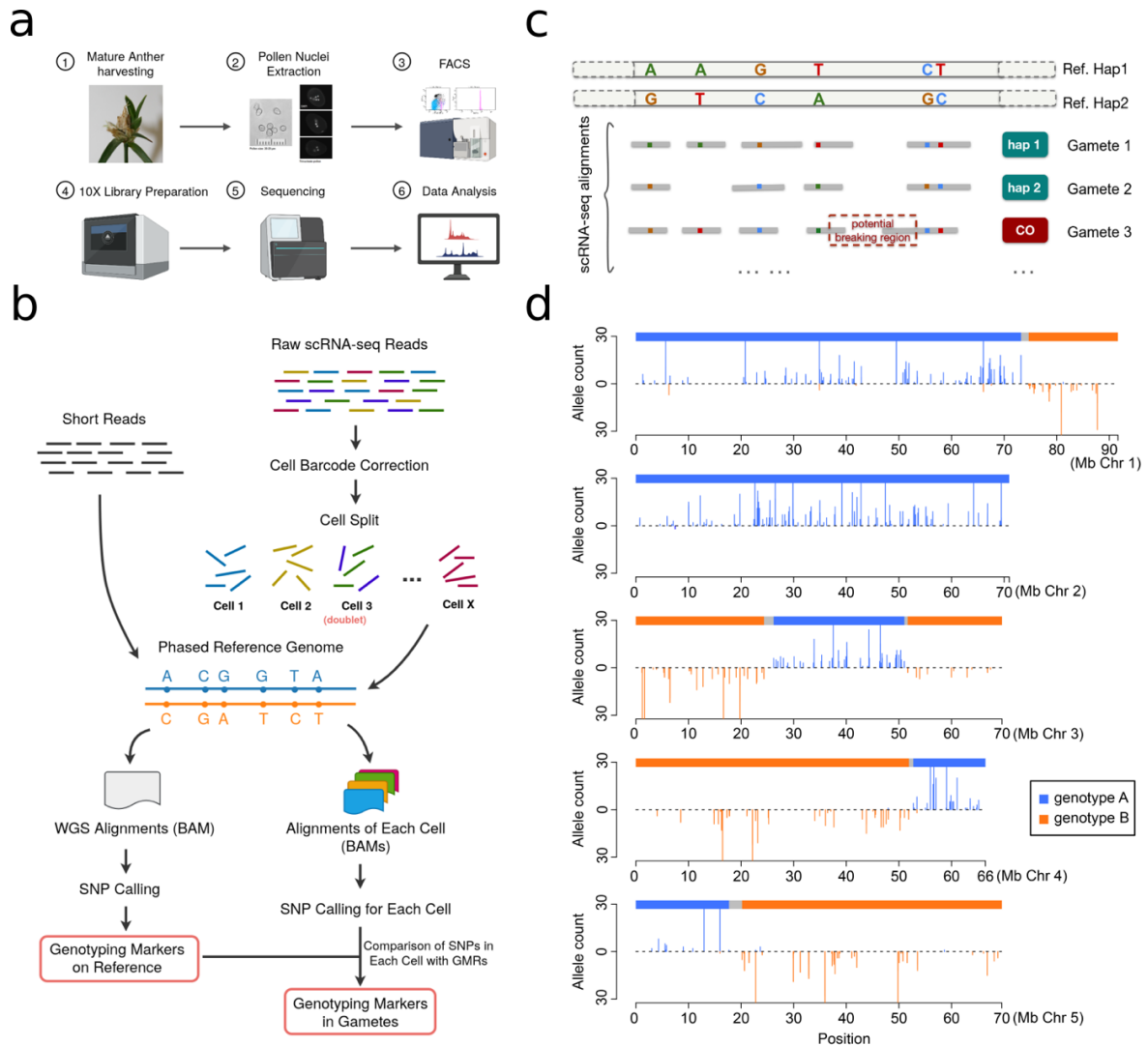
Figure 6

Overview of CO calling by scRNA-sequencing of *R. breviuscula* gametes. (**a**) Pollen sampling, library preparation and scRNA sequencing pipeline; (**b**) The strategy of obtaining genotyping markers on reference by mapping short reads and markers in gametes by mapping scRNA-seq across a large number of gametes to reference genome; (**c**) Diagram of the identification of potential CO events after alignments of scRNA reads of each gamete to phased reference genome. (**d**) An example of genotype definition by markers in a real pollen nucleus, i.e., cell barcode AAGACTCTCATCCTAT.
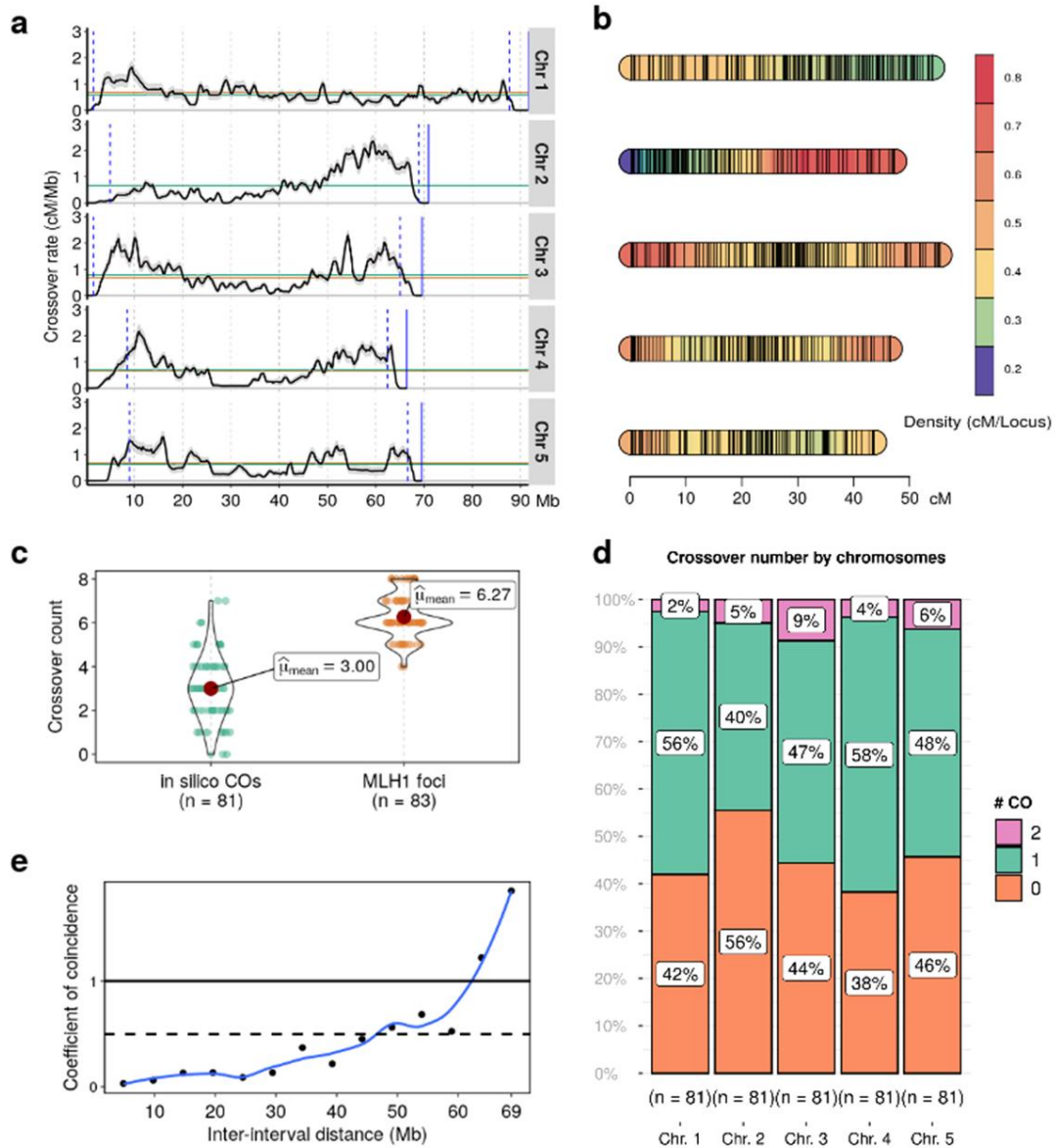
Figure 7

Meiotic recombination dynamics in *R. breviuscula* derived from single-pollen sequencing. (**a**) The first recombination landscape of the five chromosomes in *R. breviuscula* by computing crossovers in 1,641 pollen nuclei. Black line displays the CO rate, which was the mean of 500 random samplings for each CO gap. Shadow ribbons indicate one standard deviation from mean CO rate. Blue dashed vertical line: start and end of confident CO rate computation (Supplementary Figure 6). Blue solid vertical line: chromosomal end. Orange horizontal line: genome-wide average CO rate. Green horizontal line: chromosome-wide average CO rate. (**b**) Genetic linkage map with density indicated by colouring. The 705 markers were selected by 500kbp sliding window through all markers defined on reference (See Materials & Methods). (**c**) CO number by counting CO events in bioinformatic analysis and MLH1 foci in cytological observations. (**d**) CO number distribution by each individual chromosome. Note the higher incidence of double COs in chr3. (**e**) CoC curve in pollen nuclei (n = 1,641). Chromosomes were divided into 15 intervals, random sampling at CO intervals, for calculating the mean coefficient of coincidence of each pair of intervals.
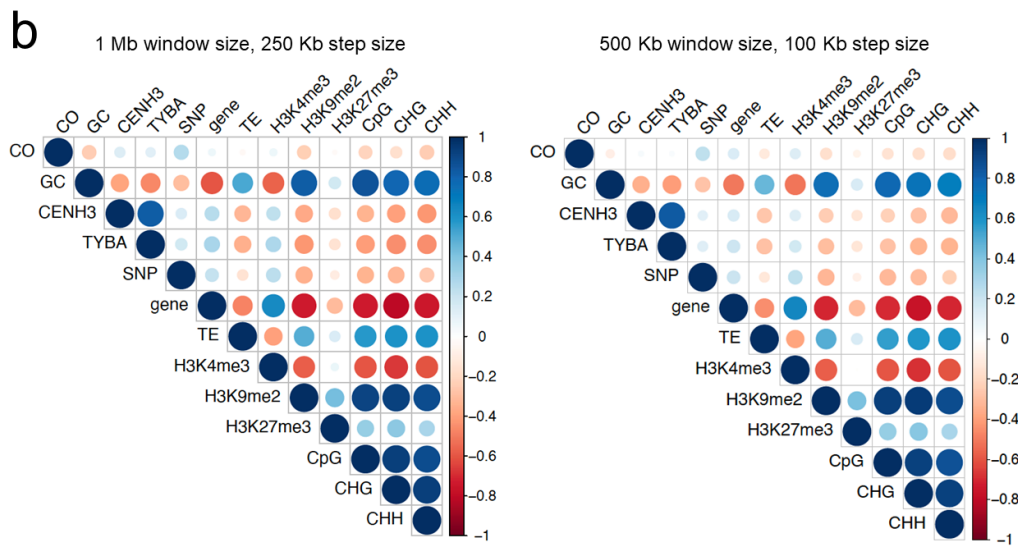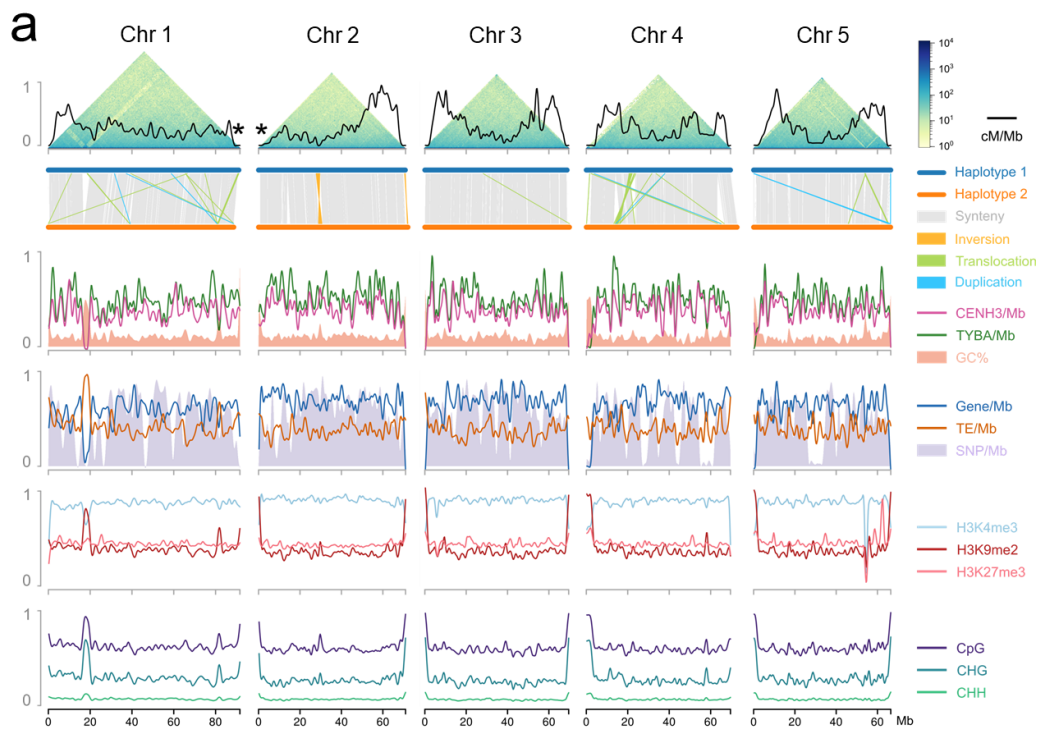
Figure 8

Broad-scale correlation of recombination landscape and (epi)genetic features in *R. breviuscula*. (**a**) Chromosome distribution of CO rate coupled with many different genetic and epigenetic features. Top: recombination landscape (black line) created with sliding windows of 500 kb at a step of 50 kb with COs detected in all single pollen nuclei (n=1,641), coupled with Omni-C chromosome conformation capture contacts. The terminal location of 35S rDNA loci on chr1 and chr2 are indicated by asterisks. For x-axis, coordinates were based on the haploid 1 assembly *R. breviuscula*. For y-axis, all features were scaled [0,1], which stands for a maximum of 2.34 for recombination frequency (cM/Mb), 5 for Tyba density, 6 for CENH3 density, 7205 for SNP density, 88 for gene density, 227 for TE density respectively; GC [33.3, 46.6], H3K4me3 [-1.494, 0.231], H3K9me2 [-1.20, 1.84], H3K27me3 [-0.671, 0.491] are scale to [0,1] by their minimum and maximum; while mCG, mCHG, and CHH are original values (0 to 100%). Crossovers are almost completely absent in a large inversion in chr2:30–35 Mb, while in homozygous regions we could not confidently call COs, for example in chr4:25–35 Mb. The large variants were confirmed within Hi-C contact maps (Figure 5). Asterisks at chromosome ends in chr1 and chr2 stands for the position of 35S rDNA clusters found in the assembly and confirmed by FISH (Supplementary Figure 3). (**b**) Correlation matrix of COs with all available (epi)genetic features. Positive correlations are displayed in blue and negative correlations in red. Colour intensity and the size of the circle are proportional to the correlation coefficients. In the right side of the correlogram, the legend colour shows the correlation coefficients and the corresponding colours. Pearson correlation coefficient for each pair of all features under 1Mb smoothing window and 250 Kb step size (left) and 500 Kb smoothing window and 100 Kb step size (right), specifically, mean CO rates, mean GC contents, CENH3 peak density, Tyba array density, SNP density, TE density, H3K4me3 RPKM, H3K9me2 RPKM, H3K27me3 RPKM, mean CpG, mean CHG, and mean CHH.

A miniature centromere effect sheds light on the fine-scale CO epigenetic regulation

As we did not find any correlation between the CO distribution and (epi)genetic features at a broad genomic scale, we tested the presence of a local centromere effects affecting CO designation in *R. breviuscula*. Although our scRNA-seq strategy is useful for delineating the recombination landscape and CO dynamics, the overall CO resolution obtained was low (median size of the location interval ~1.5 Mb, mean ~2.24 Mb), which does not allow for a precise analysis of a potential centromere effect in this particular case. To achieve precise CO resolution, we performed manual self-pollination in *R. breviuscula*. Due to its high self-incompatibility, we obtained only 63 F1 plants; we sequenced these to 3x coverage, which allowed us to detect 378 CO events at a high resolution (median 334 bp, mean ~ 2kbp). Overall, we obtained results consistent with our single-pollen sequencing strategy, confirming the robustness of our analysis (Supplementary Figure 11). We observed an increase in the genetic map length in the F1 offspring, suggesting that heterochiasmy occurs in *R. breviuscula* and that female meiosis might have slightly higher CO frequencies than male meiosis (Supplementary Figure 11A-B). We estimated the average CO number to be 6 in the F1 offspring, exactly double the average number estimated from single pollen nuclei data (Supplementary Figure 11C-D).

Holocentromeres in *R. breviuscula* are repeat-based, i.e., each centromeric unit is based on specific array of the holocentromeric repeat *Tyba* associated with CENH3, with average sizes of ~20 kb and average spacings of ~400 kb, where each chromosome harbour hundreds of individual centromeric units (Figure 9a-b; Hofstatter et al., 2022). Remarkably, we found the same epigenetic centromere identity in *R. breviuscula* (Figure 9c) as reported for *R. pubera* (Hofstatter et al., 2022). This organisation makes it possible to identify centromeric units at the DNA level by annotating *Tyba* repeat arrays (Figure 9b). We computed the observed *versus* expected by random distribution fine-scale CO positions across all available chromatin marks and genetic features. We found that COs are more frequently formed at H3K4me3 peaks and genes than what expected by random distribution (Figure 9d; Supplementary Figure 12). Within genic regions COs were preferentially formed in promoter regions (Figure 9e). Remarkably, COs were mostly suppressed inside centromeric units and heterochromatic regions (Figure 9d, f; Supplementary Figure 12), suggesting that indeed a local centromere effect exists in species with repeat-based holocentromeres. However, after computing the distances between the CO break intervals and the corresponding nearest *Tyba* arrays/CENH3 domains, COs did not show a tendency to be positioned away from or close to centromeric units (Figure 9g), suggesting a rather miniature centromere effect and that the proximity to a centromeric unit does not affect

CO formation, as long as the CO is outside of it. Moreover, we found only five cases of a CO being placed inside a region containing reduced *Tyba* repeats and CENH3-positive chromatin (Figure 9h). Our results point to the exciting finding that local CO formation in *R. breviuscula* is affected at fine-scale by repeat-based centromeric units and chromatin features in contrast to the absence of broad-scale correlation. However, the centromere effect observed seems rather limited as it does not block CO formation in the vicinity of CENH3 domains (Figure 9i).
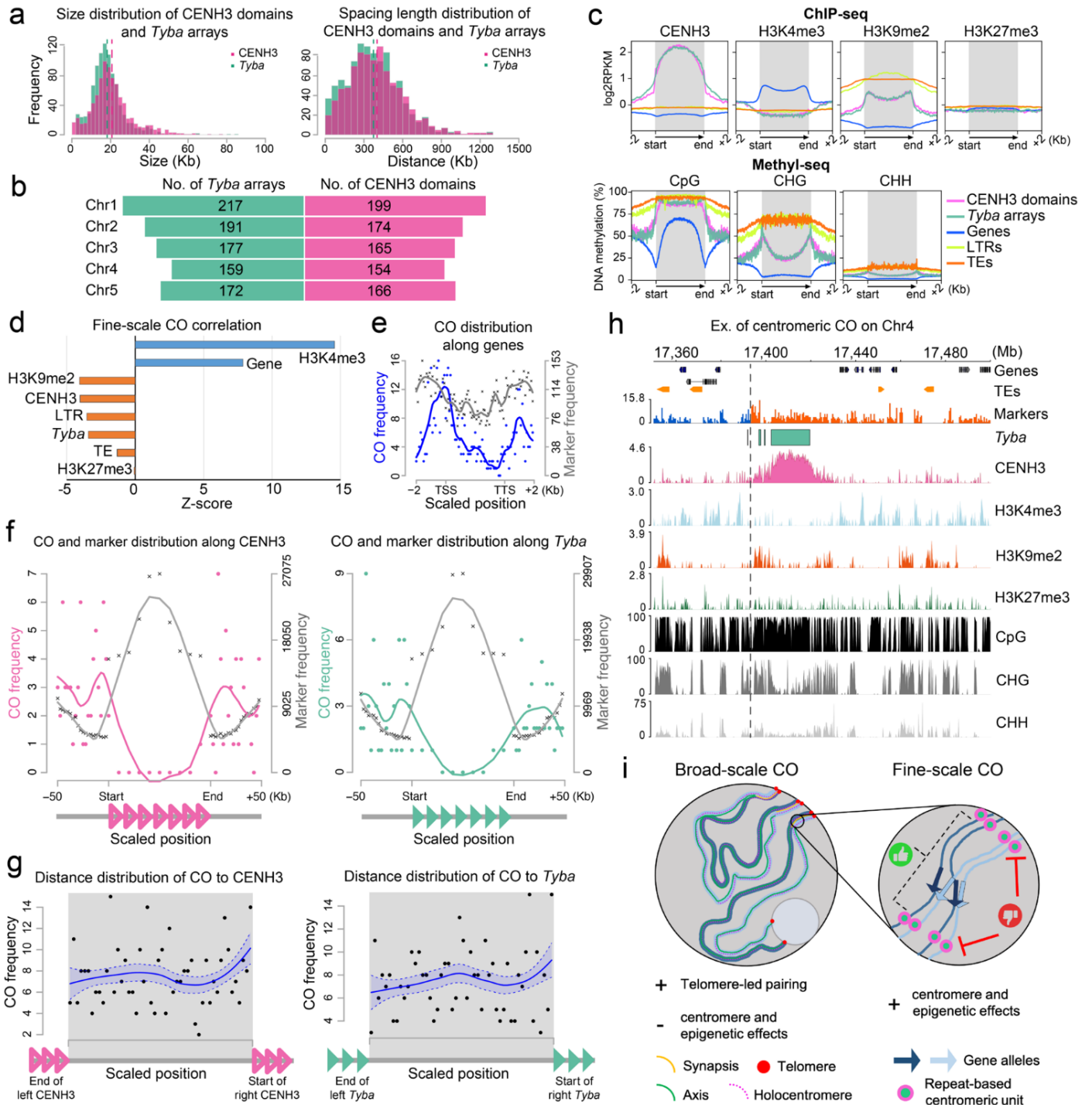
Figure 9

Epigenetic regulation and fine-scale correlation of CO position with repeat-based holocentromeres in *R. breviuscula*. **(a)** Size and **(b)** spacing length distribution of CENH3 domains and *Tyba* arrays. **(c)** Enrichment of CENH3, H3K4me3, H3K9me2, and DNA methylation in the CpG, CHG, and CHH contexts from the start and end of different types of sequences: CENH3 domains (magenta), *Tyba* repeats (green), genes (grey line), LTRs (yellow-green), and TEs (orange). ChIP-seq signals are shown as log2 (normalized RPKM ChIP/input). Grey boxes highlight the modification enrichment over the body of each sequence type. **(d)** Z-score of the overlapped CO numbers with different (epi-)genetic features to simulations of randomly distributed COs. Positive z-score indicates that COs overlap with H3K4me3 and genes more frequent than expected under the hypothesis of random distributed COs. Negative z-score implies the contrary. The higher of the absolute value of z-score, the more deviation is observed. **(e)** Within genic regions CO frequency (blue line) was higher at promoter regions or after the TTS, but lower at gene bodies, independent of marker density (grey line). **(f)** Within CENH3 domains (left) and *Tyba* arrays (right) CO frequency is reduced, despite a high marker density. **(g)** Relative distance of CO positions to the end of left and to the start of the right CENH3 domain (left) or *Tyba* array (right). The median of CO resolution 334 bp and the mean is about 2 Kb. Correlation done from 63 F1 recombinant offspring and 378 COs. Magenta-bordered and green-filled triangles represent CENH3 and *Tyba* repeat arrays, respectively. **(h)** Zoomed-in view of one of the five COs placed within a region containing CENH3-positive chromatin and *Tyba* repeats. CO resolution in this case   is 200 bp. The CO is indicated by the grey dashed line showing the haplotype switch (blue to orange) in the Marker density track. **(i)** Model for CO formation at broad- and fine-scale.

Spatial-temporal dynamics of chromosome pairing and synapsis explain the broad-scale recombination landscape

As the broad-scale CO distribution did not correlate with any (epi)genetic feature in *R. breviuscula*, a mechanism is still needed to explain the primary force driving the U-shaped recombination landscape observed. We hypothesised that pairing and synapsis progression might contribute to shaping CO frequencies in *R. breviuscula*. To investigate this, we performed immunolocalization with antibodies against ZYP1, ASY1, HEI10 and fluorescence in situ hybridisation (FISH) for telomeres on meiocytes. When combining ZYP1, ASY1 and telomere probes, we observed a tendency for telomeric signals to cluster together in one location, forming the typical "bouquet" (Blokhina et al., 2019; Niwa et al., 2000). In the proximity of this structure, we see the ZYP1 signal, representing synapsed chromosomes elongating from the telomeres until they reach the area of the nucleus that is not yet synapsed. Here, the linear signal of ASY1 was still present and represents unpaired chromosomes (Figure 10a, Supplementary Figure 2). When we combined telomeric probes with ZYP1 and HEI10, we saw that the first synapsed regions (ZYP1-stained) were also first loaded with HEI10 in the proximity of chromosome ends, exhibiting a high-intensity linear signal (Figure 10b-c). We consistently observed few telomeres that did not participate in the bouquet, coming from the terminal ends of chromosome 1 and 2 that harbour the *35S rDNA* loci; instead, these regions localized at the nucleolus (Figure 10a, Supplementary Figure 3). Remarkably, the nucleolar-positioned telomeres showed a delayed ZYP1 loading, which in many cases did not happen at all, compared to the telomeres involved in the bouquet (Figure 10b, d). Thus, the broad-scale

recombination landscape in *R. breviuscula* is better explained by early synapsis and HEI10 loading on the terminal regions of paired chromosomes rather than by any association with a centromere effect or (epi)genetic features (Figure 9i).

Discussion

Deciphering the mechanisms controlling CO formation and distribution is key to understand a main driving force for genetic diversity in eukaryotes: meiotic recombination. By combining comprehensive immunocytochemistry, chromatin, and *in silico* analyses of recombination dynamics in *R. breviuscula*, our data provide solid evidence for the role of a telomere-guided pairing (including HEI10 loading dynamics) as a major factor shaping the meiotic recombination pattern in *R. breviuscula*.
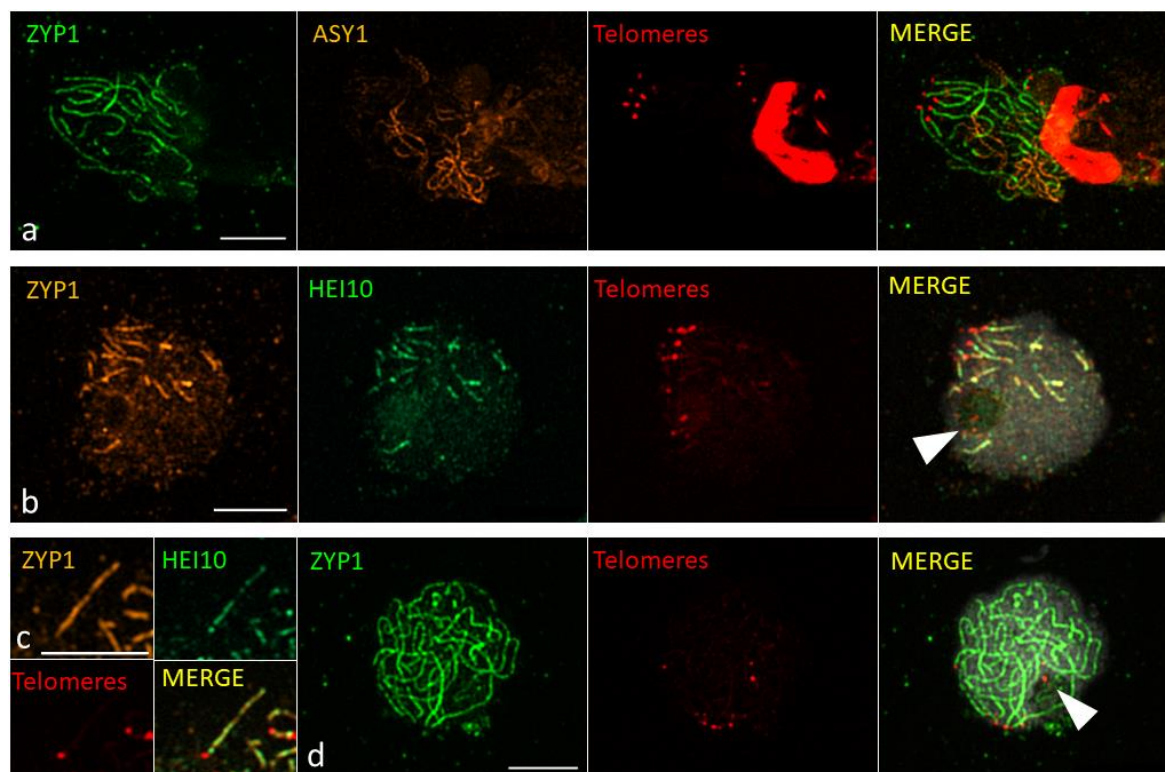
Figure 10

Immunolocalization of ZYP1, ASY1, HEI10 and telomeres. **(a)** Telomeres (red) cluster in a bouquet on one side of the cell, where ZYP1 (green) elongates as the SC is being assembled. ASY1 (orange) represents unpaired chromosomes not yet reached by ZYP1. **(b)** As ZYP1 (orange) lines elongate from telomeres, HEI10 (green) is quickly loaded onto paired chromosomes, while some telomeres (red) are at the nucleolus (white arrow), without ZYP1 and HEI10 signal. **(c)** Detail of synapsis progression: as soon as the SC (orange) is assembled, HEI10 (green) is loaded. **(d)** In late pachytene, ZYP1 (green) occupies the whole chromosomal length, and telomeres (red) are still clustered in the bouquet or at the nucleolus (white arrow). Scale bar= 5 μm.

In the new era of genomics, haplotype-phased genomes are routinely available. By applying high-throughput single-cell RNA-sequencing to individual pollen nuclei, we provide a powerful pipeline that can be used to investigate CO frequencies in any available gamete of any heterozygous individual with an available phased genome. Using haplotype-specific markers, we detected and mapped CO events from thousands of gametes for the first time in a species with repeat-based holocentromeres. Unexpectedly, recombination rates were not homogeneously distributed along the chromosomes of *R. breviuscula*, as one might expect from the absence of chromosome compartmentalization and the uniform distribution of (epi)genetic features (This study, Hofstatter et al., 2022). Instead, we mainly observed regions of higher recombination frequencies (recombination domains) at distal chromosomal regions, resulting in a U-shaped distribution of COs, similarly to most eukaryotes, including the holocentric *C. elegans* (Haenel et al., 2018; Rockman & Kruglyak, 2009; Saito & Colaiácovo, 2017). A recent study in *A. thaliana* showed that the Mb-scale CO landscape is associated with several (epi)genetic marks beyond a centromere effect, with open chromatin state showing the highest positive correlation with CO formation (Lian et al., 2022). In contrast, we could only link CO formation with centromere and (epi)genetic features at a very fine scale.

It is remarkable that despite the absence of broad-scale correlation of COs and (epi)genetic features distribution, the similar epigenetic regulation of individual centromeric-units in *R. breviuscula* as in monocentric species (This study; Hofstatter et al., (2022); Naish et al., (2021)), points to an evolutionarily conserved CO control mechanism at local scale. Notably, COs within genic regions were preferentially formed at promoter regions compared to neighbouring transcribed gene bodies. This seems to be true for several eukaryotes and may be related to open chromatin states (Lian et al., 2022; Zelkowski et al., 2019). In contrast, the miniature centromere effect found in *R. breviuscula*, which seems to prevent COs only inside centromeres, but not in their vicinity, is likely due to the closed chromatin state of centromeric units, marked by high DNA methylation. Our findings provide robust evidence for an evolutionary conserved centromere effect that, in association with (epi)genetic factors, affects CO patterning at local scale, independently of chromosome organization. By using a holocentric species like *R. breviuscula,* where centromere-effect or a compartmentalized chromosome organization are absent and cannot mask underlying factors affecting CO patterning, we revealed important mechanistic insights about evolutionarily conserved CO control.

We determined that the broad-scale U-shaped recombination landscape is mostly explained by the telomere-led pairing and synapsis as demonstrated by our combined immunostaining and telomeric-FISH approach. This result is consistent with the bouquet formation reported in many organisms, where synapsis and DNA double-strand breaks (DSBs) required for COs are mostly initiated from the telomeres (Blokhina et al., 2019; Niwa et al., 2000). Such telomere-led processes have already been proposed to influence the location of COs to be more likely at chromosome ends than in central regions (Haenel et al., 2018). Considering the level of conservation of bouquet formation and synapsis progression observed in *R. breviuscula*, and the position of high- and low- recombination domains, we propose that pairing itself, and possibly the observed telomere-led HEI10 loading dynamics, is the driving forces that shapes its recombination landscape. In fact, we observe that HEI10 is progressively loaded as chromosomes synapse from telomeres (Figure 10, Supplementary Figure 2). This early loading at ends might create a bias that increases CO rates at distal regions of chromosomes, whether or not a centromere is present. Recently, a "coarsening" model for the behaviour of HEI10 has been proposed. In this model, an enriched loading of HEI10 at chromosome ends, following the beginning of synapsis, decreases the gap between predicted and observed data in *A. thaliana*. As an abundance of loaded HEI10 accounts for an increased coarsening over time, early loading at chromosome ends would accelerate the maturation of recombination intermediates, compared to the interstitial regions of the chromosomes (Morgan et al., 2021; L. Zhang et al., 2021). These findings are even more remarkable knowing that by combining HEI10 overexpression and removal of the synaptonemal complex, the overall CO landscape did not change despite the massive increase in COs (Durand et al., 2022), suggesting that CO landscape is driven by mechanistic properties of meiotic chromosome pairing rather than synapsis. Thus, a telomere-led pairing initiation model could explain why COs mostly occur near the chromosome ends (Fozard et al., 2023; Rockmill & Roeder, 1998; Zickler & Kleckner, 2015).

We observed a gradual reduction on CO rates from the regions very adjacent to telomeres in *R. breviuscula*. Similar to the centromere effect, a telomere effect is proposed to be common across eukaryotes (Brazier & Glémin, 2022; Haenel et al., 2018) and might be explained by the recent proposed model for CO designation, i.e., the coarsening model. We hypothesise that, as pairing and synapsis proceed from telomeres and finally involve the whole length of the chromosomes, recombination intermediates are affected by the coarsening coming from both ends. Therefore, eventual recombination intermediates at telomeres will be less subject to the effect of the coarsening compared to more internal COs. Next, interstitial regions will be negatively affected

by the coarsening bias of distal regions, and will have reduced CO rates. Finally, the phenomenon of CO interference further lowers the recombination frequencies at the centre of the chromosomes, because the distal regions have already been designated for COs. These phenomena likely determine the U-shaped recombination landscape of *R. breviuscula*. The model that we just described explains the behaviour of chromosomes 3, 4 and 5. The *35S rDNA*-harbouring distal regions of chromosomes 1 and 2, however, do not participate in the bouquet formation as they stay at the nucleolus. Remarkably, these two chromosomal ends are also characterized by the lowest recombination frequencies. In the model plant *A. thaliana*, it has been proposed that ribosomal DNA is not involved in synapsis and recombination, and these regions are localized at the nucleolus (Kuttig et al., 2022; Sims et al., 2019). Indeed, we observed that these telomeres located at the nucleolus were involved later in synapsis compared to those that clustered in the bouquet. This late involvement in synapsis means a potential delay in DSBs formation and HEI10 loading, which is consistent with the lower recombination frequency observed at the *35S rDNA*-harbouring ends of chromosomes 1 and 2.

The lack of information about the spatio-temporal dynamics of DSB formation during early meiosis in *R. breviuscula* makes it difficult to assess whether DSB distribution biased by telomere-led pairing may have an effect on CO distribution. Such experiments have been performed only in a single study in *A. thaliana*, which showed a good correlation with the overall CO landscape (Choi et al., 2018).

Acknowledgments

Author contributions

AM conceived the research idea and coordinated the analyses. MC performed all cytogenetic analyses and microscopy. MC performed pollen nuclei isolation, sorting and sequencing libraries with assistance from JC. MZ performed all single-cell RNA sequencing and recombination-related analyses with assistance from HS. GT performed ChIP-seq analysis. YMS performed immuno-FISH analysis. TL and KFXM performed gene annotation and GO term enrichment analysis. MM operated the FACS machine. BH performed all sequencing. KS

supervised the single-cell analysis. MC, MZ, and AM wrote the first manuscript draft with input from all authors. All authors agreed with the last manuscript version.

Competing interests

The authors declare no competing interests.

Materials & Methods

DNA isolation of pollen nuclei, 10x sc-RNA-seq library preparation and sequencing

Protocols were adapted from Campoy et al. (2020). Briefly, to release pollen grains, anthers from fully developed flowers of *R. breviuscula* and *R. tenuis* (for multiplex purposes) were harvested and submerged in woody pollen buffer (WPB, Loureiro et al., 2007). Nuclei were extracted using a modified bursting method. The solution containing pollen grain was pre-filtered with a 100-µm strainer and pollen was crushed on a 30-µm strainer (Celltrics™). Isolated nuclei were gathered in WPB. Nuclei were stained with DAPI at 1 ug/ml and sorted on a BD FACSAria Fusion sorter with a 70µm nozzle and 483 kPa sheath pressure. A total of 10,000 nuclei were sorted into 23 µl of sheath fluid solution subsequently loaded into a 10x™ Chromium controller according to the manufacturer's instruction. A library was created according to the chromium single cell 3′ protocol. A CG000183 Rev A kit from 10x Genomics was used for the library preparation. The library was deep-sequenced (100 Gb) with an Illumina NOVAseq instrument in150bp paired-end mode.

Whole genome sequencing (WGS) of F1 recombinant offspring

In order to obtain a recombinant population of *R. breviuscula* plants, we bagged young inflorescences of our heterozygous reference *R. breviuscula* to force self-pollination. Due to its high self-incompatibility, we only obtained a total of 63 F1 plants that were sequenced at 3x coverage (~2 Gb) with Illumina HiSeq300 in 150 bp paired-end mode.

Anther fixation and immunocytochemistry

Immunostaining was performed as described by Cabral et al. (2014), with some modifications. Anthers of *R. breviuscula* were harvested and fixed in ice-cold 4% (w/v) paraformaldehyde (PFA) in phosphate buffered saline (PBS) solution (pH 7.5, 1.3 M NaCl, 70 mM Na2HPO4, 30 mM NaH2PO4) for 90min. Anthers were separated according to their size and were dissected to release the meiocytes onto glass slides. Meiocytes were squashed with a coverslip that was later removed with liquid nitrogen. Slides were stained with mounting solution (Vectashield +

0.2 µg DAPI) in order to select the meiotic stages of interest. Slides were then blocked with 3% (w/v) bovine serum albumin (BSA) in PBS + 0.1% (v/v) Triton X-100 for 1 hour at 37 °C. The antibodies used were anti-AtASY1 raised in rabbit (inventory code PAK006) (Armstrong et al., 2002), anti-AtMLH1 raised in rabbit (PAK017) (Chelysheva et al., 2010) and anti-RpCENH3 raised in rabbit (Marques et al., 2015). The anti-ZYP1 was raised in chicken against the peptide EGSLNPYADDPYAFD of the carboxyl-terminus of AtZYP1a/b (Gene ID: AT1G22260/AT1G22275) and affinity-purified (EUROGENTEC) (PAK048). The anti-RpREC8 was a combination of two antibodies raised in rabbit against the peptides CEEPYGEIQISKGPNM and CYNPDDSVERMRDDPG (Gene ID: RP1G00316120/RP2G00915110/RP4G01319620/RP5G01638170) and affinity-purified (Eurogentec). The anti-RpHEI10 was a combination of two antibodies raised in rabbit against the peptides CNRPNQSRARTNMFQL and CPVRQRNNKSMVSGGP (Gene ID: RP3G01271190/RP3G01008630/RP1G00269340/RP2G00699130) and affinity-purified (Eurogentec). Each primary antibody was diluted 1:200 in blocking solution. Slide-mounted samples were incubated with primary antibodies overnight at 4 °C. Slides were washed three times for 10min with PBS + 0.1% (v/v) Triton X-100. Samples were incubated with secondary antibodies for 2h at room temperature. Secondary antibodies were conjugated with Abberior STAR ORANGE or Abberior STAR RED (1:250, Abberior). Slides were washed again three times for 10min with PBS + 0.1% (v/v) Triton X-100 and allowed to dry. Samples were then prepared with 10 µl of mounting solution (Vectashield + 0.2 µg DAPI). Specimens were covered with a coverslip and sealed with nail polish for storage. Images were taken with a Zeiss Axio Imager Z2 with Apotome system for optical sectioning, or with a Leica Thunder Imager DMi8 with Computational Clearing. Images were deconvolved and processed with Zen 3.2 or LAS X softwares.

Sequential immunostaining and fluorescence *in situ* hybridization

Immuno-FISH was performed following Baez et al. (2020). Good quality slides obtained from immunostaining, as described above, were selected for fluorescence *in situ* hybridization (FISH) using a telomeric probe. The slides were washed with 1x PBS for 15min, fixed in 4% paraformaldehyde in 1xPBS for 10min, dried with 70% and 100% ethanol (v/v) for 5 minutes each and then probed with a direct-labelled telomeric sequence (Cy3-[TTTAGGG]$_5$; MilliporeSigma). The hybridization mixture contains formamide 50% (w/v), dextran sulphate 10% (w/v), 2× SSC and 50 ng/µl of telomeric probe. The slides were denatured at 75 °C for 5min. Stringency washes were performed following Braz et al. (2020) to give a final stringency

of approx. 72%. The slides were counterstained with 10 µl of mounting solution (Vectashield + 0.2 µg DAPI). Images were captured as described above.

Mitotic and meiotic chromosome spreads were performed as in Ruban et al. (2014), with some modifications. Briefly, tissue samples were fixed in 3:1 (ethanol: acetic acid, [w/v]) solution for 2 hours with gentle shaking. The samples were then washed with water twice for 5min and treated with an enzyme mixture (0.7% cellulase R10, 0.7% [w/v] cellulase, 1.0% [w/v] pectolyase, and 1.0% [w/v] cytohelicase in citric buffer) for 30min at 37 °C. The material was then immersed in freshly prepared 60% (v/v) acetic acid and samples were dissected on slides under a binocular microscope. The slides were then placed on a hot plate at 50 °C and the samples were spread by hovering a needle over the drop of acetic acid without touching the slide. After spreading the cells, the fixation was completed by dropping fresh 3:1 (v/v) fixative on the slides and immersing them in 60% (v/v) acetic acid for 10min. Slides were dehydrated in 100% ethanol and air-dried, ready for future applications.

Box Plots and Statistical Analyses

Box plots for HEI10 and MLH1 foci counting and relative statistics were carried out as described in Chapter 3 (See below).

Haplotype phasing and scaffolding

A phased chromosome-level genome of *R. breviuscula* was assembled using PacBio HiFi and Hi-C data available from Hofstatter et al. (2022) under the NCBI Bioproject no. PRJNA784789. First, a phased primary assembly was obtained by running Hifiasm (Cheng et al., 2021) using as input the 30 Gb of PacBio HiFi reads (~35x coverage per haplotype) in combination with Dovetail Omni-C reads, using the following command: hifiasm -o Rbrevi.phased.asm.hic --h1 hic.R1.fastq.gz --h2 hic.R2.fastq.gz hifi.reads.fastq.gz. The phased assemblies of each individual haplotype were further scaffolded in chromosome scale using Salsa2 (Ghurye et al., 2019), followed by successive round of manual curation and re-scaffolding. Genome sizes of haplotypes 1 and 2 are 418,624,405 bp and 390,890,712 bp respectively. Both haplotypes comprise five chromosomes with a length of ~370 Mbp in total and other unplaced sequences (Supplementary Table 1).

Definition of allelic SNPs as genotyping markers on the phased reference genome

To define genotyping markers for *R. breviuscula*, we first mapped all available (NCBI Bioproject no. PRJNA784789) raw WGS Illumina HiSeq3000 150 bp paired-end reads (25,899,503,075 bases, ~54x coverage) to the five pseudochromosome scaffolds in haplotype

1 of the phased reference genome with bowtie2 (v2.4.4) (Langmead & Salzberg, 2012). The alignment file was further sorted with SAMtools (v1.9) (Danecek et al., 2021). Next, the alignments of short reads to reference genome were used for SNP calling by 'bcftools mpileup' and 'bcftools call' (v1.9) (Danecek et al., 2021) (with --keep-alts, --variants-only, and --multiallelic-caller flags enabled). 1,404,927 SNPs excluding indels were derived in total. In order to distinguish two haplotypes using these SNPs, we only chose allelic SNPs as markers for genotyping. Therefore, we collected variant information such as mapping quality, alternative base coverage, and allele frequency resulting from SHOREmap conversion (v3.6) (Schneeberger et al., 2009) that converts SNP files (.vcf) into a read-friendly, tab-delimited text file. A final set of 820,601 alleles fulfilling certain thresholds (mapping quality > 50; $5 \leq$ alternative base coverage ≤ 30, $0.4 \leq$ allele frequency ≤ 0.6) was selected as markers (Figure 6b; Supplementary Figure 4).

Pre-processing single-cell RNA sequencing data from pollen nuclei

Raw scRNA-seq data usually include barcode errors and contaminations such as doublets and ambient RNA. Thus, cell barcodes (CBs) were firstly corrected by 'bcctools correct' (v0.0.1) based on 10X v3 library complete barcode list with options "--alts 16 --spacer 12" because of the 16-bp CB and 12-bp unique molecular identifier (UMI). After correction, 952,535 viable CBs were observed. This step also truncated CBs and UMIs from every pair of scRNA-seq reads. After counting the occurrence of CBs, we obtained the number of read pairs for each CB. To ensure a sufficient amount of reads for SNP calling, only CBs appearing more than 5,000 times were used for subsequent analyses. Finally, each CB was seen as one viable cell, and reads with corresponding CB were assigned to this cell (demultiplexing). 8,001 (0.84% of corrected CBs) viable cells were identified in the end with 365,771,748 (77.25% of all raw scRNA-seq) read pairs included.

Alignment of single-pollen RNA sequences to genome and deduplication

To find genotyping markers in *R. breviuscula* gametes, we firstly mapped scRNA reads of pollen nuclei to haplotype 1 chromosomes (Figure 6b) by hisat2 (v2.1.0) (Kim et al., 2019). Specifically, each cell-specific pair of reads was merged as one single-end FASTQ file, and hisat2 was run under single-end mode (-U) because the SNP-calling approach does not detect SNPs on reads whose mated reads are not mapped. Before further analyses of the alignment results, UMIs were extracted from the read alongside the CBs; hence, a fast UMI deduplication

tool, UMIcollapse (Liu, 2019), was employed to remove the PCR duplicates by collapsing reads with the same UMIs.

The sequencing library was prepared for mixed pollen nuclei of *R. breviuscula* and *R. tenuis* to enable multiple-potential analyses, necessitating a species discrimination step. We achieved this by a straightforward approach without gene expression profiling: for each cell, a) the DNA sequences were mapped to both the *R. breviuscula* and *R. tenuis* chromosomal genomes; and b) the alignment rates between the two species were compared to decide the cell identity (Supplementary Figure 5). Since the alignment rates across cells to *R. breviuscula* and *R. tenuis* were both bimodal distributions (Supplementary Figure 5A-B), it was feasible to group these cells solely based on mapping rates. It was estimated that 4,733 cells were from *R. breviuscula* and 2,709 cells were from *R. tenuis* (Supplementary Figure 5C) based on alignment fractions. The remaining 559 cells presented very similar alignment rates, which were potential doublets. Among the 4,733 *R. breviuscula* cells, we discarded those whose alignment rates were lower than 25% so 4,392 cells from *R. breviuscula* were viable for the next stage of the analysis.

SNP calling and selection of GMGs across gametes

SNP calling in all gametes adopted the same methods as reference genome SNP calling, i.e., via 'bcftools mpileup' and 'bcftools call' (v1.9), with the difference that no "--variants-only" flag was applied. After acquiring SNPs for every gamete, we extracted SNP positions, allele counts of reference, and alternative bases through 'bcftools query'. Next, comparing SNPs in every gamete with markers defined on reference resulted in reliable genotyping markers in this gamete.

However, not all cells were viable for CO calling due to insufficient markers or doublets generated during the 10X library construction. Hence, filtering is necessary before calling COs. We first discarded 2,338 cells with less than 400 markers to ensure accurate genotyping by sufficient markers. To remove doublets, we estimated the times of switches of marker genotypes across the remaining 2,054 cells. Cells with frequent switches, i.e., a switching rate (genotype switching times/number of markers) greater than 0.07, were taken as doublets (Supplementary Figure 5E). Ultimately, 402 doublets were found, with the remaining 1,652 cells proving suitable for subsequent CO calling.

CO identification

Genotyping of chromosomes was performed by adapting the haplotype phasing method proposed by Campoy et al. (2020)Campoy et al. (2020). Since the original approach was

designed based on a scDNA-seq library, which is commonly used to examine more SNPs than scRNA-seq data, we adjusted the smoothing function and parameters to define genotypes of genomic blocks accordingly. Specifically, markers were firstly smoothed by neighbouring markers (two ahead and two behind) based on allele frequency and then on presence of genotypes. After smoothing, genotype blocks containing at least five markers within 1 Mb length were qualified to assign genotypes. The genomic regions that saw the conversion of genotypes at flanks were taken as CO break positions (Figure 6c-d). In the end, we counted CO numbers in each cell and manually checked and corrected those with double COs.

Recombination landscape and CO interference

In order to have an overview of CO rates across the chromosomes of *R. breviuscula*, we summarised crossover positions in all viable cells (1,641 cells remaining after manual correction) and plotted the recombination landscape for each chromosome (Figure 7a). Recombination rate (cM/Mb) was computed by 1Mbp sliding window and 100kbp step size.

$$Recombination\ rate = \frac{Number\ of\ COs\ within\ This\ Window * 100 * 1M}{Number\ of\ Cells * Window\ Size}$$

To plot genetic linkage map (Figure 7b), we extracted 743 markers from 820,601 reference markers by selecting the median marker within each 500Kb sliding window (step size also 500Kb) from the first present marker until the last. CO interference was analysed with MADpattern (v.1.1) (L. Zhang et al., 2014), using 1,641 confident singleton pollen nuclei. Chromosome 1 was divided into 18 intervals and chromosomes 2-5 were divided into 15 intervals to compute the mean coefficient of coincidence (CoC) of every pair of intervals.

F1 offspring mapping and CO analysis

63 F1 offspring were reproduced from selfed *R. breviuscula*. Each F1 plant was sequenced with ~3X Illumina WGS data. To genotype F1 offspring, WGS Illumina sequences of each plant were firstly mapped to rhyBreHap1 reference genome with bowtie2 (v2.4.4) paired-end mode, then SNPs were called by 'bcftools mpileup' and 'bcftools call' (v1.9) (with --keep-alts, --variants-only, and --multiallelic-caller flags enabled). Next, SNPs of each F1 sample were input to TIGER (Rowan et al., 2015) for genotyping and generating potential CO positions. In addition, RTIGER (Campos-Martin et al., 2023) was also used to identify the genotypes of chromosomal segments by utilizing the corrected markers resulted from TIGER. Only the COs that agreed by both tools were kept. Recombination landscape from F1 COs were plot using the same strategy and sliding window as illustrated for pollen nuclei.

ChIP

CENH3 ChIP-seq data was obtained from Hofstatter et al. (2022). Further ChIP-experiments were performed for H3K4me3 (rabbit polyclonal to Histone H3 tri-methyl K4, Abcam ab8580), H3K9me2 (mouse monoclonal to Histone H3 di-methyl K9, Abcam ab1220), H3K27me3 (mouse monoclonal to Histone H3 tri-methyl K27, Abcam ab6002), and IgG control (recombinant rabbit IgG, monoclonal Abcam ab172730) using the same protocol described in Hofstatter et al. (2022).

ChIP-seq and analysis

ChIP DNA was quality-controlled using the NGS-assay on a FEMTO-pulse (Agilent Technologies). An Illumina-compatible library was prepared with the Ovation Ultralow V2 DNA-Seq library preparation kit (Tecan Genomics) and sequenced as single-end 150-bp reads on a HiSeq 3000 (Illumina) instrument. For each library, an average of 20 million reads were obtained.

Raw sequencing reads were trimmed by Cutadapt (Martin, 2011) to remove low-quality nucleotides (with quality score less than 30) and adapters. Trimmed ChIPed 150-bp single-end reads were mapped to the respective reference genome with bowtie2 (Langmead & Salzberg, 2012) with default parameters. All read duplicates were removed and only the single best matching read was kept on the final alignment BAM file. BAM files were converted into BIGWIG coverage tracks using the bamCompare tool from deeptools (Ramírez et al., 2016). The coverage was calculated as the number of reads per 50-bp bin and normalized as reads per kilobase per million mapped reads (RPKM). Magnified chromosome regions showing multiple tracks presented in Figure 9b was plotted with pyGenomeTracks (Lopez-Delisle et al., 2021).

***Tyba* arrays and CENH3 domains annotation**

Tyba repeats were annotated using BLAST search with a consensus *Tyba* sequence allowing a minimum of 70% similarity. Further annotation of *Tyba* arrays was performed by removing spurious low-quality *Tyba* monomer annotations shorter than 500 bp. We merged with bedtools (Quinlan & Hall, 2010) all adjacent *Tyba* monomers situated at a maximum distance of 25 Kb into individual annotations to eliminate the gaps that arise because of fragmented *Tyba* arrays and those with sizes less than 2 Kb were discarded.

CENH3 peaks were called with MACS3 (Y. Zhang et al., 2008) using the broad peak calling mode:

```
macs3 callpeak -t ChIP.bam -c Control.bam --broad -g 380000000 --broad-cutoff 0.1
```

Identified peaks were further merged using a stepwise progressive merging approach. CENH3 domains were generated by 1) merging CENH3 peaks with spacing distance less than 25 Kb using bedtools to eliminate the gaps that arise because of fragmented *Tyba* arrays or due to insertion of TEs; and 2) removing CENH3 with domain size less than 1 Kb.

Transposable elements annotation

Transposable element protein domains and complete LTR retrotransposons were annotated in the reference haplotype genome by exploiting the REXdb database (Viridiplantae_version_3.0) (Neumann et al., 2019) using the DANTE tool available from the RepeatExplorer2 Galaxy portal (Novák et al., 2020).

Enzymatic Methyl-seq and analysis

To investigate the methylome space in *R. breviuscula*, the relatively non-destructive NEBNext® Enzymatic Methyl-seq Kit was employed to prepare an Illumina-compatible library, followed by paired-end sequencing (2 x 150 bp) on a HiSeq 3000 (Illumina) instrument. For each library, 10 Gb of reads were generated.

We analyzed enzymatic methyl-seq data using the Bismarck pipeline (Krueger & Andrews, 2011) following the standard pipeline described at https://rawgit.com/FelixKrueger/Bismark/master/Docs/Bismark_User_Guide.html. Individual methylation context files for CpG, CHG, and CHH were converted into BIGWIG format and used as input tracks for overall genome-wide DNA methylation visualization with pyGenomeTracks and R plots.

Quantitative correlation of COs and (epi)genetic features

The distribution and accumulation of all the different classes of genetic and epigenetic features were correlated with the distribution of COs. Correlation matrix (Figure 8b) was calculated by pearson correlation coefficient for each pair of all features under 1Mbp smoothing window and 250kbp step size, specifically, mean CO rates, mean GC contents, CENH3 peak density, *Tyba* array density, SNP density, TE density, H3K4me3 RPKM, H3K9me2 RPKM, H3K27me3 RPKM, mean CpG, mean CHG, and mean CHH.

To inspect a possible centromere effect on CO positioning, we calculated the relative distance of 378 COs in our F1 offspring to the closest left and right centromeric unit, i.e., the CENH3 domain and *Tyba* array and normalized all distances to 0-1 such that all neighbouring centromeric units are displayed in the same scale (Figure 9g). Crossover and marker positions over the transcript bodies, CENH3 domain of *Tyba* array were normalized by their distance to

transcript start sites (TSS) and transcript termination sites (TTS), and then count by binning (Figure 9e-f).

In order to see the association of CO designations with a variety of (epi-)genetic features at a local scale, we first counted the number of COs that overlap with CENH3, *Tyba* arrays, genes, TEs, LTRs, H3K4me3 peaks, H3K9me2 peaks, and H3K27me3 peaks by 'bedtools intersect' (v2.29.0). Next, we assigned 378 COs genome-wide at random. The number of COs on each chromosome is the same as the one detected in F1 individuals (i.e., 72 COs on chr1, 69 on chr2, 76 on chr3, 84 on chr4, and 77 on chr5), while the CO break gap length was picked up from the 378 real F1 CO gaps randomly. For each simulation round, these pseudo-COs were overlapped with (epi-)genetic features again with 'bedtools intersect'. Simulations were re-iterated 5000times, and the results were then plotted as the distribution of overlapped CO numbers for each feature (Supplementary Figure 12). Finally, to evaluate the deviation of real overlapped COs with each feature to the expected overlapped CO number under the hypothesis of randomly distributed COs, Z-scores were calculated by the mean values and standard deviations of the simulated number of overlapped CO distribution (Figure 9d).
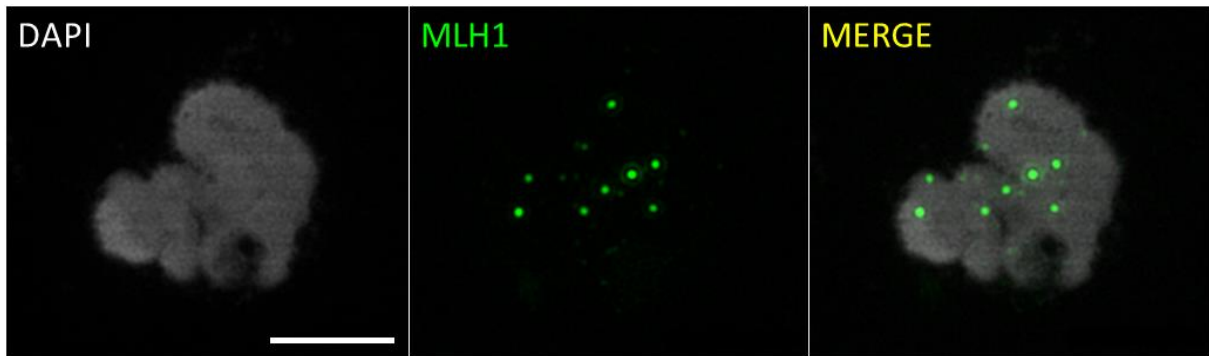
Supplementary Figure 1

Maximum number of MLH1 (green) foci observed in *R. breviuscula* at diplotene. Maximum projection is shown. DNA was counterstained with DAPI. Scale bar = 5 μm.
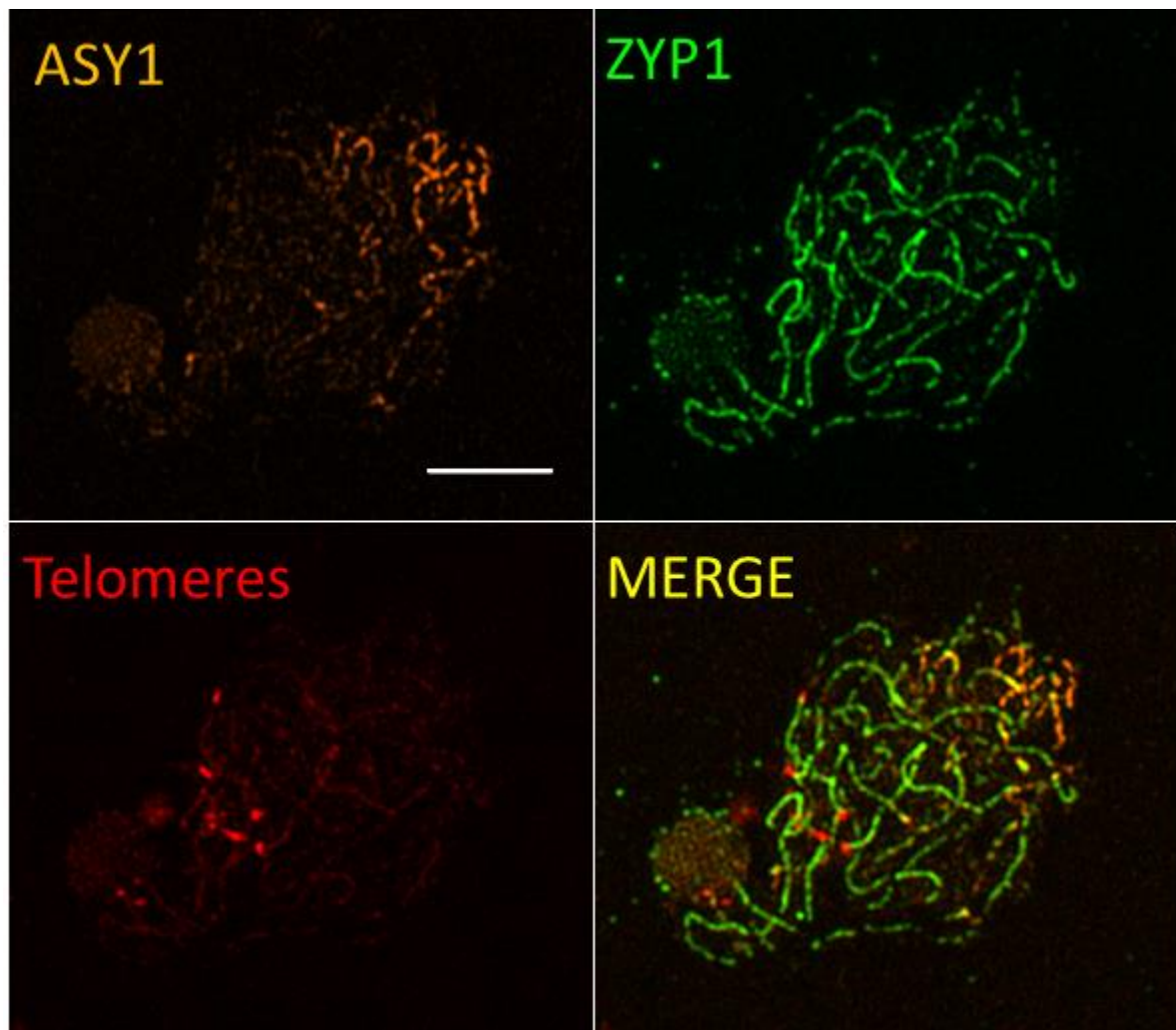
Supplementary Figure 2

Another image of a *R. breviuscula* cell at late zygotene, with immunolocalization of ASY1 and ZYP1 in addition to telomere FISH. Synapsis is almost complete and only a small portion of the cell is still displaying ASY1 signal, meaning unpaired chromosomes. Most of the cell is now covered by the linear ZYP1 signal, representing the synaptonemal complex. Telomeres are clustered in a bouquet on the left side, but some of them are present at the nucleolus. Maximum projection is shown. Scale bar = 5 μm.

| | Merged | DAPI | 35S rDNA | Telomeres |
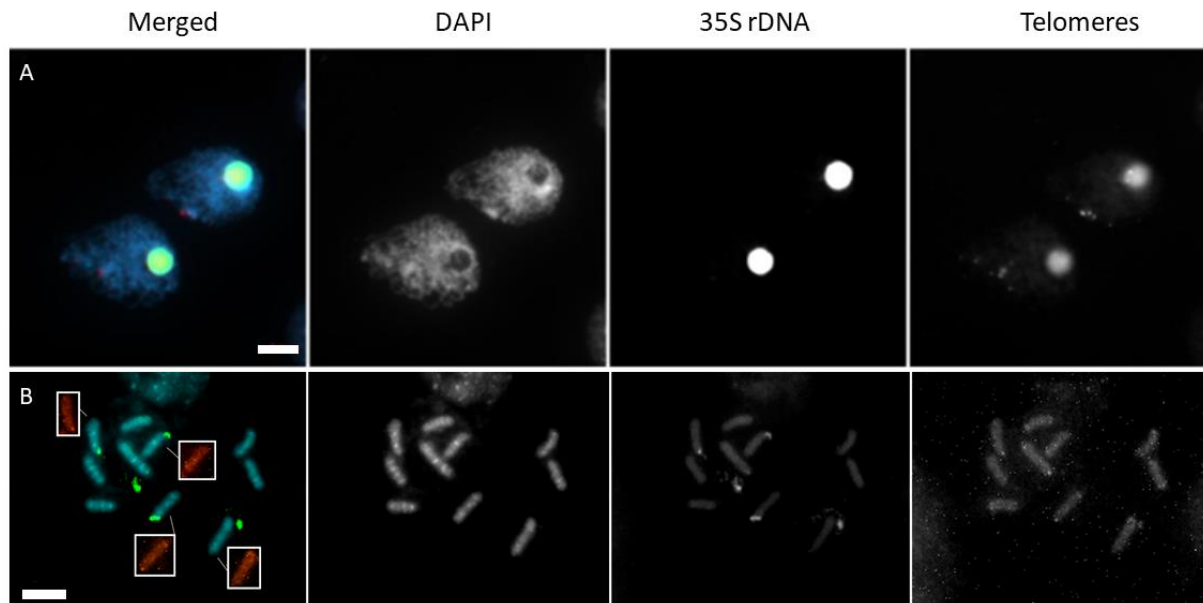
Supplementary Figure 3

FISH with 35S rDNA and telomeric probes in prophase I (**A**) and mitotic metaphase (**B**) in *R. breviuscula*. Telomeres of rDNA-harbouring chromosomes chr1 and chr2 cluster in the nucleolus. Squares in B show telomeric sequences in chromosomes with *35 rDNA*. Maximum projection is shown. Scale bar = 5 µm.

	Haplotype 1	Haplotype 2
Genome assembly size (bp)	418627160	390890803
# Contigs	1637	548
Contig assembly size (bp)	421256472	391742506
Largest Contig (bp)	35313519	43961622
Contig N50 (bp)	11938939	13764201
Contig N90 (bp)	42248	2739863
# Scaffolds	1501	457
Pseudo-chromosome size (bp)	368174147	370478156
Scaffold N50 (bp)	69585868	72168595
Scaffold N90 (bp)	45843	66381717
Largest scaffold / chr 1 (bp)	91632052	89220796
Chromosome 2 (bp)	70953004	72168595
Chromosome 3 (bp)	69585868	69956709
Chromosome 4 (bp)	66447897	66381717
Chromosome 5 (bp)	69555326	72750339
Base accuracy (QV)	30.85	32.32
Completeness (%)	85	85
GC (%)	35.91	35.60

Supplementary Table 1

Summary of genome size, contigs, and scaffolds of phased genome assemblies.

#Structural annotations			
#Variation_type	Count	Length_ref	Length_qry
Syntenic regions	229	329130991	329924075
Inversions	39	2135010	1947035
Translocations	346	3620755	3569626
Duplications (reference)	137	1472557	-
Duplications (query)	249	-	1168366
Not aligned (reference)	650	32783105	-
Not aligned (query)	808	-	33606738
#Sequence annotations			
#Variation_type	Count	Length_ref	Length_qry
SNPs	615883	615883	615883
Insertions	59142	-	2687428
Deletions	59276	3101459	-
Copy gains	87	-	126950
Copy losses	60	394961	-
Highly diverged	5660	172894800	174131686
Tandem repeats	3	482	825

Supplementary Table 2

Synteny and structural variations between two haplotypes of *R. breviuscula*.
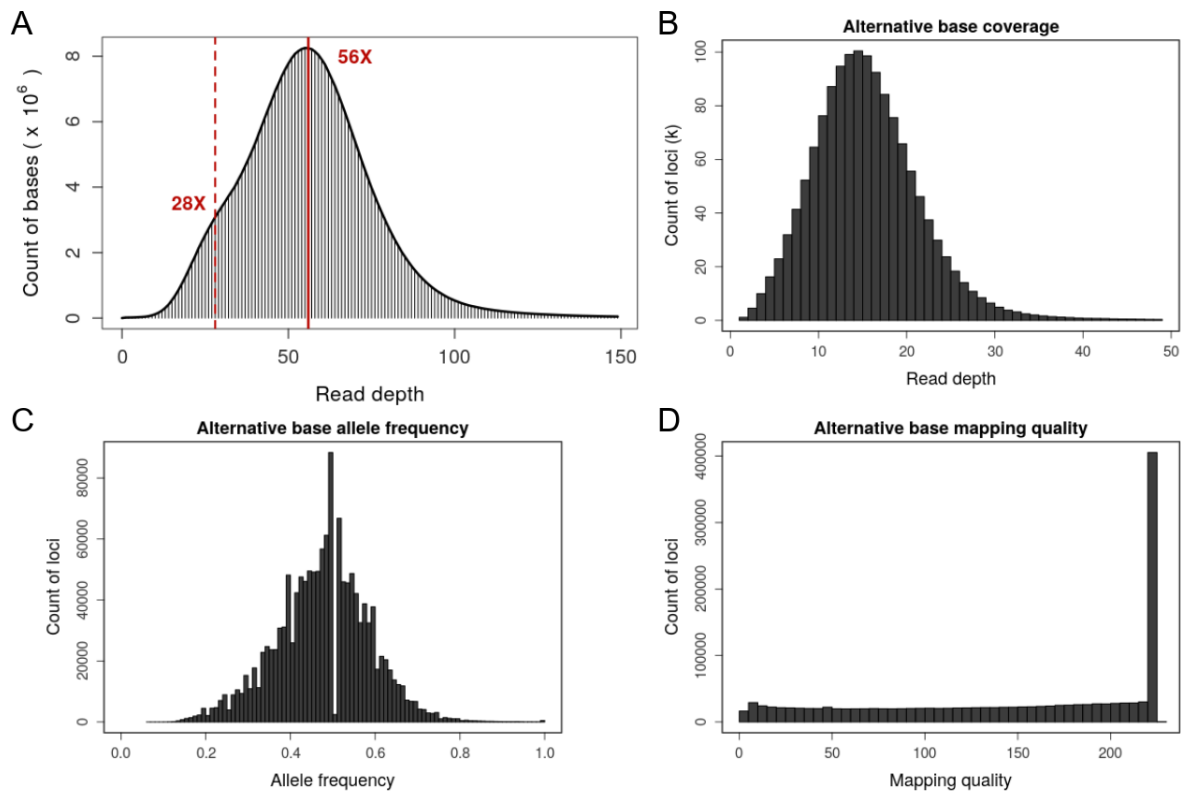
Supplementary Figure 4

Selection of genotyping markers on reference. **(A)** Read depth distribution of Illumina reads mapping to haplotype 1 of *R. breviuscula* phased genome; **(B-D)** Characteristics of alternative bases of SNPs that were called from the alignment mentioned in **(A)**. Genotyping markers on reference were selected according to the distributions of coverage **(B)**, allele frequency (**C**), and mapping quality **(D)** of alternative bases, specifically, an alternative base at a SNP position that met the requirements "5 <= alternative base coverage <= 30, 0.4 <= allele frequency <= 0.6, mapping quality > 50" was an allelic SNP, i.e., a genotyping marker.
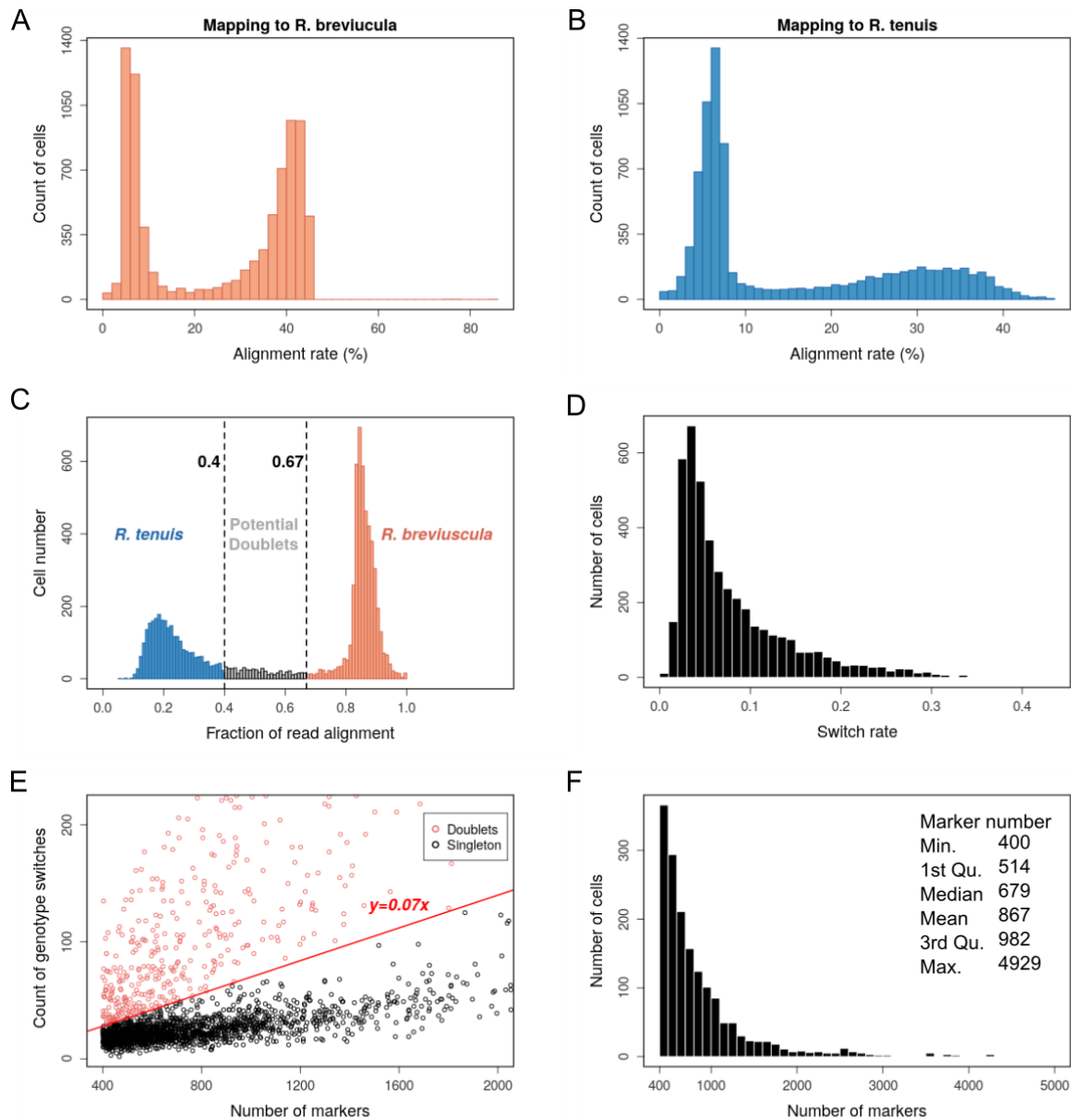
Supplementary Figure 5

Pre-processing of scRNA-seq by splitting *R. breviuscula* from *R. tenuis* cells and removing doublets. **(A-B)** Alignment rate distributions of each read to *R. breviuscula* **(A)** and *R. tenuis* **(B)**. **(C)** Distribution of the fraction of read alignment of each cell to *R. breviuscula* over read alignment to both species, i.e., for a certain cell, fraction = number of reads mapped to *R. breviuscula* / (number of reads mapped to *R. breviuscula* + number of reads mapped to *R. tenuis*). Cells with alignment fraction over 0.67 were potentially from *R. breviuscula*. Those with fraction below 0.4 were potentially from *R. tenuis*. The remaining was doublets. **(D)** Switch rate distribution across *R. breviuscula* pollens. Switch rate of a certain cell was calculated by the number of genotype switches between two consecutive markers over the number of markers in this cell. **(E)** Identification of doublets by switch rates. Cells with switch rate over 0.07 were taken as doublets. **(F)** Number of markers across *R. breviuscula* pollen cells after only keeping cells with high number (>=400) of markers and removing doublets.
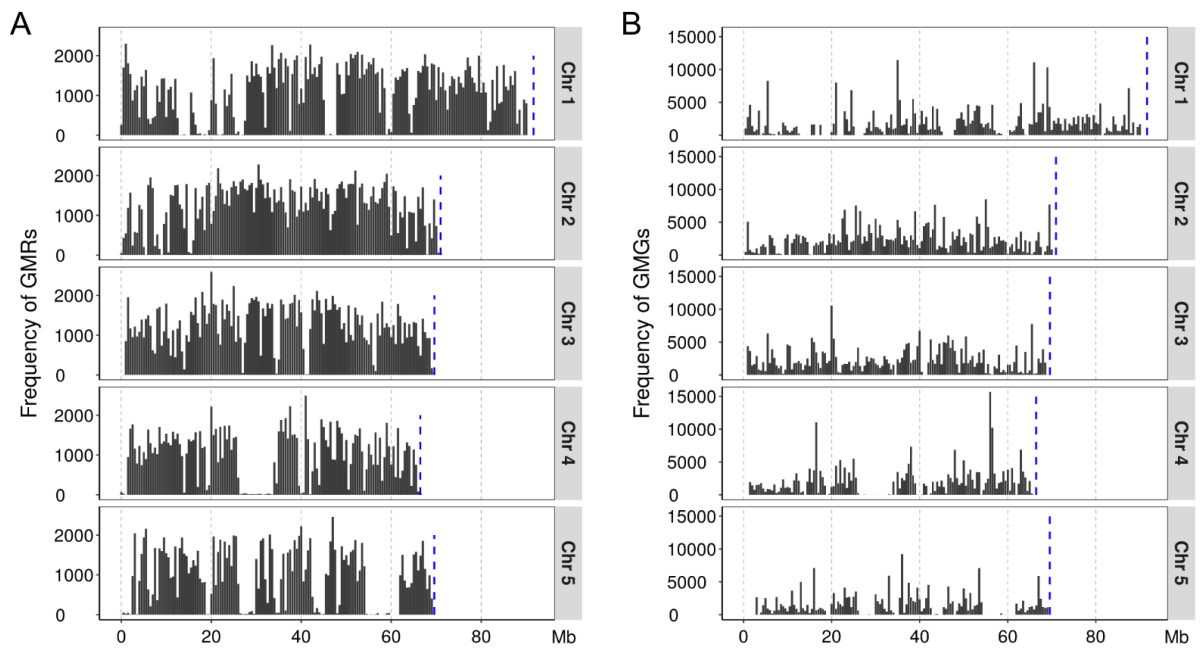
Supplementary Figure 6

Marker distribution on reference and across all viable pollen nuclei. **(A)** Frequency of genotyping markers defined along each chromosome on reference rhyBreHap1. Blue dashed lines show the end of each chromosome. GMR = Genotype Markers on Reference. **(B)** Frequency of all markers across viable pollen nuclei that were used for CO detection. GMG = Genotype Markers on Gametes
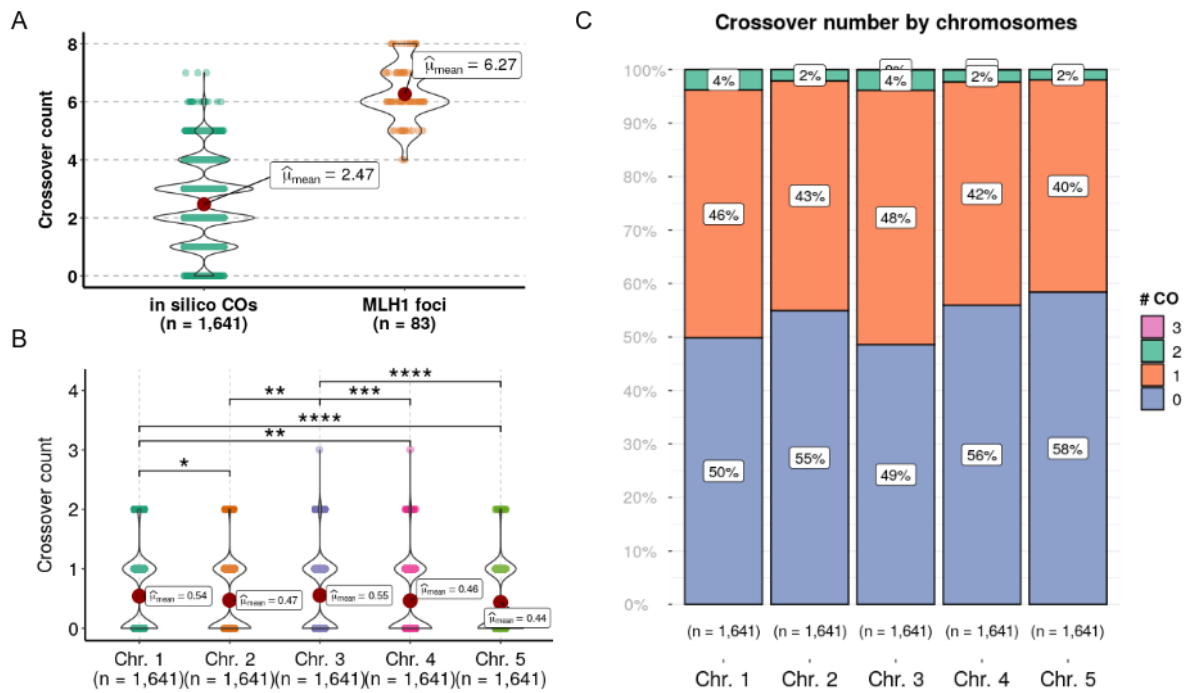
Supplementary Figure 7

Crossover number of all viable pollens. **(A)** Comparison of crossover number detected from scRNA-seq analysis of all 1641 viable pollen nuclei and counts of MLH1 foci by cytological observation. **(B)** Crossover number detected on each chromosome. The mean number of chromosomes on 5 chromosomes is 0.54, 0.47, 0.55, 0.46, and 0.44 respectively. Pairwise differences were compared by Games-Howell test and p-values were adjusted by Holm-Bonferroni method. **(C)** Proportions of CO counts across chromosomes.
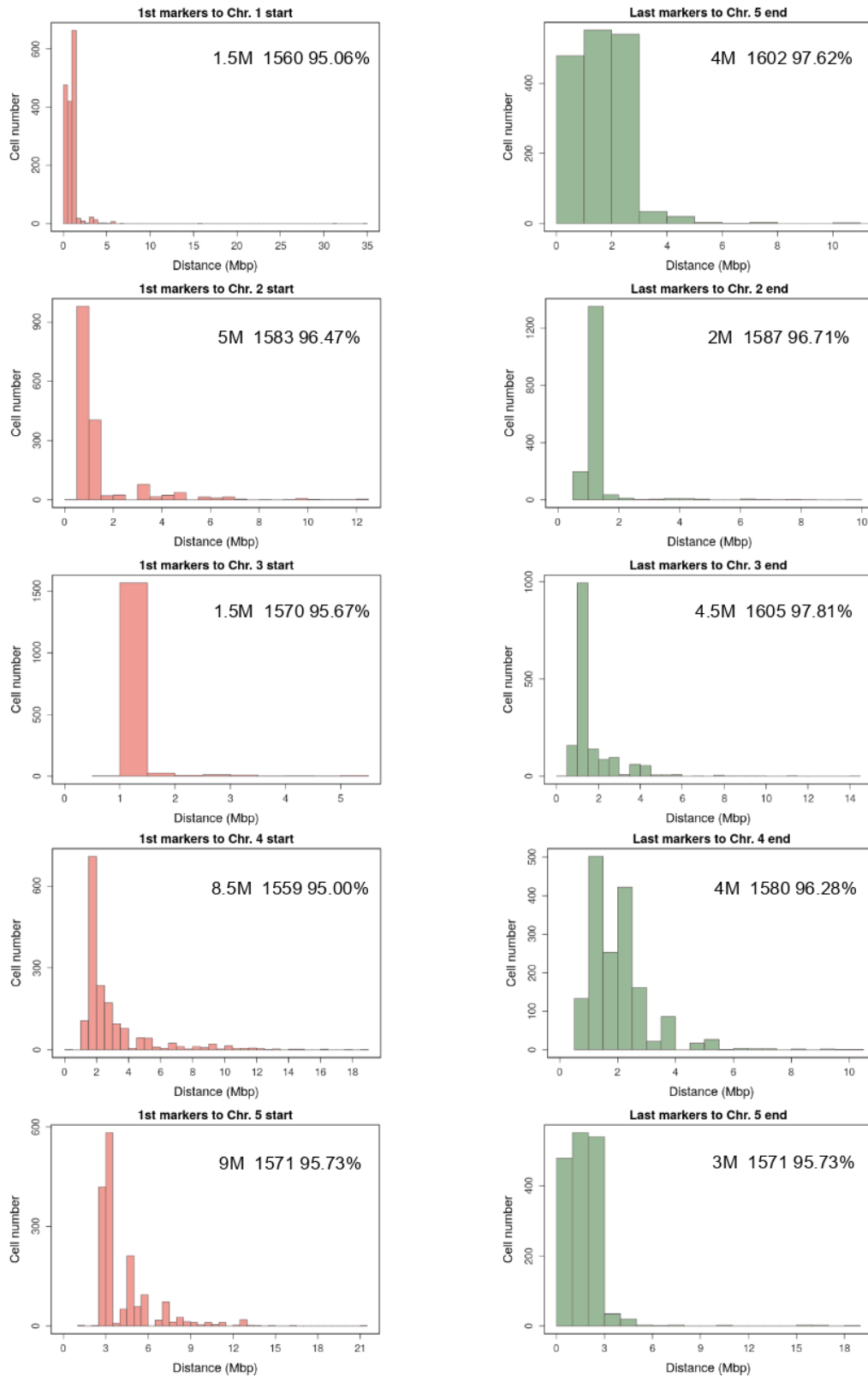
Supplementary Figure 8

Distance distribution of the first markers to chromosome start and the last markers to chromosome ends across all viable pollen nuclei. If the regions where the first or last markers appear cover at least 95% pollens, they are defined as the confident start and end of the recombination landscape. The number on each plot indicates the distance of confident regions to chromosomal ends, the number pollens covered, and the percentage of covered pollens.
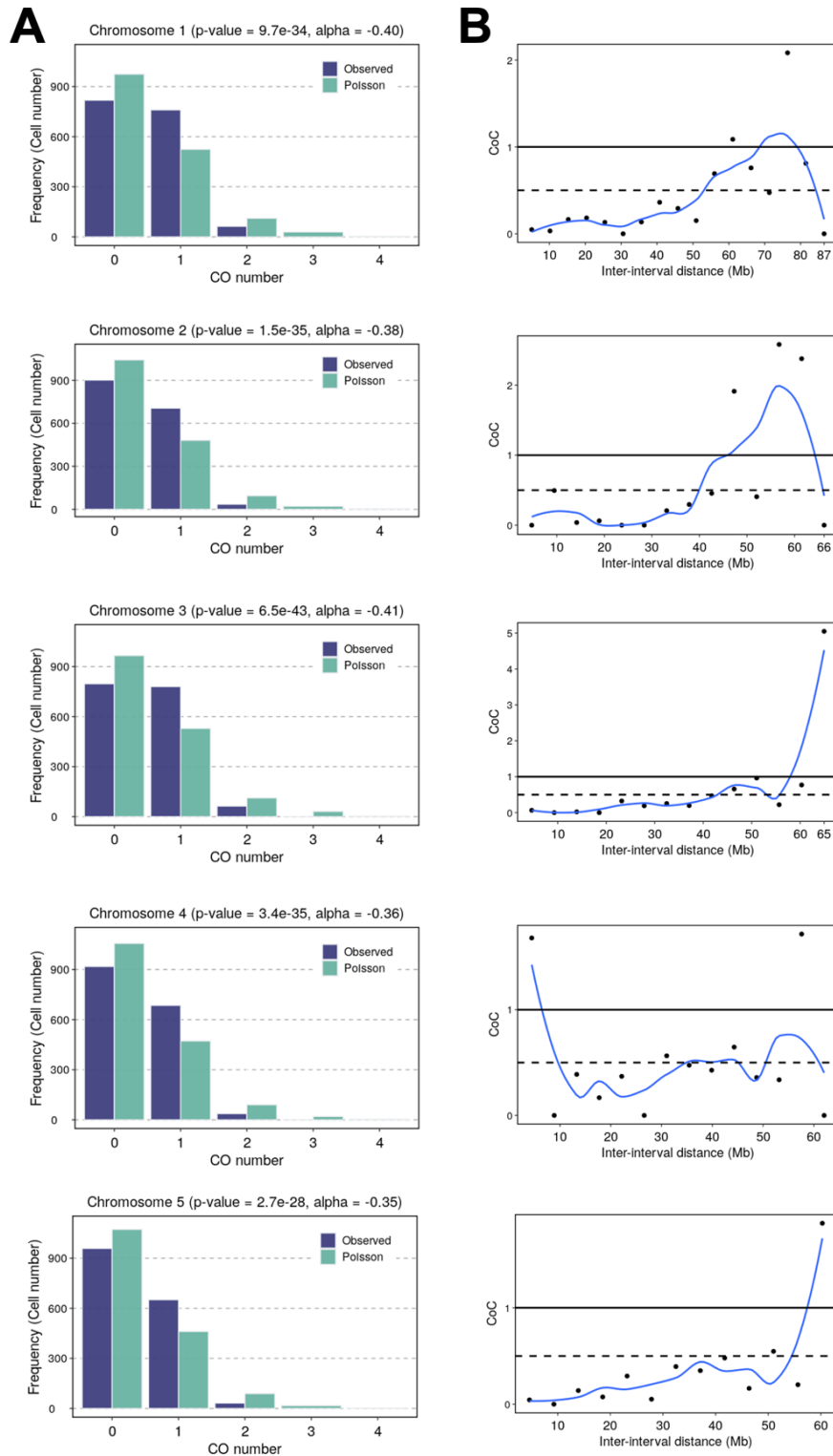
Supplementary Figure 9

CO interference on CO number. **(A)** Comparison of observed CO number and expected CO number under the assumption of no interference on chr1, chr2, chr3, chr4, and chr5. Chi-square value was firstly computed based on chi-square goodness-of-fit test with Poisson distribution. Then p-value was computed by chi-square distribution with above chi-square value and degree of freedom. Alpha value was derived from dispersion test. **(B)** CoC curve for each chromosome in pollen nuclei (n = 1,641). Chr1 was divided into 18 intervals and chr2-5 were divided into 15 intervals, random sampling at CO intervals, for calculating the mean coefficient of coincidence of each pair of intervals.

A

Sizes of CENH3 and TYBA array

B

Spacing length of CENH3 and TYBA array
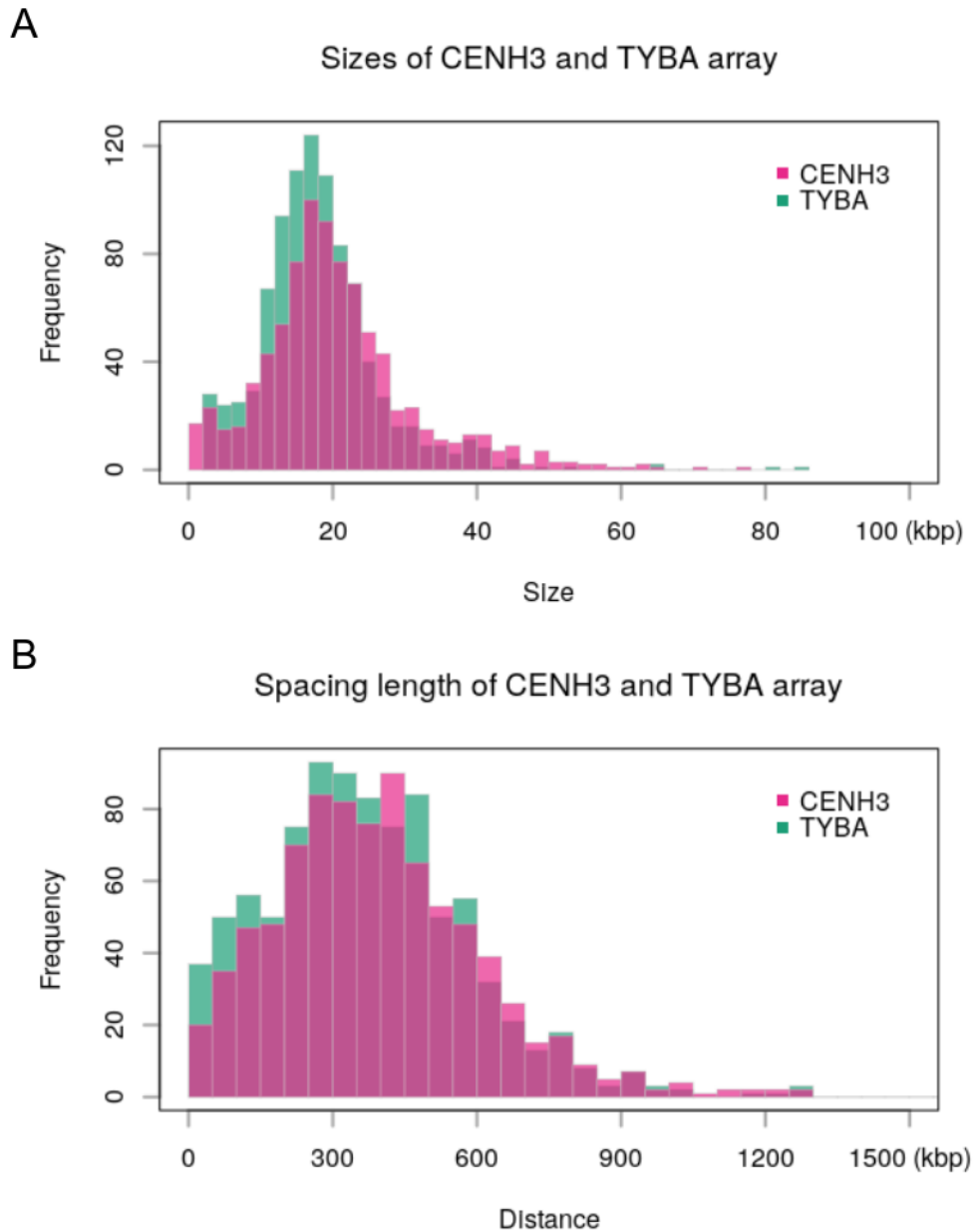
Supplementary Figure 10

Sizes and spacing distances of CENH3 and TYBA arrays. **(A)** Sizes of CENH3 and *Tyba* arrays. CENH3 median size is 19156 bp and the mean size is 20697 bp. The median of *Tyba* array size is 17424 bp and the mean is 18220 bp. **(B)** Spacing distance of CENH3 and *Tyba* arrays. CENH3 median distance is 378467 bp and the mean is 401763 bp. The median of *Tyba* array distance is 354850 bp and the mean is 374310 bp. CENH3 domains were generated by 1) merging CENH3 peaks (See Materials & Methods for peak calling) with spacing distance less than 25Kbp; 2) removing CENH3 with domain size less than 1 Kbp. *Tyba* arrays were generated by merging *Tyba* arrays with spacing distance less than 25Kbp and then discarding those with sizes less than 2Kbp.
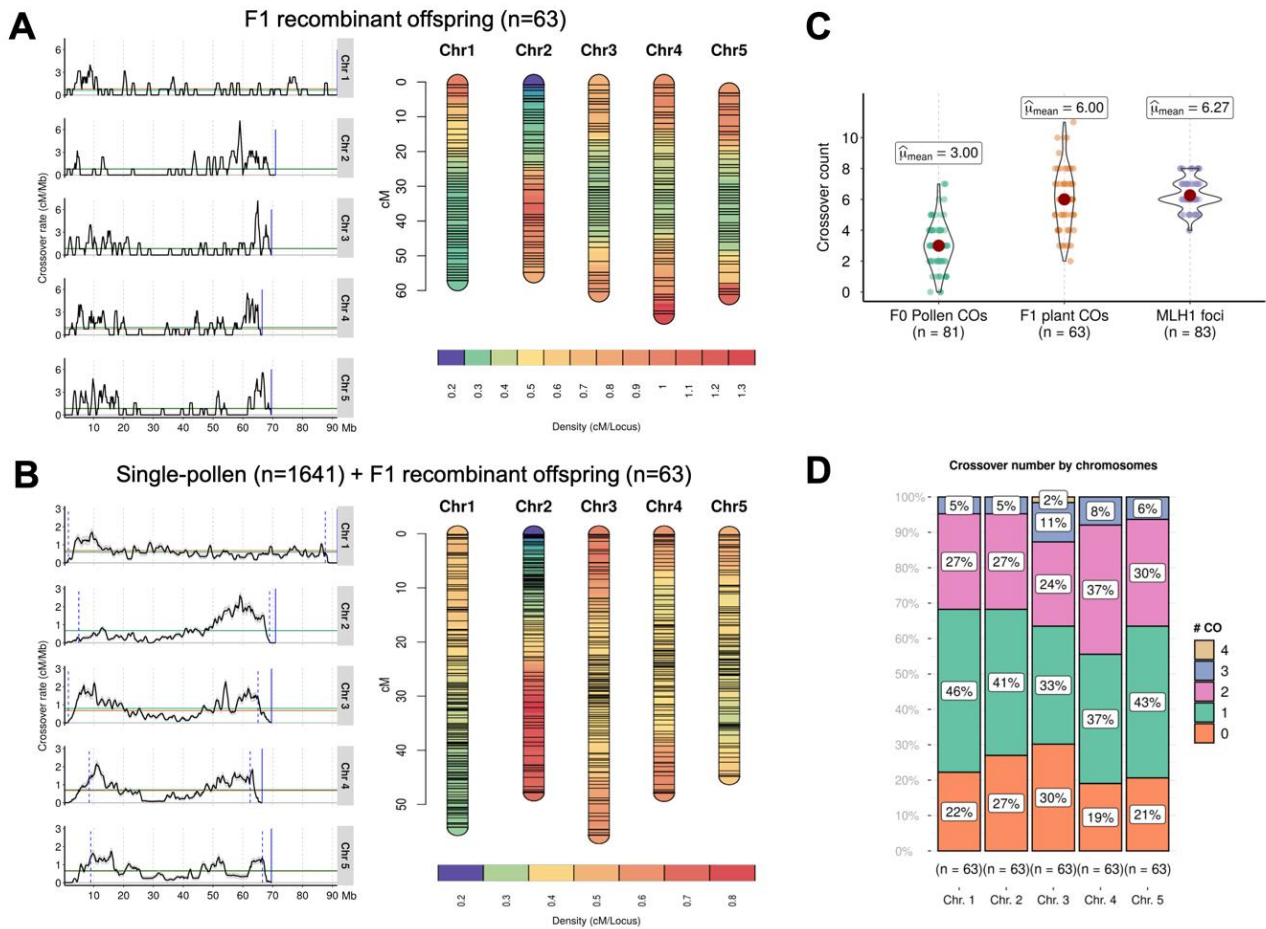
Supplementary Figure 11

Recombination dynamics in the F1 recombinant offspring and combined data (F1 + single-pollen sequencing) of *R. breviuscula*. **(A)** Recombination landscape of the five chromosomes in *R. breviuscula* by computing crossovers in 63 F1 offspring individuals (left panel). Genetic linkage map with density indicated by colouring (right panel). **(B)** Recombination landscape of the five chromosomes in *R. breviuscula* by computing crossovers in 1,641 pollen nuclei plus 63 F1 offspring individuals (left panel). Black line displays the CO rate, which was the mean of 500 random samplings for each CO gap. Shadow ribbons indicate one standard deviation from mean CO rate. Blue dashed vertical line: start and end of confident CO rate computation (Supplementary Figure 8). Blue solid vertical lines indicate chromosomal ends. Orange horizontal line: genome-wide average CO rate. Green horizontal line: chromosome-wide average CO rate. Genetic linkage map with density indicated by colouring (right panel). The 705 markers were selected by 500Kbp sliding window through all markers defined on reference (See Materials & Methods). **(C)** CO number by counting CO events in bioinformatic analysis and MLH1 foci in cytological observations. **(D)** CO number distribution by each individual chromosome in F1 offspring.
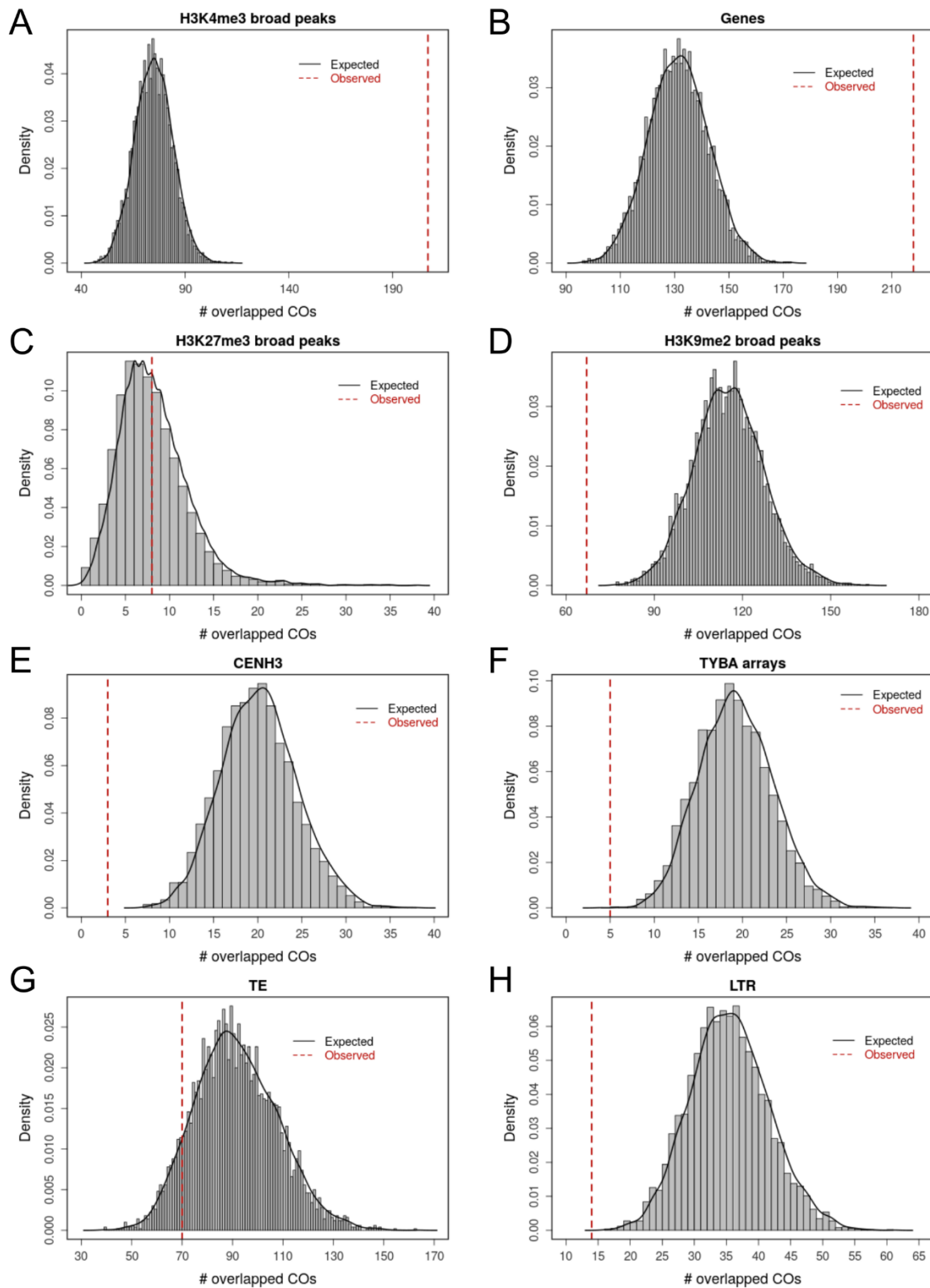
Supplementary Figure 12

Comparison of numbers of COs overlapped with (epi-)genetic features to random simulations. Observed overlapped CO number is displayed with red dashed vertical lines. Histograms show the distributions of overlapped CO numbers with H3K4me3 (**A**), genes (**B**), H3K27me3 (**C**), H3K9me2 (**D**), CENH3 (**E**), TYBA arrays (**F**), TEs (**G**), and LTRs (**H**) in 5000 times of simulation of randomly assigned COs.

Chapter 2: A new mode of sexual propagation of clonal seeds in the absence of meiotic crossovers

Authors:

Meng Zhang[#], Marco Castellani[#], Stefan Steckenborn, Lorraine Deberon, José A. Campoy, Thomas Lux, Magdalena Marek, Bruno Huettel, Klaus F. X. Mayer, Hequan Sun, Korbinian Schneeberger, Paulo G. Hofstatter, André Marques*

# equal contribution

*correspondence to amarques@mpipz.mpg.de

Abstract

The beak-sedge plant *Rhynchospora tenuis* has a genome composed of only two holocentric chromosome pairs. Because of this unusual centromere organization, this species performs inverted meiosis, where the first meiotic division involves an equational segregation of sister chromatids, while reductional segregation of homologous chromatids occurs at the second meiotic division. Furthermore, no chiasmata have been observed during male meiosis in *R. tenuis*. Because of the lack of recombination, haplotypes are expected to accumulate large sequence divergence. Here, we exploited this high heterozygosity of *R. tenuis* to obtain a haplotype-phased chromosome-scale reference genome. Following single-gamete sequencing of pollen nuclei and NGS sequencing of the progeny of two selfed mother plants, we confirmed that there is no evidence of meiotic recombination in this species. We validated our results by immunocytochemistry using recombination specific-protein markers and their visualization in meiotic prophase I. Our results provide evidence for a case of bisexual achiasmy and absence of recombination in a sexually propagating organism. Furthermore, our study sheds light on novel mechanisms for achieving clonal seed propagation despite maintenance of sexual reproduction.

Key words: achiasmatic meiosis, holocentric chromosomes, apomixis, single-cell sequencing, meiotic recombination

Introduction

Meiosis is a specialized cell division process that sexually reproducing organisms undergo in order to reduce their ploidy before fusing their gametes. Additionally, meiotic recombination reshuffles genes and generates genetic diversity in the progeny (Mercier et al., 2015). Meiotic recombination is the exchange of genomic material between homologous parental chromosomes that first induce fragmentation of their own chromosomes, which are then repaired using non-sister template, resulting in a crossover (CO). The physical manifestation of a CO is the chiasma, a physical link between homologous chromosomes that can be observed at the end prophase I, in a stage called diakinesis (Keeney, 2008; Mercier et al., 2015).

During early meiosis a series of meiotic-specific proteins are required for proper placement of CO, pairing and synapsis. These proteins retain conserved patterns that can be studied using cytology and microscopy. DMC1 is a meiotic-specific protein involved in the single-strand invasion following a double strand break (SDB). In early meiotic stages, DMC1 localizes as many foci on chromosomes (Da Ines et al., 2013). ASY1 is a solid cytological marker for the beginning of prophase I and especially the stage of leptotene. During this stage, chromosomes are condensed into thin threads, but are not yet paired. ASY1 represents the chromosome axis that is formed on unpaired chromosomes, and it is necessary for both pairing and later stages of recombination (Armstrong et al., 2002; Lambing, Kuo, et al., 2020). REC8 is another robust cytological marker for sister chromatid cohesion. REC8 is widely used to visualize the process of pairing, when homologous chromosomes are brought together to process recombination intermediates. As a result of this process, REC8 form and intense linear signal as chromosomes are paired (Kuttig et al., 2022; Lambing, Kuo, et al., 2020; Lambing, Tock, et al., 2020). ZYP1 is the transverse filament of the synaptonemal complex (SC), a zipper-like structure assembled to tie together homologous chromosomes. When pairing is complete, at the stage of pachytene, ZYP1 can be visualized as a linear signal running along the chromosomes (Higgins et al., 2005; M. Wang et al., 2010).

It is known that recombination frequencies within and among species are subject to fluctuations. Heterochiasmy is the phenomenon of having different recombination frequencies between the two sexes (Lenormand & Dutheil, 2005; Saini et al., 2020; Stapley et al., 2017). This difference can be so strong that recombination is absent in one of the two sexes, i.e., achiasmy. Heterochiasmy has been observed in many eukaryotic model organisms, including plants. Generally, organisms with canonical meiosis can have incorrect or failed recombination. In this

case, there are dire consequences, as chiasmata are necessary for correct segregation and evolution in general. Otherwise, organisms (or specific chromosomes) can be entirely achiasmatic, which means there is never occurrence of crossovers during meiosis in one or both sexes. One of the most famous example is the male meiosis of *Drosophila melanogaster*, where recombination does not take place, chiasmata is absent and no synaptonemal complex is formed, although there is evidence for pairing (Beadle, 1932; John et al., 2016; McKee et al., 2012). In addition, given the absence of chiasmata, other mechanisms must be adopted to ensure proper non-random chromosome segregation.

Although meiotic recombination is essential for proper segregation of chromosomes, it is also essential for reshuffling genetic material preventing the retaining of deleterious mutations (Melamed-Bessudo et al., 2016). Thus, it plays an important role on creating new allelic combination and disrupting negative linkage disequilibrium. Therefore, the absence of recombination would have an evolutionary toll on achiasmatic organisms. The process of gene conversion would be impaired and this would allow to a systematic accumulation of many mutations in various loci in different chromosomes (Veller et al., 2017). With time, the accumulation of a large number of mutations in both homologous chromosomes would make them significantly different from each other, the so-called 'Meselson effect' (Birky, 1996; Butlin, 2002; Ceplitis, 2003; Mark Welch & Meselson, 2000; Weir et al., 2016). Another expected consequence of the lack of recombination is the accumulation of deleterious alleles and the pseudogenization of alleles, which cannot be rescued anymore by gene conversion.

In the past years, the holocentric plant species *R. tenuis* attracted our interest because of its low chromosome number (n=2), the lowest found among plants (Vanzela, A.L.L., 1996) and its achiasmatic meiosis (Cabral et al., 2014). More recently, we have shown that this very low chromosome number has resulted from three end-to-end chromosome fusions from an ancestral karyotype with n=5 (Hofstatter et al., 2022). In contrast to monocentric chromosomes, where a single size-restricted centromere is found, holocentric chromosomes in *Rhynchospora* are typically composed by hundreds of small centromeric units encompassing the whole length of the chromosome (Hofstatter et al., 2022; Marques et al., 2015). In fact, holocentric chromosomes evolved several times independently across many animal and plant groups (Marcial Escudero et al., 2016). Transition to holocentricity is normally associated with the evolution of several meiotic adaptations to deal with this new condition (Cabral et al., 2014; Heckmann et al., 2014; Hofstatter et al., 2021; Marques & Pedrosa-Harand, 2016). Indeed, we have previously reported that *Rhynchospora* species display inverted meiosis, where bi-

orientation of sister chromatids allows their early separation at anaphase I, while homologous chromatids are only segregated at anaphase II (Cabral et al., 2014; Marques et al., 2016b). Remarkably, male meiosis in *R. tenuis* is even more special, because homologous chromosomes do not pair nor form chiasma, displaying 4 univalents at the diakinesis stage (Cabral et al., 2014). Strikingly, formation and repair of double-strand breaks (DSBs) are likely occurring as evidenced by the presence RAD51 foci, a protein involved in DSB repair (Cabral et al., 2014). Further separation of sister-chromatids at anaphase I and segregation of homologs only at anaphase II confers *R. tenuis* an inverted order of the main meiotic events (Cabral et al., 2014). As in *R. tenuis* no bivalents are formed, univalents align perpendicular to the equatorial plate at Metaphase I. Sister chromatids then assume a bi-orientation, facing sister kinetochores at opposite poles, instead of a canonical mono-orientation. After the segregation of the sister chromatids at Anaphase I, the two products are still diploid. During meiosis II, homologous non-sisters finally segregate, terminating meiosis with four haploid products (Cabral et al., 2014). However, lack of genetic data in *R. tenuis* hampers the conclusion that this species is fully achiasmatic.

R. tenuis, with such a mosaic of features such as holocentricity, low chromosome number, absence of chiasmata and inverted meiosis, presents a very unique model system to understand the impact of lack of recombination in genome evolution and sexual reproduction. Therefore, it is of great interest to study how these features are integrated in a single species, if they are associated with specific adaptations and if (and how) they could interact with each other in a meiotic context. Here we uncover the meiotic recombination mechanics and outcomes of *R. tenuis*. With a combined approach involving single-gamete sequencing of pollen nuclei, NGS sequencing of an F1 offspring population and immunocytochemistry, we propose a model in which *R. tenuis* is surviving a challenging evolutionary state with a mosaic of unexpected adaptations.

Results

Prophase I is impaired in *R. tenuis*

Prophase I of meiosis can be cytologically studied by immunocytochemistry using antibodies to detect conserved proteins and their behaviour. Different markers can be used to study different meiotic stages. The holocentric nature of *R. tenuis* is highlighted by CENH3 that appears as a linear signal along the entire chromosome length (Supplementary Figure 15a-c). In *R. tenuis,* at early prophase I, we can observe DMC1 appearing as many foci located on the

DNA, not yet condensed into thin lines (Figure 11a). At the stage of leptotene, ASY1 forms a linear intense signal (Figure 11b). Later stages can be visualized with REC8 and ZYP1, and indeed REC8 forms a signal that is linear but partial, not covering the whole length of the presumed paired chromosomes. ZYP1 is supposed to be loaded when REC8 forms its linear signal, but we can only see a scattered signal that, even if present in proximity of the REC8 signal, does not display a full linear structure (Figure 12a). We cannot observe any conserved behaviour of meiotic proteins in later stages. Rare instances hint at a possible beginning of synapsis, that might be soon aborted. There are traces of HEI10 loading, however it seems to be delayed and/or less abundant compared to observation is related species (See Chapter 1 and 3) (Figure 12b). Therefore, it seems that prophase I is occurring canonically in its initial part, but somehow, when pairing is involved and meiosis I reaches stages typically characterised by the processing of recombination intermediates, markers are not behaving normally.
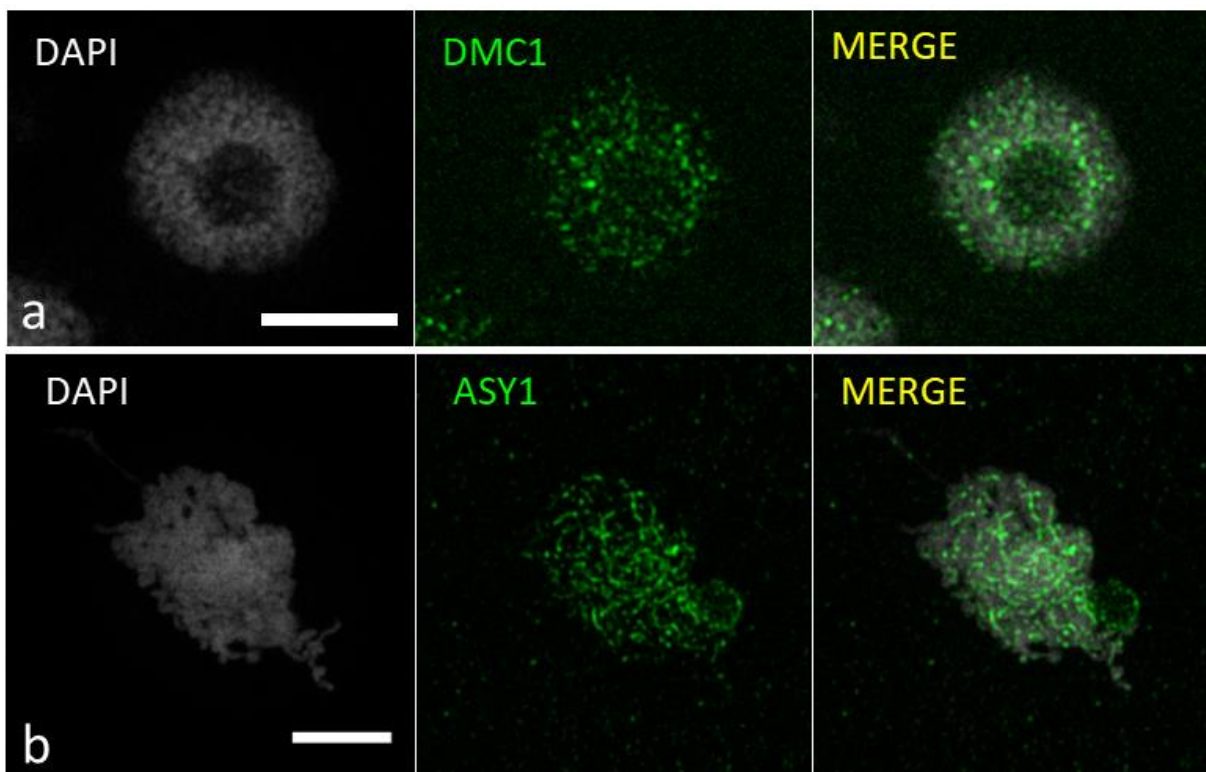
Figure 11

Immunolocalization of meiotic proteins during prophase I of male meiosis of *R. tenuis*. **(a)** Early prophase I cell with DMC1 (green) localizing as foci. **(b)** Leptotene cell with ASY1 (green) forming a linear signal. Maximum projection is shown. DNA is counterstained with DAPI. Scale bar = 5 μm.
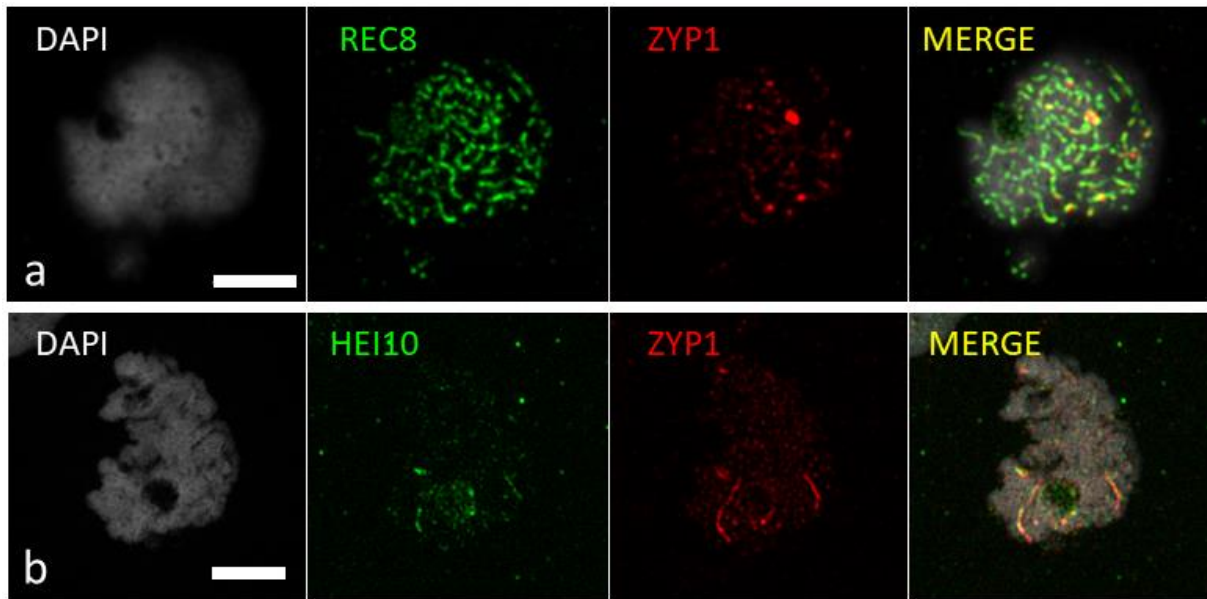
Figure 12

Immunolocalization of meiotic proteins in male meiosis of *R. tenuis*. (**a**) Intermediate prophase I cell stained with ZYP1 (red) and REC8 (green). REC8 forms a linear signal, but ZYP1 cannot be distinguished as a linear signal and it displays a dispersed or scattered pattern. (**b**) Rare case of a cell displaying a linear ZYP1 signal (red), that appears incomplete. Additionally, HEI10 (green) appears as a very weak and even less intense signal than ZYP1. Maximum projection is shown. DNA is counterstained with DAPI. Scale bar = 5µm.

The meiotic machinery repertoire of *R. tenuis* is conserved and likely functional

In order to study whether the absence of recombination is due to mutations or rearrangements in fundamental meiotic genes, we investigated their sequences and expression. Interestingly we found that at the sequence level most of the known actors of meiosis are present in the genome of *R. tenuis*. In addition, they also are expressed and their gene function is maintained. Only SHOC1, a protein essential for mid-to-late recombination progression in *Arabidopsis* and mammals (Guiraldelli et al., 2018; Macaisne et al., 2008), is not found in our expression dataset. However, its sequence seems incomplete and predicting a functional protein (Table 1).

Phased genome assembly of *R. tenuis*

The high degree of heterozygosity of the genome of *R. tenuis* is around 2% (Hofstatter et al., 2022). This feature was exploited to obtain a phased genome assembly. Applying the same genome assembly method as demonstrated for *R. breviuscula* (See Chapter 1), we successfully obtained a phased genome assembly of *R. tenuis* (Table *2*; Figure 13), which then allows for whole chromosome genotyping. The assembly result shows that *R. tenuis* has a comparable genome size to *R. breviuscula*, but *R. tenuis* has only two pairs of chromosomes, the least number we know in plants so far. *R. tenuis* has a high degree of synteny between two haplotypes with several inversions and some small duplications and translocations (Figure 13).

No occurrence of COs in both male and female meiosis

To ascertain the absence of crossovers in *R. tenuis* at the genetic level, we genotyped male gametes and selfed F1 offspring using the same type of data, i.e., scRNA sequences from pollen nuclei and WGS Illumina sequences from F1 plants, and the same CO detection methodology used for *R. breviuscula* (See Chapter 1). Remarkably, we confirmed that no COs could be detected among 1861 haploid pollen nuclei and 50 F1 offspring diploid plants (Figure 14). Strikingly, all F1 individuals showed heterozygous genotypes on both chromosomes, indicating a potential mechanism of heterozygosity assurance in *R. tenuis*. It is important to note that the same pipeline we implemented here was used to successfully detect COs in *R. breviuscula.* This acts as a cross-validation, making our pipeline even more robust. Therefore, our analysis indicates that neither male nor female gametes of *R. tenuis* undergo formation of meiotic recombination events, i.e., COs.

Non-random segregation of chromosomes

Since recombination is absent in male gametes of *R. tenuis*, the genotype is supposed to be predictable, i.e., AA, AB, BA, BB for chromosome 1 and 2, where "A" represents haplotype 1 and "B" represents haplotype 2. Meiosis canonically follows Mendelian segregation; therefore, four genotypes should appear with the same frequencies in male gametes. After genotyping the 1861 pollen nuclei, we counted the frequency of the four possible genotype combinations of two chromosomes. Surprisingly, it was found that the chromosomes belonging to the same haplotype have a higher chance of being segregated together in male gametes (Figure 15A), suggesting a non-random segregation of chromosomes. Our results suggest a potential mechanism that bias the segregation of *R. tenuis* chromosomes in meiosis despite the absence of COs. Indeed, synteny comparison between chromosome 1 and 2 of the same haplotype revealed a small 1 Mb-long region to be translocated between these chromosomes (Figure 15B). These high-homology regions could be exploited to sort univalents in a non-random disposition.

Table 1

Expression and functional domain conservation of key meiotic genes in *R. tenuis*. We used BLAST on characterized *Arabidopsis thaliana* proteins of interest in order to find their *R. tenuis* homologs. Eight genes, ASY3, DFO, FANCM, MSH4, PRD1, SHOC1, SPO11-1, and ZYP1a had more complete sequences when applying *Arabidopsis* or *R. pubera* annotation than when using the *R. tenuis* in-house annotation. PRD1 is not annotated but the coding sequence is conserved and is translated to a functional protein (See Materials & Methods).

Gene	Gene code	Expression	Functional domain sequences conserved	Comment
ASY1	rtenuis.r2.1_h1G00285630	Present	Yes	Cytologically observed
ASY3	NA	Present	Yes	
ASY4	rtenuis.r2.1_h1G00328940	Present	Yes	
DFO	NA	Present	No	Conserved regions disrupted when compared to related species
DMC1	rtenuis.r2.1_h1G00029300	Present	Yes	Cytologically observed
FANCM	rtenuis.r2.1_h1G00134510 & rtenuis.r2.1_h1G00134520	Present	Yes	
HEI10	rtenuis.r2.2_h1G00739780	Present	Yes	Cytologically observed, altered pattern
HOP2	rtenuis.r2.1_h1G00261110	Present	Yes	
MER3	rtenuis.r2.1_h1G00058540	Present	Yes	
MLH1	rtenuis.r2.1_h1G00249290	Present	Yes	
MND1	rtenuis.r2.2_h1G00798220	Present	Yes	
MSH4	rtenuis.r2.2_h1G00811930	Present	Yes	
MSH5	rtenuis.r2.1_h1G00064650	Present	Yes	
MTOPVIB	rtenuis.r2.1_h1G00319210	Present	Yes	
MUS81	rtenuis.r2.2_h1G00783800	Present	Yes	
PCH2	rtenuis.r2.1_h1G00017140	Present	Yes	
PHS1	rtenuis.r2.2_h1G00752030	Present	Yes	
PRD1	NA	Present	Yes	
PRD2	rtenuis.r2.2_h1G00806080	Present	Yes	
PRD3	rtenuis.r2.2_h1G00833000	Present	Yes	
PTD	rtenuis.r2.1_h1G00191640	Present	Yes	
REC8	rtenuis.r2.2_h1G00749550	Present	Yes	Cytologically observed, altered pattern
RECQ4	rtenuis.r2.1_h1G00097360	Present	Yes	
SCEP1	rtenuis.r2.1_h1G00047920	Present	Yes	
SCEP2	rtenuis.r2.1_h1G00103630	Present	Yes	
SHOC1	rtenuis.r2.1_h1G00097360	Absent	Yes	
SPO11-1	rtenuis.r2.1_h1G00247890	Present	Yes	
SPO11-2	rtenuis.r2.2_h1G00849990	Present	Yes	
ZIP4	rtenuis.r2.1_h1G00300290	Present	Yes	
ZYP1a	rtenuis.r2.1_h1G00007590	Present	Yes	Cytologically observed, altered pattern
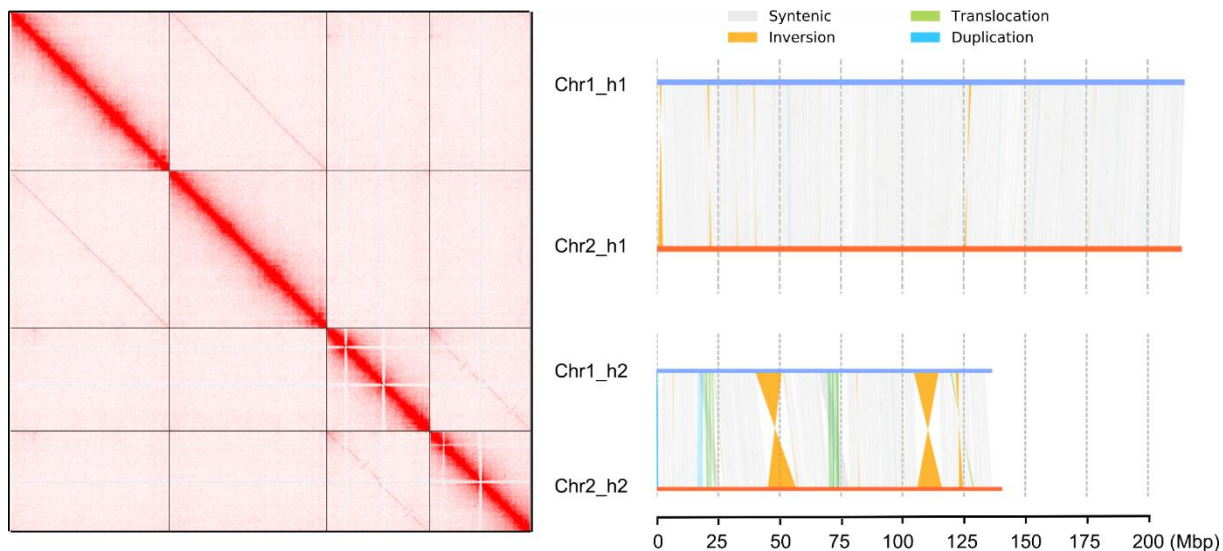
Figure 13

Hi-C map and haplotype comparison. The left heatmap shows the Hi-C interactions of *R. tenuis* chromosomes, indicating the success of phasing two haplotypes of *R. tenuis*. The right figure is a comparison between two haplotypes. The synteny blocks and structural rearrangements were analysed by Syri and plotted by plotsr (See Materials and Methods).

Table 2

Summary of the assemblies of the two haplotypes of the genome of *R. tenuis*.

	Haplotype 1	Haplotype 2
Genome assembly size (bp)	397748830	371283995
GC (%)	35.70	35.47
# Scaffolds	1,635	592
Pseudo-chromosome size (bp)	350,419,914	352,251,097
Scaffold N50 (bp)	215,061,937	212,800,643
Scaffold N90 (bp)	38,266	139,450,454
Largest scaffold / chr 1 (bp)	215,061,937	212,800,643
Chromosome 2 (bp)	135,357,977	139,450,454
Base accuracy (QV)	39.5	44.3
Completeness (%)	70.6	70.9
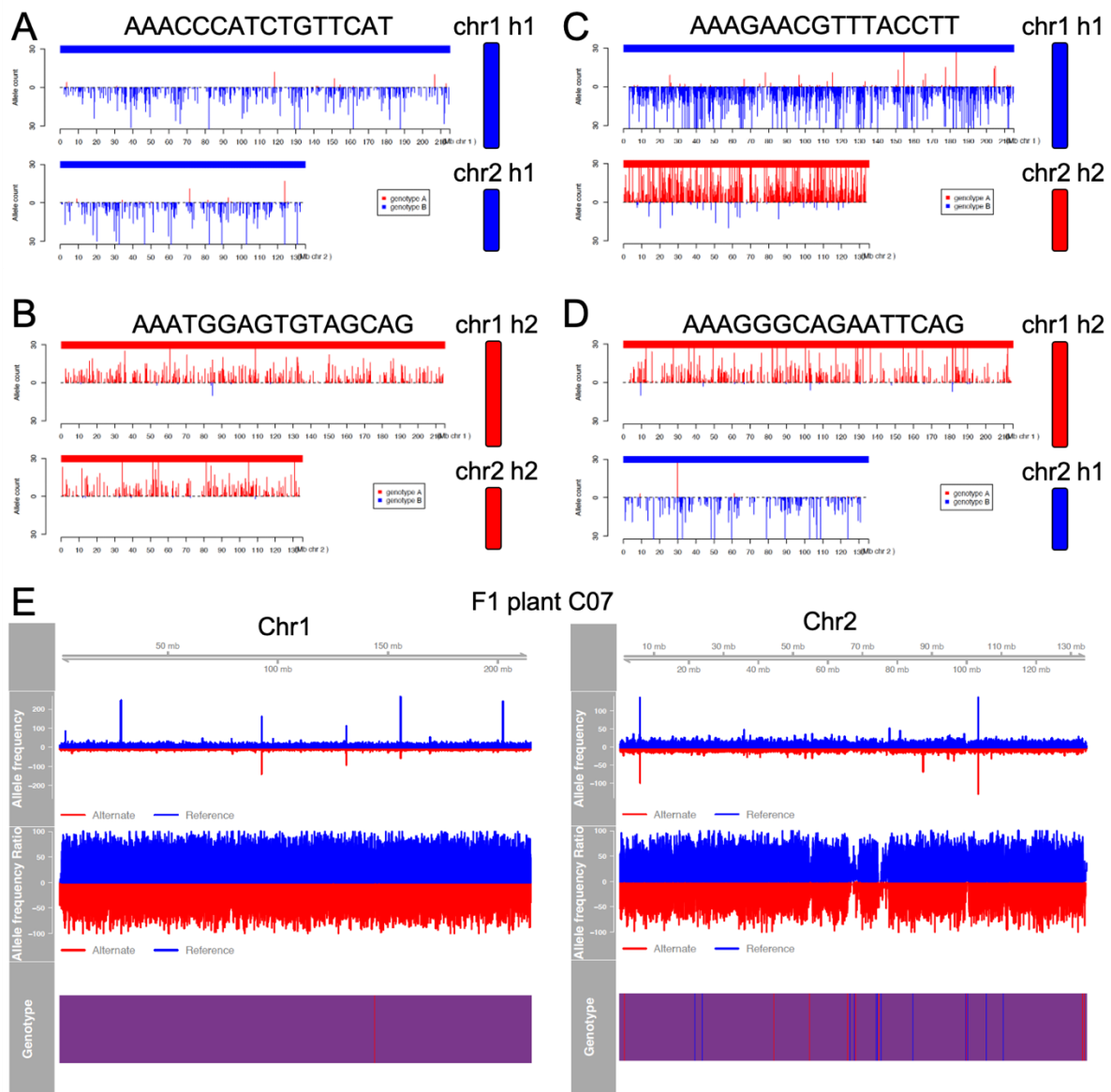
Figure 14

Bisexual lack of COs in *R. tenuis*. (**A-D**) Four examples of sequenced gametes showing complete absence of COs and segregation of haplotypes. (**E**) All F$_1$ plants obtained by selfing two heterozygous mother plants show lack of COs and the same heterozygous haplotype combination of the mothers.

Discussion

Both our cytological and bioinformatic analyses confirms that no recombination is taking place in male meiosis of *R. tenuis*. To our knowledge this is the first case of a plant species, and possibly eukaryotic organism, showing complete lack of COs in both sexes, but at the same time keeping its sexual reproduction ability. Furthermore, *R. tenuis* combines a very specific set of features that allow it to produce fertilized clonal seeds in a way that differs from typical apomixis, which typically derive from parthenogenesis (Underwood & Mercier, 2022). These key features are: 1- holocentric chromosomes; 2- inverted meiosis; 3- bisexual lack of COs; 4-extreme low chromosome number; 5- a possible homozygous state incompatibility that confers only heterozygous seeds (Figure 16).

We show that the same single-cell gamete sequencing pipeline that was able to detect COs in chapter 1, was not able to detect any genotype conversion in the pollen of *R. tenuis*. This means that there is no evidence of exchange of genetic material between homologous chromosomes during meiosis. Moreover, by sequencing the progeny of selfed F1 offspring, we could only detect the same identical genotype of the mother plants, always resembling a combination of
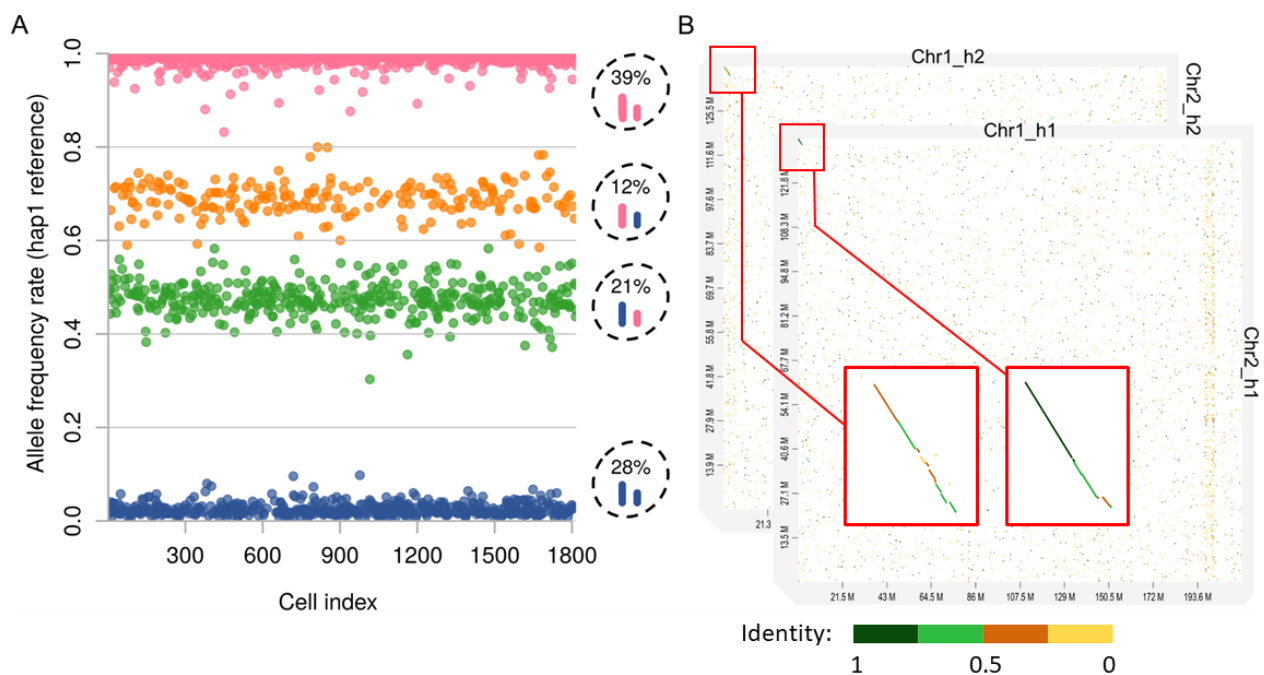
Figure 15

Biased segregation of chromosomes in *R. tenuis* male gametes. **(A)** The allele frequency rate was computed for each pollen nuclei and haplotype 1 as a reference. 39% of pollen nuclei have two chromosomes both from haplotype 1; 12% of pollen nuclei have chr 1 from haplotype 1 and chr 2 from haplotype 2; 21% of pollen nuclei have chr 1 from haplotype 2 and chr 2 from haplotype 1; 28% of pollen nuclei have two chromosomes both from haplotype 1. **(B)** Synteny dotplot comparison between chr1 and chr2 of the same haplotype, with magnifications showing a small 1 Mb region of homology at the very end of each chromosome. Doplots were generated by D-GENIES.

both heterozygous haplotypes. This result is very exciting as supports the hypothesis that also female meiosis is achiasmatic and that a clonal reproduction is being achieved through seeds. Our crossing results further supports that these seeds are not generated by parthenogenesis or apomixis, but rather produced by sexual reproduction. However, the exclusively heterozygous progeny generated is intriguing. We speculate that some homozygous state incompatibility is likely taking place in *R. tenuis* due to the accumulation of deleterious alleles or due to the loss of gene copies that are likely single copy in the diploid genome. However, future experiments are necessary to validate this hypothesis.

Our immunocytochemistry observation report that even if most of prophase I is carried out completely and without major impairment, when the cells get close to the stages when the crucial recombination mechanisms are supposed to happen, meiotic recombination is prevented or aborted. The presence of a linear signal on the chromosome axis (ASY1) and a partial one
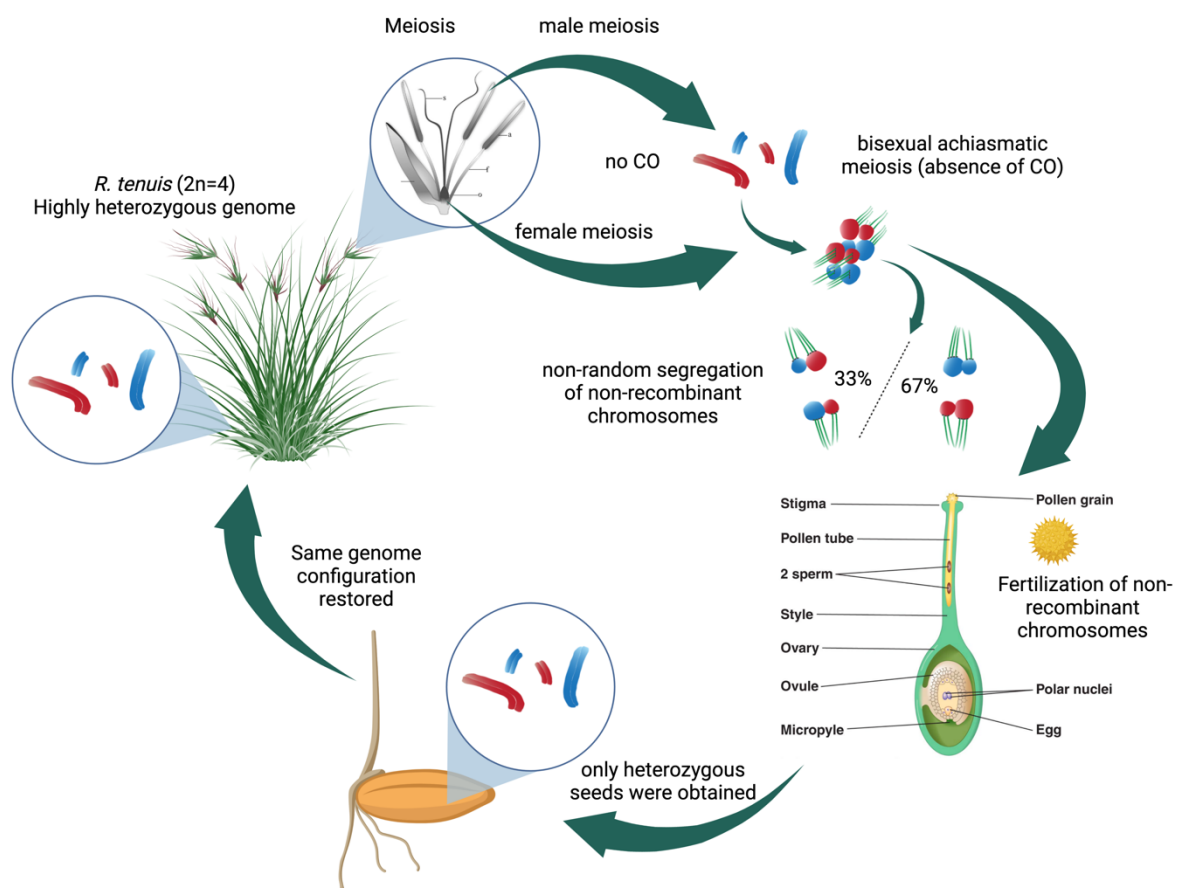
Figure 16

The sexual reproduction cycle of *R. tenuis* maintains its heterozygosity due a combination of key features. Whether an incompatibility of male and female gametes with a homozygous combination of chromosomes is taking place is yet unknown.

representing sister chromatid cohesion (REC8), support a model where the beginning of

prophase I is happening canonically. However, the absence of a linear signal, representing pairing and synapsis (ZYP1), being progressively formed, suggests that indeed pairing and synapsis, that were not observed in previous studies, are the missing steps that prevent recombination from happening. Despite missing data from SPO11 activity, previous observations of RAD51 (Supplementary Figure 16; Cabral et al., 2014) and our cytological evidence of DMC1 (Figure 11a) support a conserved beginning of recombination, that would exclude an upstream CO abortion. It is important to note that from genomic analyses, the entire meiotic machinery repertoire is present and expressed. However, SHOC1, even if present at the sequence level as a complete protein, is not expressed, contrary to what is observed in closely related species like *R. pubera*. SHOC1 mutants reported in mammals and *A. thaliana* show a severe reduction or complete lack of recombination. Interestingly, the mutant phenotype still has a conserved progression of early meiosis. In *A. thaliana* synapsis is not affected, but in human the SC cannot fully extend on the chromosome axis. This behaviour is consistent with our observations in *R. tenuis*.

Now that we have a more robust proof that recombination is indeed absent, we need to delineate a model to explain how this plant can maintain its fitness and can carry so many peculiar traits that in other eukaryotes are not only rare, but could also be deleterious, when present. We speculate that *R. tenuis* lost the ability to recombine and became achiasmatic. It is still hard to speculate what could be the driving force, but the absence of SHOC1 expression hints at the disruption of a related pathway. In a normal sexual eukaryote this would be a great evolutionary challenge. The first obstacle is how to properly segregate chromosomes, as there are no chiasmata to link them. Due to the fact that chiasmata are absent, meiotic segregation would be random, but a low chromosome number automatically reduces the complexity of segregation, simplifying the alignment and the separation of homologous chromosomes and sister chromatids. Indeed, we have recently shown that a series of end-to-end fusions allowed *R. tenuis* to reduce its chromosome number (Hofstatter et al., 2022). In addition, our genomic analyses hint at homology-based pairing that helps the 4 chromosomes to assume a non-random disposition at diakinesis (Supplementary Figure 15d; Cabral et al. (2014)). This way, the cell can correctly segregate sister chromatids at anaphase I and prepare the homologs for the second division. Additionally, when we sequenced the pollen, we encountered a bias towards chromosome pairs with the same haplotype. This bias gives to the meiotic product a non-mendelian segregation, the mechanism of which is still unclear. By sequencing the progeny, finally, we observed that individuals were identical to the mother. This means not only the absence of recombination, but also the restoration of the mother genotype, without

other allelic variants. Thus, we speculate a possible additional mechanism of gamete selection either at the moment of fertilization or during embryo development, that would guarantee that only the heterozygous genotype is viable (Figure 16).

In summary, we show that *R. tenuis* has developed a new mode of sexually propagated clonal seeds in the absence of COs in both male and female meiosis. Understanding the molecular mechanisms that confer *R. tenuis* this special type of chromosome segregation will potentially unveil new ways of engineering apomixis in crops.

Materials & Methods

Immunocytochemistry & Cytology

All cytological methods were performed on anthers coming from inflorescences of *R. tenuis* plants. Protocols are the same described in Chapter 1. Additionally, the anti-RpDMC1 was a combination of two antibodies raised in rabbit against the peptides CIDTEGTFRPDRIVPI and CMLRKGKGEQRVAKII (Gene ID: RP5G01801410/RP4G01420350/RP2G00748220/RP1G00419100) and affinity-purified (Eurogentec).

Selection of genotyping markers on the reference genome of *R. tenuis*

The genome-wide markers used for genotyping in *R. tenuis* were defined by aligning ~60Gbp WGS Illumina sequences (~142x mean coverage) to haplotype 1 of the phased genome of *R. tenuis* (rhyTenHap1). After calling SNPs based on the alignments, 1,648,186 haplotype-specific SNPs (~1SNP/213bp on average) on chromosomes were selected as markers for genotyping (Supplementary Figure 13B-D). These reference markers are almost evenly distributed along the chromosomes (Supplementary Figure 13E). Additionally, homology regions between chromosomes belonging to the same haplotype were visualized using plotsr (Figure 15B) (Goel & Schneeberger, 2022)

Identification of COs in *R. tenuis* with scRNA-seq of pollen nuclei

Extraction of pollen nuclei, library preparation and sequencing were performed as described in Chapter 1. The same strategy of CO detection as illustrated for *R. breviuscula* was employed for *R. tenuis*. As mentioned in Chapter 1, pollen nuclei of the two species were discriminated from the same mix based on alignment rates. 2709 *R. tenuis* pollens were selected by alignment fraction no less than 60%. After discarding 33 cells with a mapping rate of less than 15%, 701 cells with a marker number less than 500, and 159 doublets (Supplementary Figure 14A), 1816

cells were left for confident detection of COs. Genotyping and CO identification were implemented by the same method demonstrated for *R. breviuscula* in Chapter 1.

F1 offspring analysis

50 F1 offspring plants were reproduced from the selfed *R. tenuis* reference. Each F1 plant was sequenced with ~5X Illumina WGS data. CO detection was performed by the same method used for *R. breviuscula* F1 individuals, i.e., for each F1 sample, SNPs were called based on the alignments of WGS Illumina sequences to the rhyTenHap1 reference genome. SNPs of each F1 sample were run through TIGER for genotyping and CO detection. RTIGER was also used to further validate the results from TIGER. Details are described in Chapter 1.

Conservation of meiotic genes

We used BLAST on *Arabidopsis thaliana* sequences found in the the *Arabidopsis* Information Resource (Berardini et al., 2015) to find homologs of the genes of interest in *R. pubera* and *R. tenuis*. We then aligned the identified protein sequences and judged the completeness of amino acid sequences in *R. tenuis* by the absence of extended non-conserved regions, gaps, and early protein termination compared to homologous proteins in *A. thaliana* and *R. pubera*. When available, we also made use of existing literature to identify key functional domains. In case of ambiguity, we cross-compared the in-house *R. tenuis* annotation with the ones from *A. thaliana* and *R. pubera*. Gene expression was performed by analysing the location corresponding to the protein sequences in transcriptomic data from flower buds of *R. tenuis*.
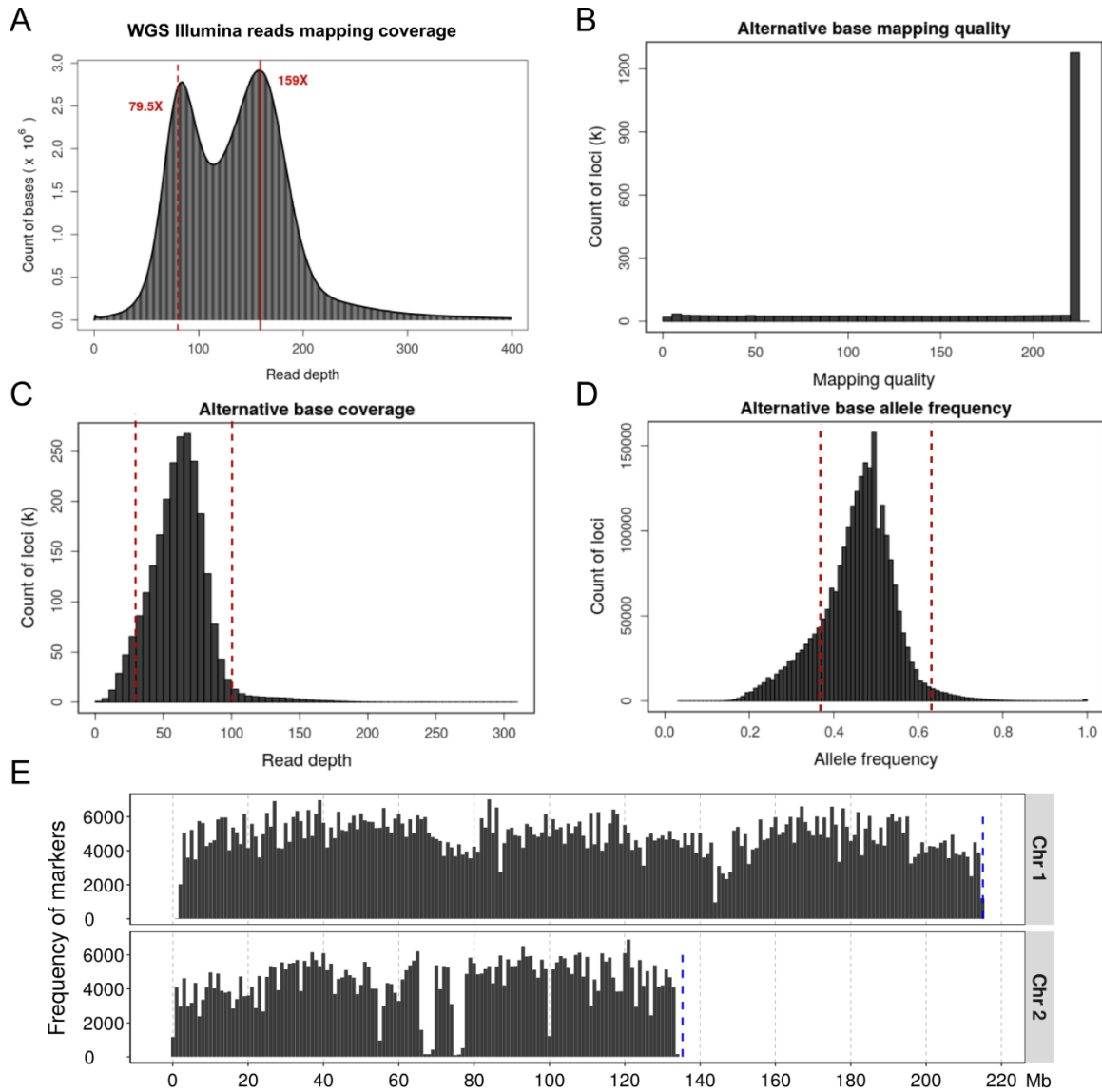
Supplementary Figure 13

Selection of genotyping markers on the reference genome. **(A)** Read depth distribution of Illumina reads mapping to haplotype 1 of *R. tenuis* phased genome; **(B-D)** Characteristics of alternative bases of SNPs that were called from the alignment in **(A)**. Genotyping markers on reference were selected according to the distributions of mapping quality **(B)**, coverage **(C)**, and allele frequency **(D)** of alternative bases, specifically, an alternative base at a single-nucleotide variant position that met the requirements "30 < alternative base coverage < 100, 0.37<= allele frequency <= 0.63, mapping quality > 100" was an allelic SNP, i.e., a genotyping marker. **(E)** Distribution of reference genotyping markers across chromosomes. Marker frequency was counted in 1Mbp windows. Blue dashed lines show the chromosomal ending positions.

A

Count of genotype switches

y=0.075x

○ Doublets
○ Singleton

Number of markers

B

Marker number distribution across pollen nuclei

Marker Number	
Min.	500
1st Qu.	785
Median	1126
Mean	2035
3rd Qu.	2052
Max.	18334
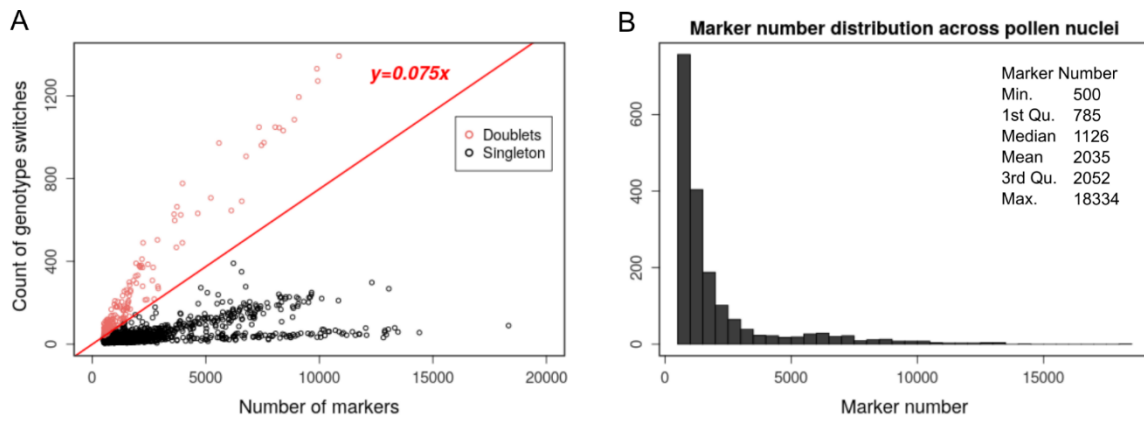
Marker number

Supplementary Figure 14

Selection of viable pollen nuclei for CO identification. (**A**) Identification of doublets by switch rates. Cells with a switch rate of over 0.07 were taken doublets. (**B**) The number of markers across *R. tenuis* pollen nuclei after filtering.
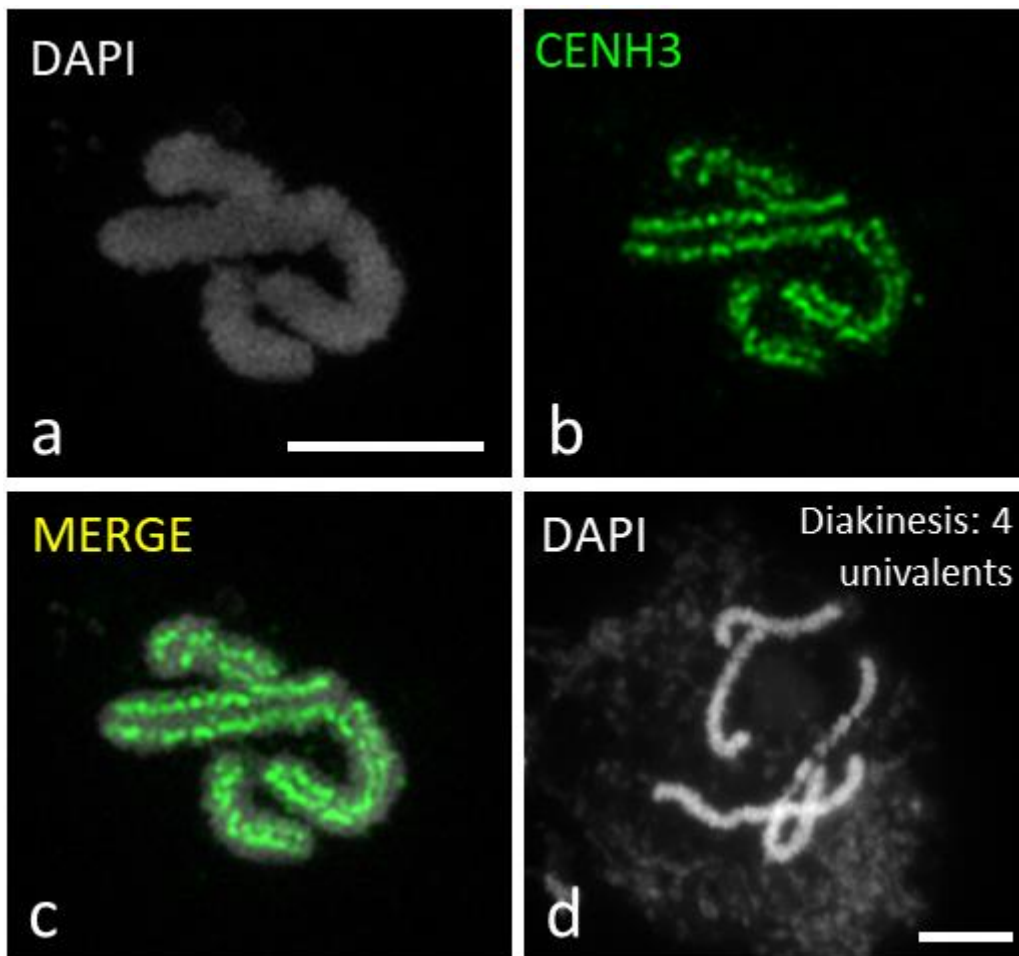
Supplementary Figure 15

General behaviour of *R. tenuis* chromosomes. **(a, b, c)** At mitosis, CENH3 (green) can be detected as a linear signal occupying the entire chromosomal length. **(d)** At the meiotic stage of diakinesis, only 4 univalents can be detected, hinting at the absence of chiasmata. DNA is counterstained with DAPI. Maximum Projection is shown. Scale bar = 5µm
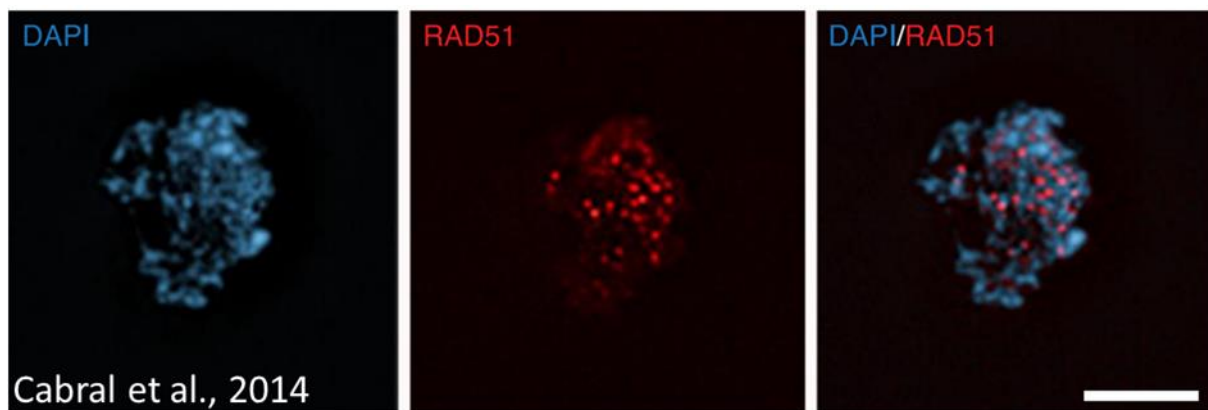
Supplementary Figure 16

RAD51 (red) localization as foci in early meiotic stage of *R. tenuis* (Cabral et al. 2014). DNA is counterstained with DAPI. Scale bar = 5µm.

Chapter 3: Recombination dynamics hint at a fully diploidized meiosis in the holocentric (hidden) octoploid *R. pubera*

Authors:

Marco Castellani & Andre Marques

Abstract

Polyploidy is a ubiquitous phenomenon that involves the doubling of a species genome, resulting in an additional set of chromosomes. Polyploid species are largely present across the tree of life, and despite established polyploids being able to cope very well with this condition and perform correctly all physiological functions, neo-polyploid needs to adapt to this mutation. Meiosis is a process that reshuffle genes in a process greatly challenged by polyploidy, as chromosomes could incorrectly pair with their new homologs or homeologs, leading to chromosome segregation errors and possibly aneuploidy. The genetic basis of meiotic adaptation to polyploidy is still unclear. Holocentricity is another feature of many plants and, similarly to polyploidy, its effects on recombination and eventual adaptations are still mostly unknown. *Rhynchospora pubera* is a holocentric model plant, recently discovered to hide an octoploid state due to a complex chain of end-to-end chromosome fusions that diploidized its chromosome number. Here we study the adaptation of the meiotic machinery of *R. pubera* to both holocentricity and polyploidy. With immunocytochemistry techniques, we investigate the behaviour and the level of conservation of meiotic recombination proteins. Interestingly, we observe that being holocentric and having multiple genome copies does not fundamentally impair meiotic recombination, that is conserved and carried out correctly, suggesting this species has a fully diploid meiotic behaviour. However, we detected altered mechanics of pairing and synapsis and speculate whether it is a result or an adaptation to *R. pubera* being a mosaic of challenging evolutionary features. Taken together, our results constitute the first meiotic overview of a holocentric organism hiding an octoploid state, confirming *R. pubera* as a suited model for cytological approaches and a promising tool to study meiotic adaptations to both polyploidy and holocentricity. Furthermore, we propose a model where end-to-end chromosome fusions have contributed to its genome re-diploidization.

Introduction

The advent of genomics has brought with it the discovery of the ubiquity of polyploidy. In fact, every major eukaryotic taxon has witnessed events of WGD (Whole-Genome Duplication) and the occurrence of polyploid species. However, plants can be considered the most prone to polyploidy. The long-term consequence of polyploidy is subject of discussion. However, it is the consensus that new raw genetic material following a WGD is useful to adaptation and the evolution of complexity. The short-terms effect of a WGD event are equally important, as neo-polyploids underwent a severe mutation that pose a challenge to their fitness (Van de Peer et al., 2017).

One of the challenges that a neo-polyploid must face is meiosis. Meiosis is a specialized cell division that sexually reproducing eukaryotes use to reduce their ploidy and form gametes that will be subsequently fused to form new progeny. Meiosis is essential as it ensures the generation of viable gametes that will lead to successful fertilization. Moreover, it is essential for gene reshuffling and evolution, as meiotic recombination generates variability in the gametes and subsequently in the progeny. Correct segregation of homologous chromosomes during meiosis is essential for the production of viable gametes and fertility in general (Lambing et al., 2017; Mercier et al., 2015). Neo-polyploids often display errors during meiotic segregation and aneuploidy, whereas established polyploid usually display a diploid-like meiosis. Therefore, neo-polyploids need to undergo adaptations to tailor meiosis to their new condition. Normally, homologous chromosomes exchange genetic material and form a structure called bivalent, that is resolved at the end of prophase I with the segregation of homologs. However, in the case of polyploids the situation becomes more complex. Autopolyploids will have an additional copy of the homologous chromosome, running the risk of the formation of multivalents, that might be incorrectly resolved, unevenly segregating chromosomes and resulting in aneuploidy. Allopolyploids instead will have homoeologous chromosomes coming from different genomes. Based on the sequence similarity between the two genomes the risk is of homology-based pairing between them and incorrect segregation leading to aneuploidy (Bomblies, 2022; Mercier et al., 2015).

The Cyperaceae family has the peculiar characteristic to host species with holocentric chromosomes. In holocentric organisms, centromeric determinants are not single entities defined in a specific region of the chromosome, but are numerous and equally dispersed on the whole length of the chromosomes. Just like polyploidy, holocentricity is a challenge for meiosis

and requires adaptations. In fact, the abundance of centromeric determinants could lead to errors in the attachment of the spindle fibres, resulting in mis-segregations of chromosomes and aneuploidy (Melters et al., 2012). *Rhynchospora* species adapted to this condition by developing inverted meiosis. Their meiosis is post-reductional and involves the segregation of sister chromatids first, following with the segregation of homologous chromosomes at meiosis II. Even if these species cope very well with this alternative type of meiosis, the consequences on meiotic recombination have not yet been explored (Cabral et al., 2014).

Meiotic molecular adaptations to polyploidy have been the subject of many recent studies. Despite the absence of a clear picture, hints point at an adapted pairing and/or synapsis machinery (Bomblies, 2022). A similar thing can be said for holocentricity: scientists have only scratched the surface of how holocentric species have adapted their meiosis to this challenging condition. Despite many holocentric species coping very well with it, the molecular mechanisms at the basis of their adaptations are still unclear.

Rhynchospora pubera has been proposed as a model organism for holocentric plants as it presents features that allow easy cytological approaches (Cabral et al., 2014; Hofstatter et al., 2022; Marques et al., 2015, 2016a), easy self-propagation and high seed viability. However, a recent breakthrough study revealed that *R. pubera*, thought to be a canonical diploid organism due to a diploid-like meiosis, does instead hide an octoploid state. We found that its genome underwent multiple rounds of WGDs followed by a complex chain of chromosome end-to-end fusions which restored the pre-WGD ancestral chromosome number. This resulted in a plant with an unusual large genome size, quadruplicated gene copy number and a diploid-like meiosis (Hofstatter et al., 2022).

In this chapter I will display a cytological overview of male meiosis of *R. pubera*. With immunocytochemistry methods I will show the level of conservation and the cytological patterns of meiotic proteins, including differences that might be due to specific adaptations to polyploidy and/or holocentricity.

Results

Cytological overview of *R. pubera*

First, we assessed the holocentric nature of its chromosomes. Immunocytochemistry experiments performed with antibodies against the centromeric protein CENH3 showed how this appears on the chromosomes as a linear signal during mitotic metaphase, made of multiple units closely spaced (Figure 17a). Moreover, as reported in previous studies, at the end of the

first meiotic prophase, at diakinesis, five bivalents appear in male meiocytes (Figure 17b)(Cabral et al., 2014; Marques et al., 2016a). This is strong evidence that meiotic recombination is taking place, as bivalents represent homologous chromosomes connected by chiasmata, which is the physical outcome of recombination. Bivalents can be distinguished in different shapes. They can appear as elongated rod-like bivalents, thus having only one distal chiasma, or circular ring-shaped bivalents, formed by two distal chiasmata. This is evidence that CO assurance (e.g. at least one chiasma per bivalent) is maintained. The fact that not only rod-shaped bivalents can be observed, moreover, is evidence that more than one crossover can take place on a chromosome, differently from *C. elegans*, a holocentric nematode where only one chiasma is allowed per bivalent (Garcia-Muse & Boulton, 2007).

Axis structure and meiotic recombination are mostly conserved

We investigated meiotic recombination mechanics in *R. pubera* using immunocytochemistry with antibodies against main meiotic proteins. Early stages of prophase I involve homologous chromosome that are not paired already, and appear as thin threads. This stage is called leptotene. ASY1 is a protein forming the chromosome axis and is fundamental for pairing and recombination (Armstrong et al., 2002; Lambing, Kuo, et al., 2020). As reported in other model species, ASY1 in *R. pubera* appears as a linear signal on the whole length of unpaired chromosomes (Figure 18). After leptotene, chromosomes start to pair and be connected by the synaptonemal complex (SC), a zipper-like structure. This transition stage is called zygotene and ends at pachytene, when chromosomes are fully paired and synapsed. ZYP1 represents the traverse filament of the SC and it is a robust marker for its assembly. Moreover, ZYP1 is in
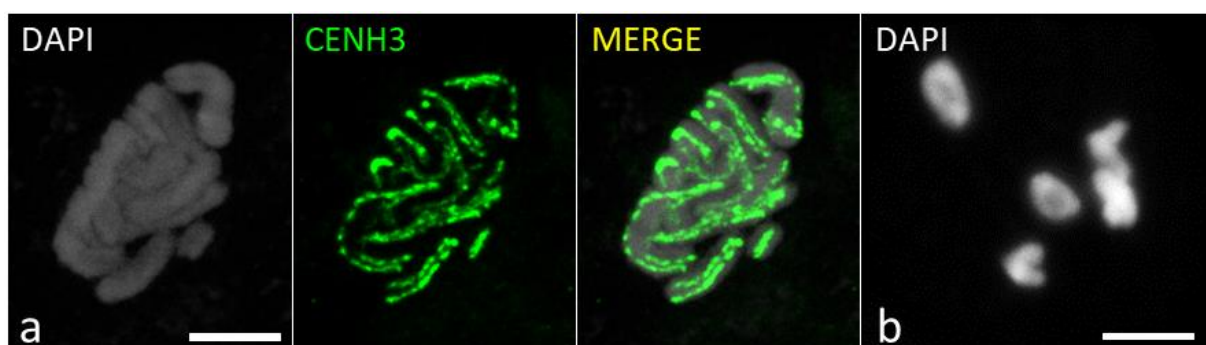
Figure 17

Immunocytochemistry of mitosis and male meiosis of *R. pubera*. **(a)** Mitotic prophase, CENH3 signal is linearly distributed as a double line after the duplication of genomic material. **(b)** Meiotic stage of diakinesis, where five bivalents can be distinguished, evidence of the presence of chiasmata as a result of recombination. Maximum projection is shown. DNA is counterstained with DAPI. Scale bar = 5 μm.

many species essential for recombination and imposition of CO interference (Barakate et al., 2014; Capilla-Pérez et al., 2021). Interestingly, despite having the formation of a linear signal from ZYP1, we cannot ever see instances where it is covering the entire chromosome length (Figure 19a). Even more intriguing is the different length of the stretches we see. At the same time, we see very long lines and very short fragments, indicating an incomplete or uneven synapsis. HEI10 is a key recombination protein, responsible for the maturation of recombination intermediates. HEI10 is supposed to be loaded as many closely spaced foci, thus forming lines. Later on, most of the foci will disappear, except for a few that will grow in intensity, marking final class I COs (Chelysheva et al., 2012; Morgan et al., 2021; K. Wang et al., 2012). Remarkably, we observed a similar behaviour of HEI10 in *R. pubera*, where its loading is subordinate to the formation of the SC as it colocalizes with ZYP1 (Figure 19a). Indeed, we noticed that despite the uneven extension of ZYP1 lines in late pachytene, COs are being processed into few high-intensity HEI10 foci. No HEI10 signal appear in absence of ZYP1 (Figure 19a). At late prophase I (diplotene and diakinesis), ZYP1 signal disappears and 5-8 HEI10 foci are mostly observed (Figure 19b).

The last stage of prophase I is diakinesis, where homologous chromosomes are represented by bivalents and connected by chiasmata. MLH1 is a robust marker widely used in other models to mark final class I COs. MLH1 is responsible for the final resolutive step to finalize COs (Chelysheva et al., 2010; Lhuissier et al., 2007). Similar to HEI10, during diakinesis in *R.*
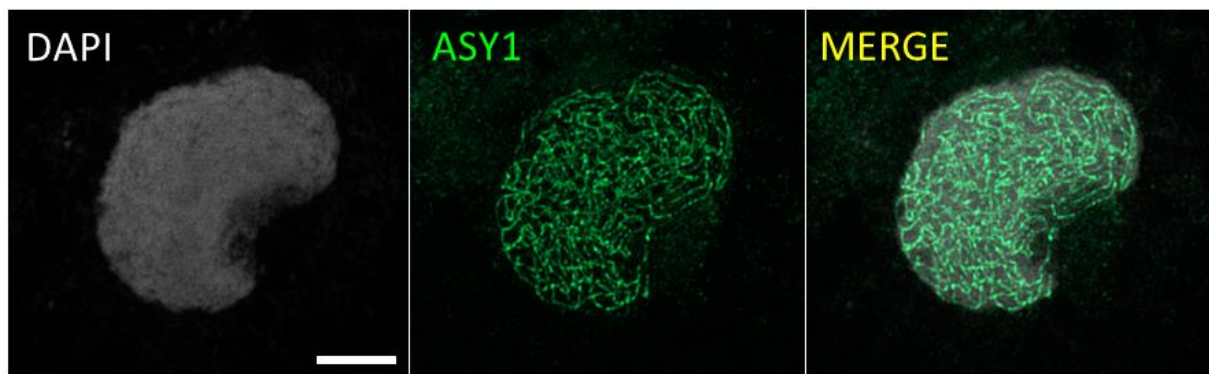
Figure 18

Meiotic stage of leptotene, where the linear signal of the axis component ASY1 can be seen as lines running over the entire length of unpaired chromosomes. Maximum projection is shown. DNA is counterstained with DAPI. Scale bar = 5µm
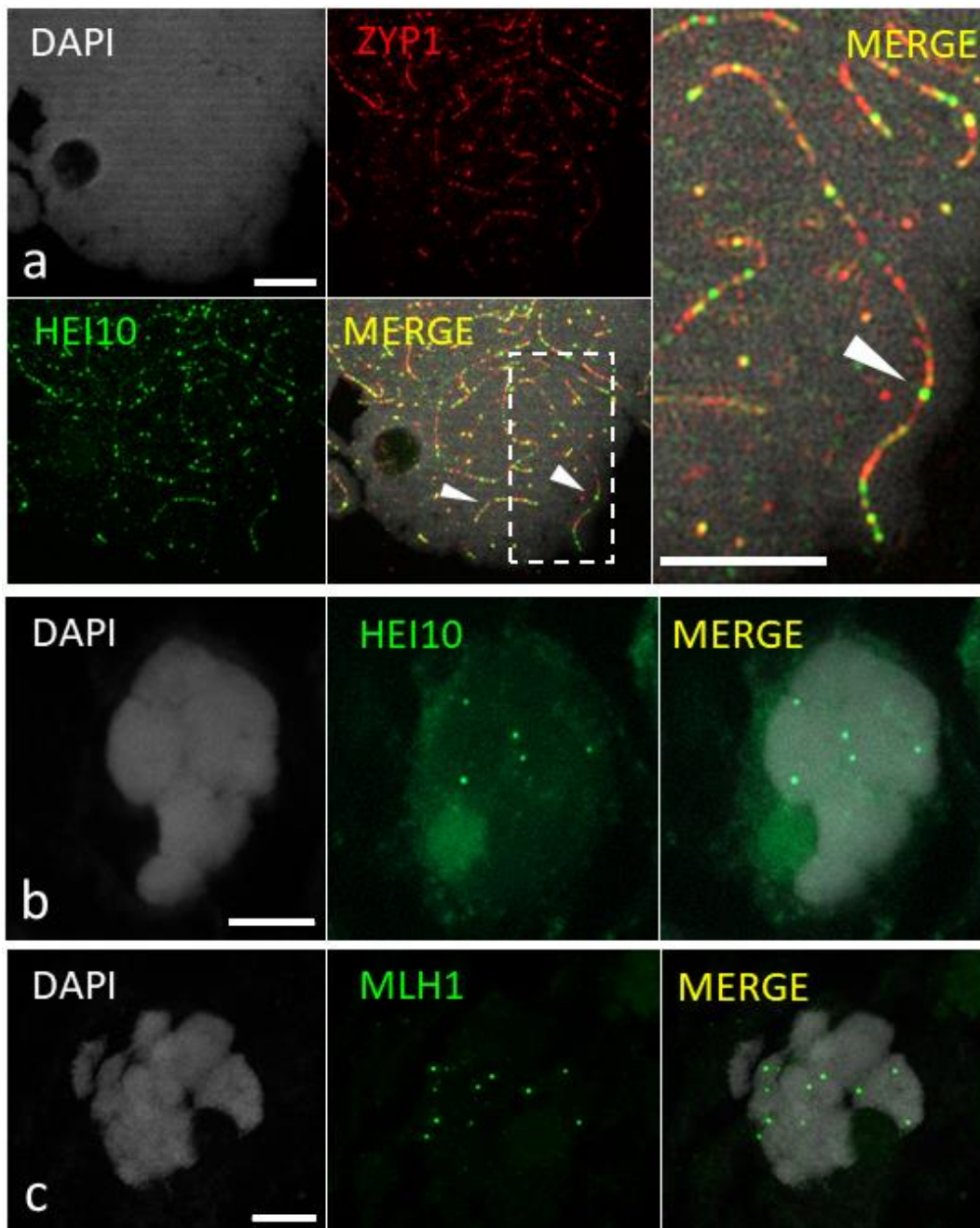
Figure 19

Immunolocalization of meiotic recombination proteins in male meiosis of *R. pubera*. **(a)** Pachytene cell with the formation of ZYP1 lines representing SC (red) and coarsening of HEI10 signal into final recombination intermediates (green). Note the different lengths of SC, despite HEI10 being already processed into foci, hinting at an altered loading of ZYP1 (white arrows). The detail highlights the processing step of HEI10 (green) being displayed as high intensity foci on SC segment (red). **(b)** Late prophase I cell where HEI10 (green) is only displayed as foci, marking recombination spots. **(c)** MLH1 (green) is loaded as foci in late prophase I stages, where it marks COs and chiasmata. Maximum projection is shown, and DNA is counterstained with DAPI. Images were acquired with a Zeiss Axio Imager Z2 with Apotome system. Scale bar = 5 µm.

pubera, MLH1 signal appears as foci on bivalents, marking class I COs (Figure 19c, Figure 20).

Moreover, we used MLH1 to study foci positioning, confirming that usually rod-shaped

bivalents have one focus in the middle, whereas ring-shaped bivalents have two foci at each
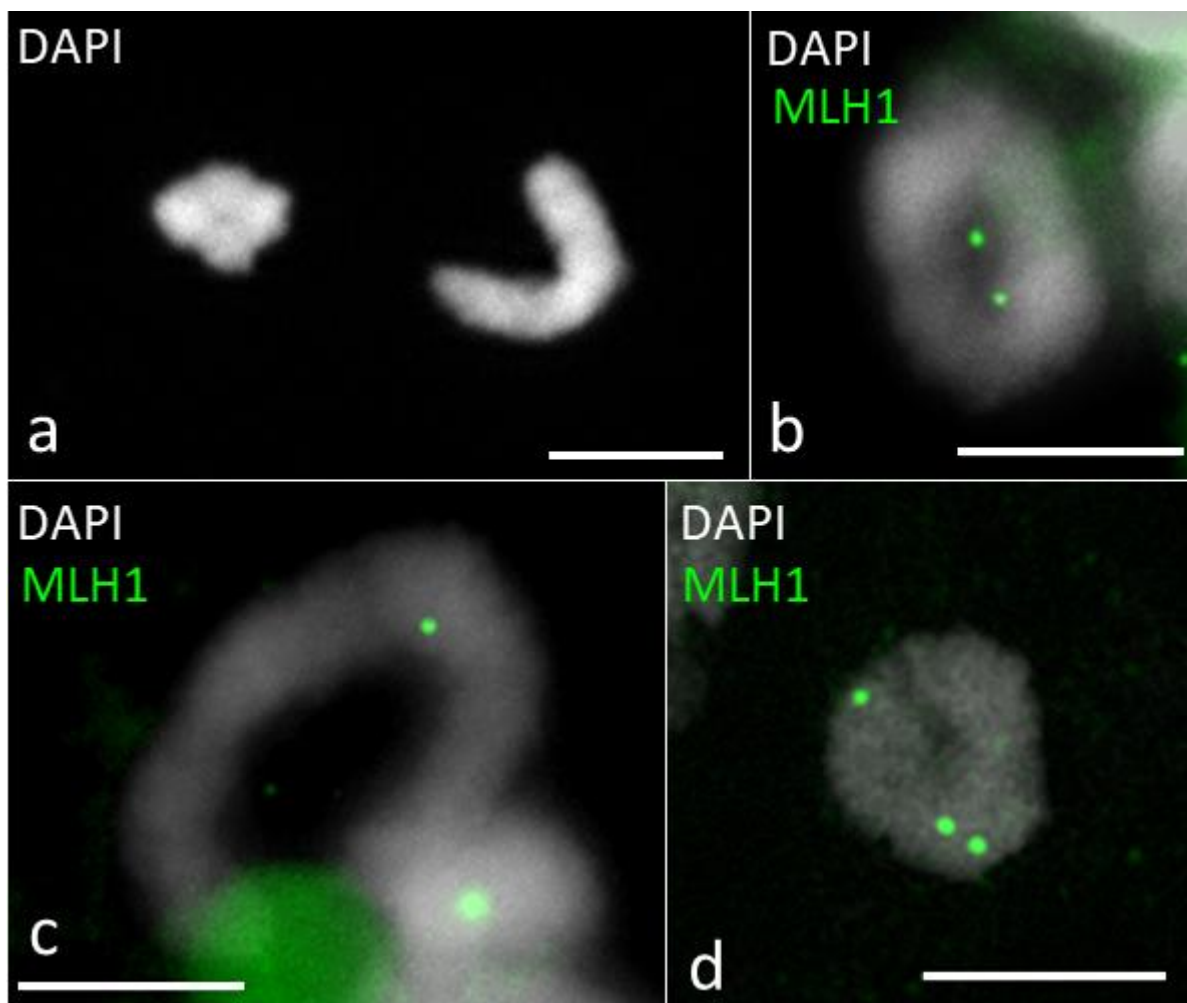
Figure 20

Cytological study of bivalents shapes in *R. pubera*. **(a)** Most bivalents assume a circular and compact ring shape (left) or an elongated rod shape (right) with the homologous chromosomes usually not aligned. **(b)** Ring-shaped bivalents appear with two CO foci (green) on opposite extremities, hinting at recombination happening at distal regions. **(c)** Rod-shaped bivalents only carry one CO focus (green) in the middle, hinting at recombination taking place at only one distal region. **(d)** Other shapes are rarer, but occasionally we observe 3 foci, two of which seemingly happening close to each other. Maximum projections are shown. Chromosomes are counterstained with DAPI. Scale bar = 5 μm.

chromosome ends. However, rare instances hint at other shapes generated by three CO foci, two of which are positioned towards the same chromosome end, close to each other (Figure 20b, c, d). We further computed the number of HEI10 (n=31) and MLH1 (n=84) foci and found a median of 7 foci for both, despite HEI10 showing a slightly significantly lower mean number (Figure 21). Interestingly, we found a slightly higher number of MLH1 foci in *R. pubera* when compared to the true diploid *R. breviuscula*, which share the same chromosome number but no recent WGD event (Figure 22).

RHP1 (*Rhynchospora* HEI10 Paralog 1)

During the genomic analysis of *R. pubera* we investigated the level of conservation of its meiotic machinery. As was done for *R. tenuis* (See Chapter 2, Table 1), we assessed the presence of the most important genes involved in the Class I CO pathway of *R. pubera* (not shown). Our first observation was that all genes were present as multiple copies as expected by the hidden octoploid nature of the *R. pubera* genome. The copies resulting from the quadruplication share a very high degree of identity, and almost no polymorphisms at paralogous CDS copies. However, we encountered an additional copy of the key meiotic gene HEI10, that recently gathered a lot of attention. HEI10 has been reported recently to be the very most important

R. pubera

$W_{\text{Mann-Whitney}} = 819.50$, $p = 1.79e\text{-}03$, $\hat{r}_{\text{biserial}}^{\text{rank}} = -0.37$, $CI_{95\%}$ [-0.56, -0.15], $n_{\text{obs}} = 115$
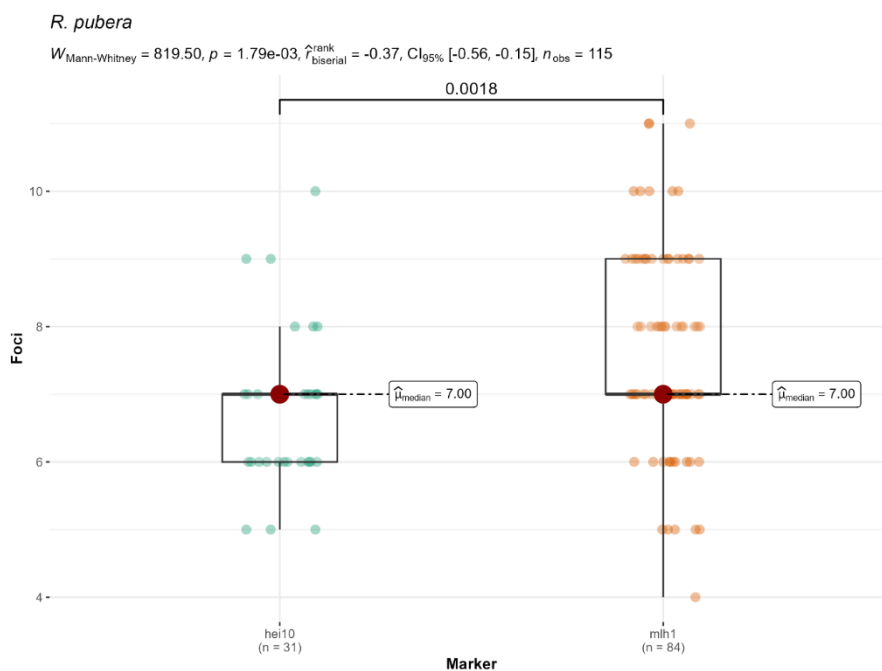
Figure 21

Foci counting for HEI10 (left) and MLH1 (right) in *R. pubera*. Both counting respect the model that includes CO assurance and presence of two ring-shaped bivalents and three rod-shaped bivalents, thus explaining the median of 7 foci. However, there is a significant difference between HEI10 and MLH1 (p=0.0018). Plots were made in R using the ggstatsplot package (Indrajeet Patil 2021).

MLH1 Foci Count

$W_{\text{Mann-Whitney}} = 1588.50$, $p = 7.27e\text{-}10$, $\hat{r}_{\text{biserial}}^{\text{rank}} = -0.54$, $CI_{95\%}$ [-0.65, -0.40], $n_{\text{obs}} = 166$
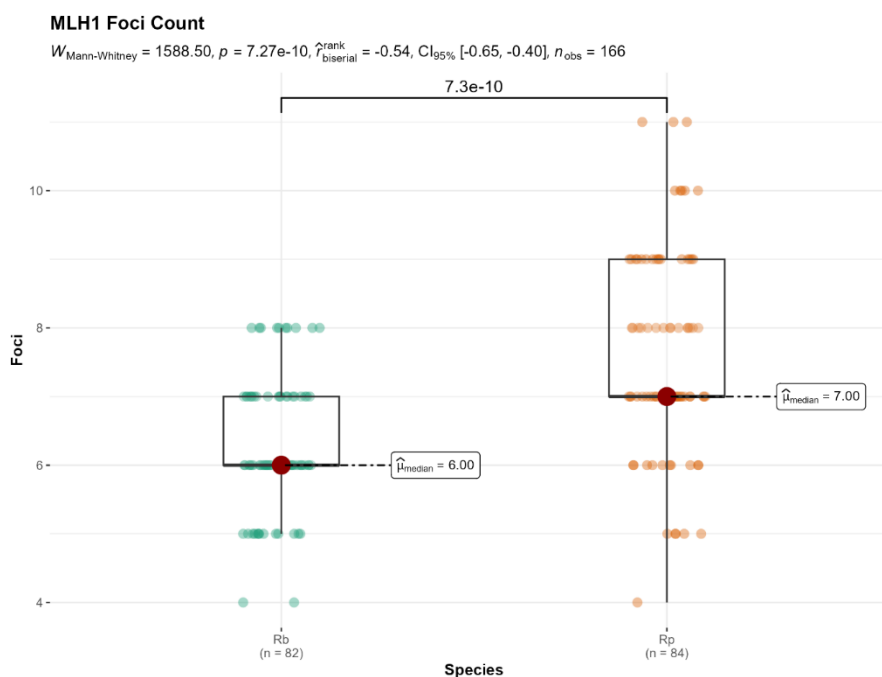
Figure 22

Comparison of MLH1 counted for *R. breviuscula* (left) and *R. pubera* (right). Despite the same chromosome number, there is a significant difference (p=7.3e^-10) in MLH1 foci number. The plot was made in R with the package ggstatsplot (Indrajeet Patil 2021).

regulator of meiotic recombination. The paralog, that we named RHP1 (*Rhynchospora* HEI10 paralog 1), is uniquely shared by both Cyperaceae and Juncaceae lineages (Figure 23). Interestingly, both lineages have species with holocentric chromosomes. The protein alignment showed conserved functional domains, but divergency in the rest of the sequence, especially at the c-terminus (Figure 24). This feature was exploited to design specific antibodies able to discriminate the paralog from the original copy. When these antibodies were used in the first immunocytochemistry experiments, the results were unexpected. In late prophase I stages
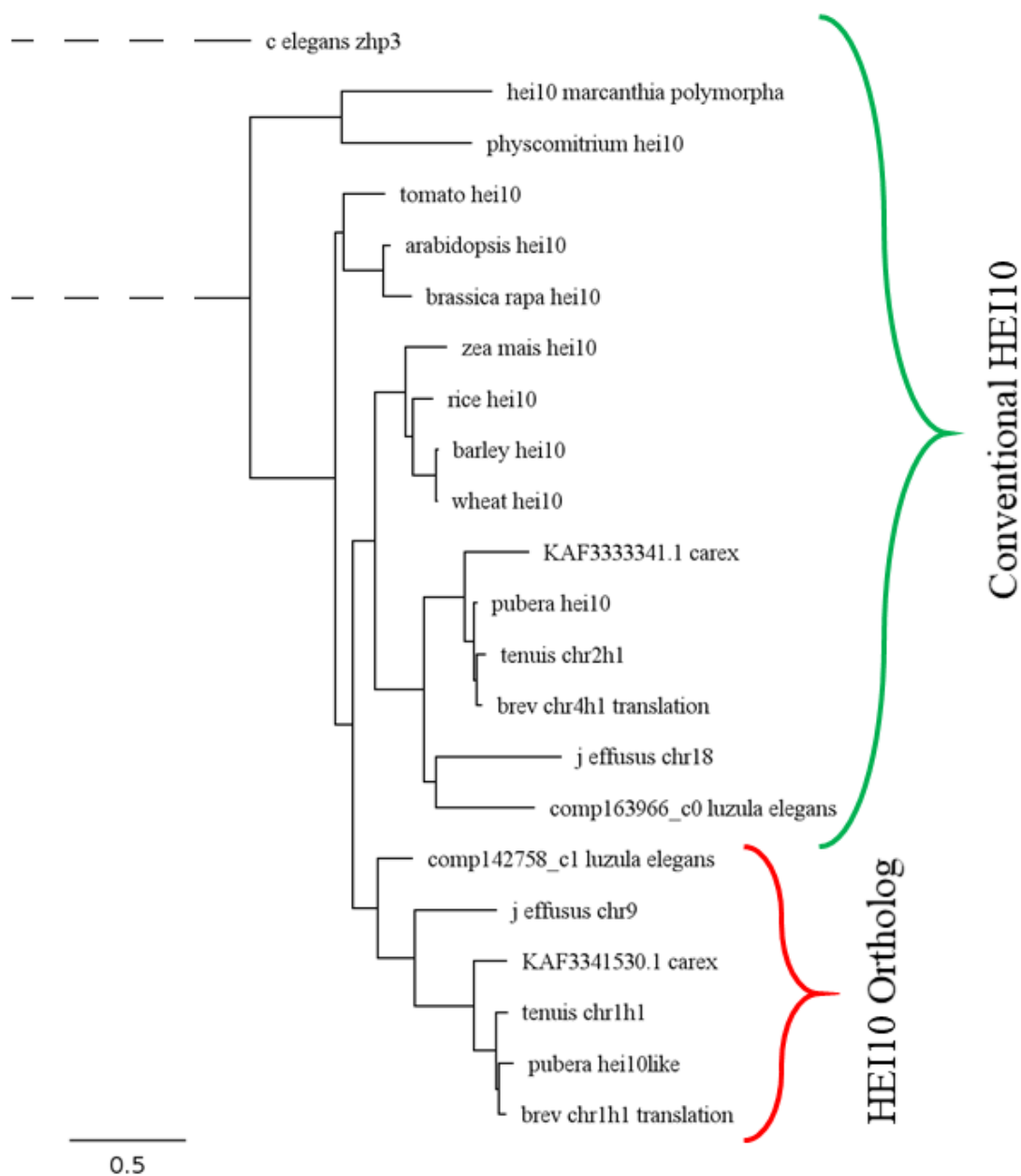
Figure 23

Phylogenetic tree showing the duplication of HEI10 specific to Juncaceae (*Luzula* and *Juncus*) and Cyperaceae (*Carex* and *Rhynchospora*) in the red bracket.

(diplotene and diakinesis), RHP1 maintains the same localization pattern as HEI10: high intensity foci marking class I COs, colocalizing with both HEI10 and MLH1 (Figure 25). When counted, RHP1 foci number was not significantly different from HEI10 or MLH1 (Figure 26). However, when observed in earlier stages (zygotene and pachytene), where HEI10 is displaying its "coarsening" behaviour (See Chapter 1), RHP1 shows no signal at all (Figure 27). Formally, RHP1 displays the exact same pattern as MLH1. These analyses were repeated and further confirmed in *R. breviuscula* (See Chapter 1).

Discussion

Our cytological results show a mostly conserved scenario of meiotic recombination for *R. pubera*. The conservation of MLH1 and HEI10 pattern at the end of prophase I as foci on five bivalents, is strong evidence that recombination is happening and the final result, chiasmata, can be achieved consistently. Moreover, the number of counted foci is evidence of the conservation of CO assurance and CO interference. The first is the assurance that at least one CO will happen per bivalent, the second is the phenomenon that prevents multiple COs from happening in close proximity to each other. The same level of conservation can be observed for the first steps of prophase I, where we see a conserved behaviour of ASY1, appearing as lines on unpaired chromosomes. However, the situation becomes more complex if we look at the intermediate stages, represented by zygotene and pachytene. In fact, we never observed a full synapsis, where ZYP1 linear signal is involving the whole length of all five chromosome pairs. We do not have evidence of altered pairing itself, that might be achieved completely even without the full extension of the SC. If we compare the maturation of HE10 foci with the
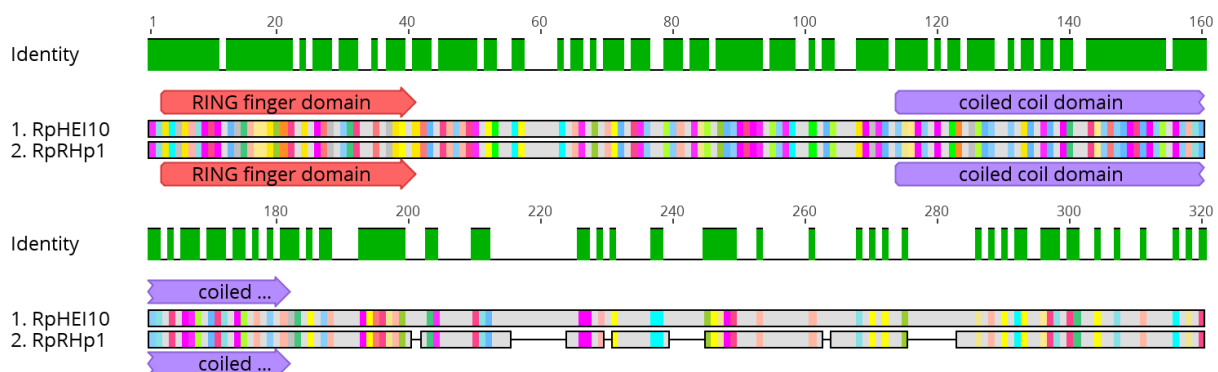
Figure 24

Protein alignment between HEI10 and the paralog RHP1. Sequences become gradually divergent towards the end of the AA chain. The RING finger domain and the coiled coil domain are the most conserved regions. Sequence divergence was exploited to design paralog-specific antibodies.
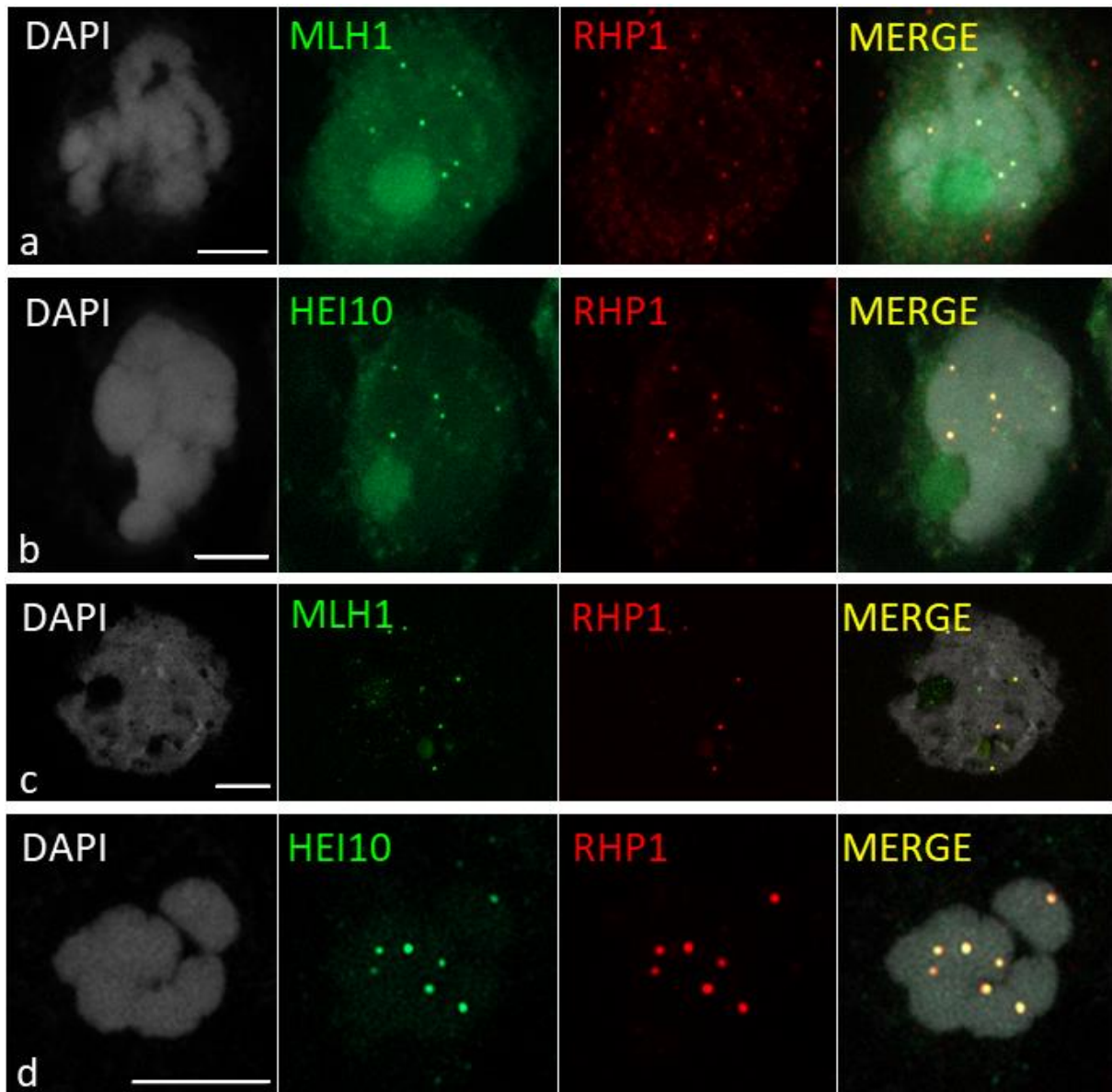
Figure 25

Immunocytology study of RHP1, HEI10 and MLH1 at late prophase I stages (diplotene and diakinesis). In *R. pubera*, RHP1 (red) appears as bright foci on bivalents at the end of recombination, co-localising with both HEI10 and MLH1 (green) (a, b). In *R. breviuscula* the situation is the same, with RHP1 (red) marking Class I COs and co-localising with HEI10 and MLH1 (green) (c, d). Maximum projection is shown and DNA is counterstained with DAPI. Scale bars = 5 μm.

extension of the SC, something seems inconsistent. In fact, the emerging of high-intensity foci of HEI10 is supposed to happen at pachytene, when synapsis is complete. However, when HEI10 displays this pattern, we see a variance of length in the stretches of ZYP1, where some of them are long, but others are relatively much shorter. The robustness of HEI10 as a marker and its behaviour at diakinesis, cast no doubt that HEI10 is very conserved and most likely not the issue.

On the other hand, pairing and synapsis proteins have been pointed out as possible responsible for adaptations to polyploidy in other species. However, we must note that the genome of *R. pubera* is different from the most commonly studied polyploid, as *R. pubera* underwent several rounds of chromosomal end-to-end fusions. It is speculated that one of the first meiotic adaptations for neo-polyploids is the reduction of the total number of crossovers, as a strategy to reduce the possible negative outcomes, mostly the formation of multivalents. When studying COs detected cytologically, we compared *R. pubera* with its relative *R. breviuscula*, that maintained the ancestral chromosome number without undergoing WGDs or end-to-end fusion. We noticed a significant difference between MLH1 foci number in the two species (Figure 22). However, the difference does not reflect the two rounds of WGD in *R. pubera*. Actually, the end-to-end fusions restored the original chromosome number of *R. pubera*, and chromosome number is an important drive to regulate CO number, as only one CO is necessary for each chromosome pair (CO assurance). The current CO number of *R. pubera* might be the result of an initial increase generated by the WGDs. Then, the plasticity granted by the holocentric nature of its chromosomes allowed to reduce its chromosome number by end-to-end fusions, making an increased number of COs unnecessary and undesired, encouraging the species to go back to ancestral recombination frequencies similar to the ones of *R. breviuscula*.

The research on polyploid plants has been only scratching the surface of how the synapsis machinery can adapt to polyploidy, but none of the well-studied polyploid plants have had extensive end-to-end chromosome fusions. On the other hand, chromosome fusions have been studied only in few models, like *C. elegans*. As an additional layer of complexity, these two features have never been studied together in a holocentric eukaryote at the meiosis level. In summary, our results report how meiotic recombination can be highly conserved even in an organism with a unique genomic configuration, made of a combination of polyploidy, end-to-end chromosome fusions and holocentricity. Specifically, the observations made at zygotene and pachytene, where no continuous and complete synapsis can be observed, create an interesting and deep gap of knowledge that recent and future advances in plant biology regarding meiotic adaptations to holocentricity, polyploidy and chromosome fusions, might help to fulfil.

In addition, the discovery of the HEI10 paralog RHP1 gives increased value to the genus *Rhynchospora*. HEI10 is gaining great attention as the key regulator of recombination, and a

R. pubera

$\chi^2_{Kruskal-Wallis}(2) = 10.68, p = 4.80e\text{-}03, \hat{\varepsilon}^2_{ordinal} = 0.06, CI_{95\%} [0.03, 1.00], n_{obs} = 174$

R. breviuscula

$\chi^2_{Kruskal-Wallis}(2) = 12.91, p = 1.58e\text{-}03, \hat{\varepsilon}^2_{ordinal} = 0.08, CI_{95\%} [0.04, 1.00], n_{obs} = 159$
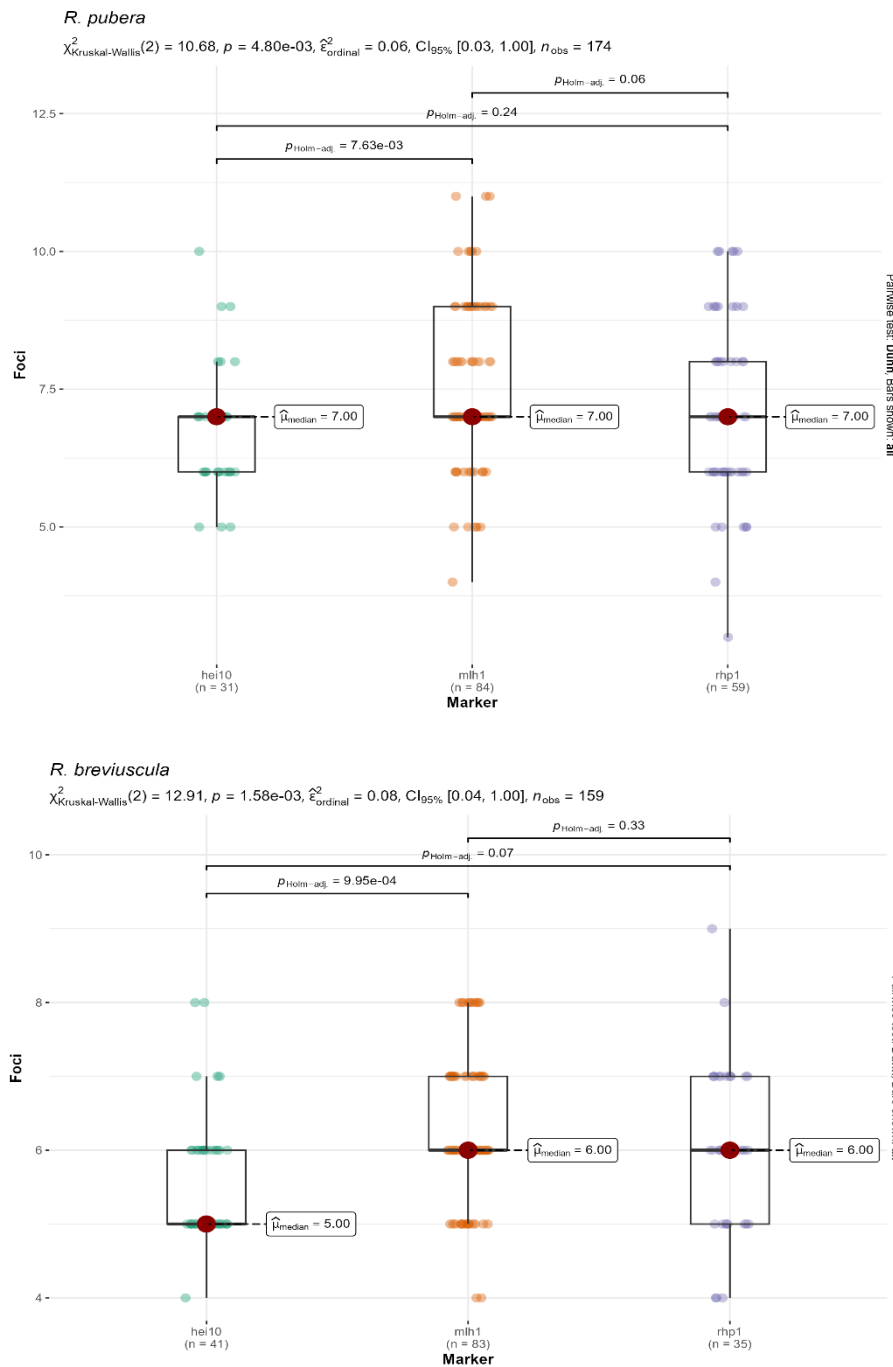
Figure 26

RHP1 foci counting compared with MLH1 and HEI10, for *R. pubera* (top) and *R. breviuscula* (bottom). RHP1 foci number was found to be not significantly different from HEI10 and MLH1 foci number for both species (p>0.05). Plot was made in R with the package ggstatsplot (Indrajeet Patil 2021).

paralog with a putative different function might help to shed light on the original gene. In fact, we demonstrate how RHP1 is a robust cytological marker for COs, as it colocalizes with both MLH1 and HEI10. However, the absence of its signal prior to diplotene poses an interesting novelty. The molecular function of HEI10 is still not well understood, but the fact that the paralog has a very specific and different pattern to the original copy in different stages, might hint that HEI10 has a dual function in two different steps of recombination. A first "coarsening" function at zygotene and pachytene, where it promotes maturation of putative CO sites, and a stabilization function in later stages, where it interacts with recombination intermediates already designated to be final COs. We propose that RHP1 might have lost the first coarsening function, but retained the second stabilizing function. Nevertheless, with this work we show how an

environmentally successful organism can evolve as a mosaic of challenging genomic conditions.
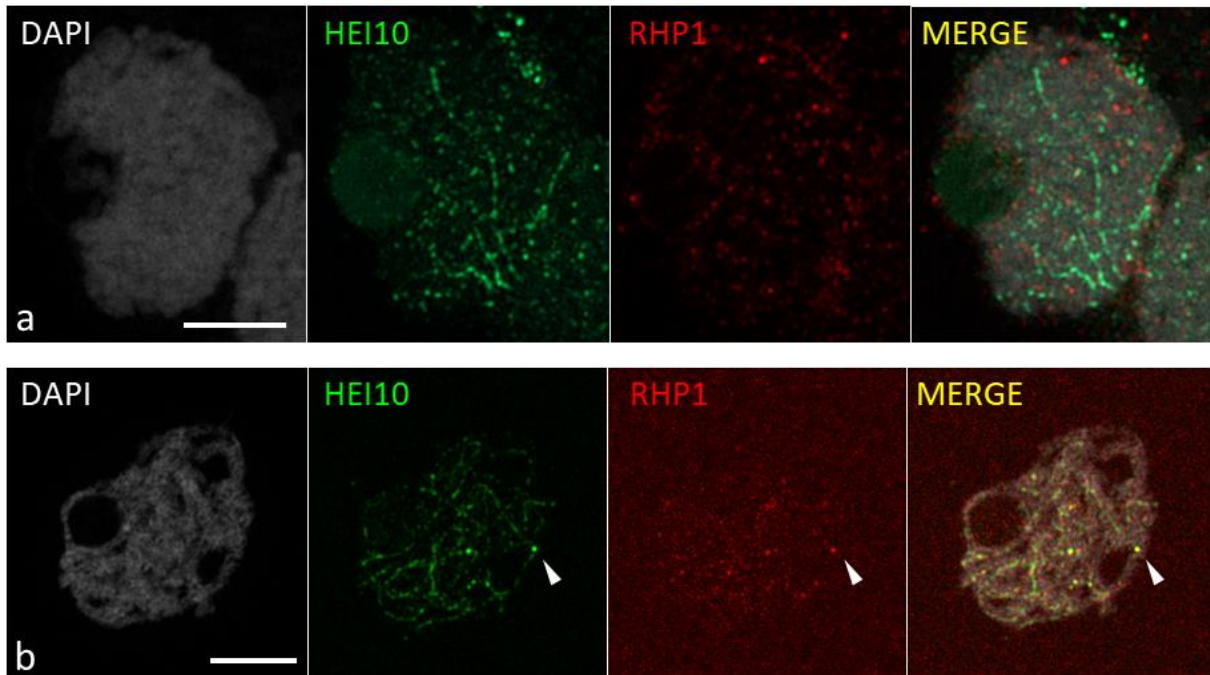
Figure 27

Immunocytochemistry experiment on RHP1 in zygotene (**a**) and pachytene (**b**) showing examples in *Rhynchospora*. (**a**) In *R. pubera*, at zygotene, HEI10 (green) begins to appear as a linear signal on paired chromosomes, however, RHP1 (red) does not appear as a distinguishable signal. Exposure time: green = 150ms, red = 1.200ms. (**b**) In *R. breviuscula*, at late pachytene, when HEI10 (green) is displaying its typical coarsening behaviour (weak linear signal, intense foci signal), RHP1 (red) does not appear as lines. However, we note that the at this stage RHP1 starts to be loaded as foci, consistent with the behaviour detected in later stages (**b**). Exposure time: green = 300ms, red = 300ms. Maximum projection is shown and DNA is counterstained with DAPI. Scale bars = 5 µm.

Materials & Methods

Immunocytochemistry & Cytology

All cytological methods were performed on anthers coming from inflorescences of *R. pubera* plants. Protocols and antibodies, including their working concentrations, are the same described in Chapter 1. The anti-RpRHP1 was a combination of two antibodies raised in rabbit against the peptides CIDIMSDSRDMLRQGKREREEIW and CDTDSAVNMGPPSGDTSNR (Gene ID: RP5G01653920/RP4G01302190/RP2G00897890/RP1G00298020) and affinity-purified (Lifetein).

Identification of RHP1

The HEI10 paralog was identified based on the reference genome of *R. pubera*. The phylogenetic tree was produced by aligning the protein sequences of HEI10 homologs from *C. elegan, M. polymorpha, P. patens, S. lycopersicum, A. thaliana, B. rapa, H. vulgare, O. sativa, Z. mays, T. aestivum, Luzula elegans, J. effusus, C. littledalei, R. pubera, R. tenuis* and *R. breviuscula.* All sequences were downloaded from publicly available databases, or obtained directly by us (Hofstatter et al., 2022). The phylogenetic tree was generated with PhyLM 3.0 (Guindon et al., 2010). The comparison of protein sequences between HEI10 and RHP1 was made by generating consensus sequences for each gene from multiple copies of HEI10 and RHP1 of *R. pubera*. AA sequences were aligned using MAFFT v7.309 (E-INS-I algorithm, BLOSUM62 scoring matrix) (Katoh & Standley, 2013).

Box plots and statistical analyses

HEI10 and MLH1 foci were counted with cytological observations during multiple independent experiments carried out using the same preparation described in Chapter 1. Box plots were generated in R v4.2.3 (R Core Team, 2022) using the ggstatsplot package (Indrajeet Patil, 2021). Statistical significance was verified by Kruskal-Wallis test on case of three groups (Kruskal & Wallis, 1952) and Mann-Whitney test in case of two groups (Mann & Whitney, 1947).

General Conclusions

With this work we have collected observations over three holocentric *Rhynchospora* species with different evolutionary stories: *R. breviuscula*, *R. tenuis* and *R. pubera*. We have now new important insights on how these species adapted their meiotic recombination pathways to conditions such as holocentricity, achiasmy and polyploidy.

The first striking observation is how early meiosis and particularly meiotic recombination are not at all affected by holocentricity itself, despite striking adaptations to meiotic chromosome segregation, i.e., inverted meiosis. If we look at *R. breviuscula*, we clearly see that the meiotic recombination machinery is very well conserved. Not only the presence, but the proximity and distribution of centromeric determinants on the whole chromosomal length does not disturb at all the broad-scale distribution of class I COs. Only a miniature centromere effect was observed at fine-scale. This observation highlights the importance of meiotic recombination among eukaryotes, and how much it can remain conserved even after drastic structural chromosome changes like the transition to holocentricity. Additionally, research about meiotic recombination in plants has always put emphasis on the centromere effect and how it shapes the recombination landscape of species. This work represents the first instance of a recombination overview in plants that is not affected by centromeres in a canonical way. The additional importance of it is that the centromere effect might mask underlying factors shaping CO distribution, like pairing and synapsis progression, that we propose as having a greater than expected effect on the maturation of recombination intermediates. In fact, a telomere-led pairing might give distal genomic regions an advantage, allowing them to process recombination intermediates earlier, therefore increasing recombination rates towards chromosome ends.

The other two species, *R. tenuis* and *R. pubera,* display more challenging conditions like achiasmy and polyploidy. Here it is important to note that in these cases holocentricity is not a burden anymore, but it becomes a tool, as the increased genome plasticity given by the tolerance to chromosome fissions and fusions, is a mean to faster adapt to other mutations like polyploidy and achiasmy. By modulating chromosome number, holocentric *Rhynchsopora* plants can avoid the formation of multivalents and the risk of aneuploidy. The drastic reduction of chromosome number in *R. tenuis* is proposed as a way to cope with achiasmy and a method to narrow segregation scenarios, reducing the chance of aneuploidy, together with other species-specific adaptations. *R. pubera,* in order to cope with the two rounds of WGD, reduced its chromosome number by end-to-end fusions. This prevents the formation of multivalents that might lead to aneuploidy, a common challenge in neo-polyploid plants. Curiously, when other

conditions apart from holocentricity are brought into the equation, meiotic recombination begins to be affected. Achiasmy by itself is a quite unique condition among eukaryotes, and it is interesting that a species could survive this challenge by exploiting being holocentric. Polyploidy, on the other hand, is a common condition among plant species, but *R. pubera* offers a unique example of adaptation through reduction of chromosome number. In both cases, interestingly, the steps of pairing and synapsis seem to be the most delicate checkpoints of meiotic recombination. The recombination machinery of *R. tenuis* is mostly conserved, but we found that SHOC1, an essential actor in meiotic recombination, is not expressed. SHOC1 mutants in other model organisms display impaired synapsis and CO maturation. In *R. pubera*, on the other hand, recombination in achieved normally. However, possibly due to its hidden polyploid nature, pairing and synapsis seem to encounter problems. This suggests that, as reported in recent studies in other plant models, the synaptonemal complex might be the key subject to meiotic adaptations to polyploidy.

Taken together, our results offer new valuable insights into the evolution of holocentricity in the framework of meiotic recombination. The genus *Rhynchospora* is confirmed to be a robust model to study the adaptations of meiotic recombination to drastic centromeric reorganizations. This knowledge will be useful in the future to assess recombination mechanics related to centromeres, and possibly unlock new strategies to improve plant breeding and push the agriculture of the future to tackle global challenges.

Appendix: Protocol for *Agrobacterium* mediated transformation of *Rhynchospora pubera*

Marco Castellani, Gokilavani Thangavel, André Marques – 2020

Updated – 1 Aug 2022

Starting material:

Take *Rhynchospora pubera* flowers. Under a microscope, open flowers looking for immature seeds.

Immature seeds are mostly green (early) or green with brown spots and stripes (late). Both these stages are suitable to isolate immature embryos. The shell must be hard. Do not take mature seeds (completely brown with a harder shell) or seeds that are not ready yet (small, green and very soft).

Gather seeds and place them in a 2ml tube. If seeds are too many the procedure can be scaled up with a 5ml tube. Proceed with the surface sterilization.

Rhynchospora **seeds surface sterilization:**

Materials:

- 2ml sterile tubes (5ml tubes in case of many seeds)
- Saturated Trisodium Phosphate solution (Na3PO4). To prepare this, dissolve an excess of Na3PO4 into water, until the crystals cannot dissolve any further
- Tween-20
- Sodium Hypochlorite solution or commercial bleach. Concentration around 5%.
- Sterile water

Procedure:

1. Place seeds in a 2ml tube and add 1ml of Trisodium Phosphate Saturated solution. Then add a drop of Tween-20 (in case of 5ml tubes, add 3ml of solution)
2. Leave in gentle agitation for 30 min
3. Discard the solution and add 1ml of Sodium Hypochlorite and a drop of Tween-20
4. Leave in gentle agitation for 1 h
5. Discard the solution and under a sterile ventilated hood start rinsing the seeds with sterile water.
6. Wash 5 times or until the smell of Sodium Hypochlorite is gone.
7. Place a disc of sterile blue germination paper on a sterile glass petri dish
8. Place seeds on the paper with some water in preparation for the embryo dissection
9. Note: You can use pre-made solutions of Trisodium Phosphate + 0.1% tween (store at room temp) and Sodium Hypochlorite 5% + 0.1% tween (store at 4°C or room temp)

Now that immature seeds have been cleaned from superficial contaminants, they can be dissected.

Embryo dissection:

Materials:

- Ventilated sterile hood
- Stereomicroscope (*Rhynchospora* seeds are small)
- Sterile forceps and small-blade scalpel
- Sterile water
- Plates of RCI medium

Sterilization and dissection should be done the same day

Procedure:

1. Using a small sterile spoon, take some seeds and place them on a blue germination paper on a sterile support (plastic or glass petri dish) under the microscope. Work with small batches of seeds and change the support frequently. This will minimize the spreading of endophytic contaminations among the sample.
2. Take a seed using forceps and scalpel
3. Holding the seed with the forcep, perform an incision using the scalpel. Cut at one of the extremities of the seed, in order to not damage the embryo at the centre.
4. The embryo sac contains the endosperm and the embryo. If the sac is transparent it can be discarded as it´s not developed enough. Proceed only if the sac is white.
5. (optional) remove the outer membrane of the sac
6. Place the embryo on RCI medium
7. Close the plate with parafilm (otherwise the medium will dry fast) and incubate in darkness at 28°C for 2 weeks. Transfer to fresh medium every 2 weeks and make sure to discard non-embryogenic calli (dark, watery, soft). After 1 week of induction calli are competent for transformation (after 2 weeks they will be bigger, for better manipulation). Calli health will drastically decrease after 5-6 months.

Infection and co-cultivation:

Preparation of *Agrobacterium* culture beforehand:

- Inoculate a single colony of Agro (with vector of interest) into 50ml of liquid YEP + required antibiotics. Grow for 2 nights at 28°C 220rpm
- This is called seed culture that can be stored in the fridge (4°C) for up to 1 month.
- The day before the infection, prepare 3 batches of 50ml YEP + antibiotics. Inoculate different amounts of seed culture in the batches (25ul, 125ul, 250ul) in order to choose the optimal growth rate for Agro the following day. Do this at 6.00 p.m. Use 200ml flasks to allow aeration.

- The day of the transformation, measure the OD600 of the different batches (use clean YEP as control). Do this at around 9.00 a.m. An OD600 < 0.6 is preferred because Agro is supposed to be in exponential phase and very active. Select the desired batch for transformation.

Note: All steps that involve the manipulation of plant tissues must be carried out in sterility conditions with sterile tools and disposables

Infection:

- Take 4ml from the selected Agro batch and divide them into two 2ml tubes.
- Centrifuge 7000 rpm for 5 min to pellet Agro (higher rpm can damage cells)
- Prepare a 50ml tube with 25ml of RAS liquid medium and add 10ul Acetosyringone (from 1M stock) and 50ul Dicamba (2.5 mg/ml stock).
- Remove the supernatant from the 2ml tubes and gently resuspend the pellet with 100ul of RAS liquid medium each
- Transfer the resuspended Agro cells from each 2ml tube into the 50ml tube.
- Take the calli (from 2 to 4 weeks old) developed from embryos from the RCI plate and drop them into the 50ml tube with the RAS liquid medium and Agro.
- Pierce some holes in the lid of the tube. Place a small round sterile filter paper between the lid and the tube and close the tube.
- Place the tube in a vacuum pump for 5-10 minutes.
- Discard the RAS liquid medium by tilting the tube or using a pipette
- Place the calli on RAS-Co (co-cultivation) medium.
- Seal petri dishes with surgical tape and incubate in darkness at 20-22°C for 48h

The transfer of the T-DNA has happened, now it´s time to kill Agro and select transformant calli.

Antibiotic wash and selection:

- Prepare a 50ml tube with 25ml sterile water and add 15ul of Timentin (from 300mg/ml stock)
- Take calli from the RAS-Co plates and drop them into the tube. Wash calli for a few minutes. (when you take calli from the Ras-Co plate you should see small patches of Agro under the calli. This is proof of successful co-cultivation)
- This washing can be repeated in the future in case of agro overgrowth.
- Discard the washing liquid by tilting the tube or with a pipette
- Dry calli on sterile filter paper and place them on RCI + Hyg50 + Tim medium. Seal plates with parafilm.
- Subculture for 14 days at 28°C in darkness, then move calli on fresh medium. Repeat this step again and subculture for 2 more weeks. 4 weeks (in total) are more than enough to distinguish resistant calli from untransformed calli. After this move calli to regeneration.

You should see calli turning completely black. Some calli will develop an individual mass of white, fast-growing, healthy tissue with embryogenic characteristics (mentioned before). White transparent micro-calli that form on the surface of dying calli (similar to bubbles) should be ignored.

Regeneration:

- Selection should be maintained during regeneration (Hyg30).
- Move calli to RpReg medium supplemented with 1 mg/l BAP and 0.5 mg/l NAA. Use this medium to induce a faster greening and shoot development. After shoots have developed, the rotting process can be sped up by using the regeneration medium K4N.
- Subculture every 14 days, seal plates with parafilm and keep at 28°C and long day conditions.
- Calli that developed both roots and shoots can be moved to hormone-free, antibiotic-free ½ MS rooting medium to develop and then to soil

Media preparation:

Note: Media plates must be prepared in sterility conditions and using sterile disposables. Let the media dry well in order to avoid excess condensed water in the plates. Hormone-free media can be stored at room temperature. Media with hormones and antibiotics must be stored at 4°C.

Rhynchospora Callus Induction Medium (RCI)
December 4, 2020:

To induce callus after embryo dissection and before Agro transformation

Part I: 2X Gelrite

Component	Stock concentration	Final concentration	Amount for 1 litre
Gelrite	-	4 g/l	4 g

Dissolve in 500 ml water in a 1 litre bottle and autoclave.

The next day...

Part II: 2X RCI

Component	Stock concentration	Final concentration	Amount for 1 litre
MS salts (M0221)	-	4.4 g/l	4.4 g
Sucrose	-	30 g/l	30 g
Casein hydrolysate	-	1 g/l	1 g

Mix everything, adjust pH to 5.8 – 5.6 with 1M KOH, bring volume to ~490 ml.

Add the following components under sterile hood:

Component	Stock concentration	Final concentration	Amount for 1 litre
100X Vitamins BCI	100X	1X	10 ml
$CuSO_4.5H_2O$	1.25 mg/ml (5mM)	1.25 µg/ml (5 µM)	1 ml
Dicamba	2.5 mg/ml	5 µg/ml	2 ml

Filter sterilize

Part III: RCI

Warm the 2x gelrite and the 2x BCI at 50-60°C in a water bath.

Add the 2X BCI into the bottle with 2X gelrite. Mix together.

Pour the BCI into petri dishes.

***Rhynchospora* Callus Induction Medium + Hygromycin + Timentin (RCI + Hyg + Tim) December 4, 2020**:

To select propagating calli and remove Agrobacterium after infection

Part I: 2X Gelrite

Component	Stock concentration	Final concentration	Amount for 1 litre
Gelrite	-	4 g/l	4 g

Dissolve in 500 ml water in a 1 litre bottle and autoclave.

The next day...

Part II: 2X RCI

Component	Stock concentration	Final concentration	Amount for 1 litre
MS salts (M0221)	-	4.4 g/l	4.4 g
Sucrose	-	30 g/l	30 g
Casein hydrolysate	-	1 g/l	1 g

Mix everything, adjust pH to 5.8 – 5.6 with 1M KOH, bring volume to ~490 ml.

Add the following components under sterile hood:

Component	Stock concentration	Final concentration	Amount for 1 litre
100X Vitamins BCI	100X	1X	10 ml
$CuSO_4.5H_2O$	1.25 mg/ml (5mM)	1.25 µg/ml (5 µM)	1 ml
Dicamba	2.5 mg/ml	5 µg/ml	2 ml
Hygromycin B	50mg/ml	50mg/l	1 ml
Timentin	300mg/ml	150mg/l	0.5 ml

Filter sterilize

Part III: RCI

Warm the 2x gelrite and the 2x BCI at 50-60°C in a water bath.

Add the 2X BCI into the bottle with 2X gelrite. Mix together.

Pour the BCI into petri dishes.

Rhynchospora Regeneration Medium adapted from rice (RpReg)
(FOR SHOOT DEVELOPMENT) - June, 2021:

To regenerate selected calli and induce shoots.

Part I: 2X Gelrite

Component	Stock concentration	Final concentration	Amount for 1l
Gelrite	-	4 g/l	4 g

Dissolve the gelrite in a 1l bottle with 500ml H2O, autoclave.

The next day…

Part II: 2x RpReg

Component	Stock concentration	Final concentration	Amount for 1l
MS salts (M0221)	-	4.4 g/l	4.4 g
Sucrose	-	30 g/l	30 g
Sorbitol		15 g/l	15 g

Mix everything in a 500ml bottle, adjust pH to 5.6-5.8 with 1M KOH, bring volume to **500 ml** H2O

Component	Stock concentration	Final concentration	Amount for 1 liter
6-BAP	1 mg/ml	1 mg/l	1 ml
Hygromycin B	50 mg/ml	30 µg/ml	600 µl
NAA	1mg/ml	0.5mg/l	500 µl
Timentin	300mg/ml	150mg/l	500 µl

Filter sterilize.

Part III: RpReg

Warm up 2x gelrite and 2x RpReg at 50-60°C in a water bath.

Mix them together.

Pour into petri dishes.

Rhynchospora Regeneration Medium + BAP (K4N + BAP)
(FOR ROOT DEVELOPMENT) - December 4, 2020:

To regenerate selected calli and induce shoots and roots.

Part I: 2X Gelrite

Component	Stock concentration	Final concentration	Amount for 1 litre
Gelrite	-	4 g/l	4 g

Dissolve in 500 ml water in a 1 litre bottle and autoclave.

The next day...

Part II: 2X K4N

Component	Stock concentration	Final concentration	Amount for 1 litre
Macronutrients	25X	1X	40 ml
Micronutrients	1000X	1X	1 ml
FeNaEDTA	1000X	27.5 mg/l	1 ml
KNO$_3$	-	3640 mg/l	3.64 grams
Sucrose	-	30 g/l	30 g
Glutamine	-	146 mg/l	146mg
Gamborg B5 Vitamins	112 mg/ml (1000X)	112 mg/l (1X)	1 ml

Mix everything, adjust pH to 5.8 – 5.6 with 1M KOH, bring volume to 500 ml.

Add the following components under sterile hood:

Component	Stock concentration	Final concentration	Amount for 1 litre
6-BAP	1 mg/ml	0.225 mg/l	225 µl
Hygromycin (Roche)	50 mg/ml	30 µg/ml	600 µl
Timentin	300mg/ml	150mg/l	500 µl

Filter sterilize

Part III: K4N + BAP

Warm the 2x gelrite and the 2x K4N at 50-60°C in a water bath.

Add the 2X BCI into the bottle with 2X gelrite. Mix together.

Pour the BCI into petri dishes.

Rhynchospora **Rooting Medium (1/2 MS)**
December 4, 2020:

To allow regenerating calli to develop into full plants in hormone-free medium, after the appearance of shoots and roots

Component	Stock concentration	Final concentration	Amount for 1 litre
MS salts (M0221)	-	2.2 g/l	2.2 g
Gelrite	-	4 g/l	4 g
Sucrose	-	15g/l	15 g

Bring to volume with water, autoclave and pour into sterile glass pots.

Rhynchospora **Infection Medium (RAS)**
December 4, 2020:

For infection of Rhynchospora embryos with Agrobacterium

Part I: Concentrated medium without Cysteine and Acetosyringone

Component	Stock concentration	Final concentration	Amount for 500 ml
MS salts (M0221)	-	4.4 g/l	2.2 g
Sucrose	-	20 g/l	10 g
Glucose		10 g/l	5 g
Casein hydrolysate	-	1 g/l	0.5 g
100X Vitamins BCI	100X	1X	5 ml
L-Cysteine	8 g/l (1000X)	8 mg/l (1X)	0.5 ml

Mix everything, adjust pH to 5.8 with 1M KOH, bring volume to **500 ml**, filter sterilize, keep at 4°C.

Part II: Final medium with Dicamba and Acetosyringone

Prepare fresh for each transformation experiment. For one transformation, take 25 ml of **Part I (above)** in a 50ml tube and add the following:

Component	Stock concentration	Final concentration	Amount for 25 ml
Dicamba	2.5 mg/ml	5 ug/ml	50 ul
Acetosyringone	1 M	400 µM	10 µl

Rhynchospora Co-cultivation Medium (RAS-Co)
December 4, 2020:

For co-cultivation of Rhynchospora embryos with Agrobacterium and T-DNA transfer

Part I: 2X Gelrite

Component	Stock concentration	Final concentration	Amount for 500ml
Gelrite	-	4 g/l	2 g

Dissolve the gelrite in a 500ml bottle with 250 H2O, autoclave

Part II: 2x Ras-Co

Component	Stock concentration	Final concentration	Amount for 500 ml
MS salts (M0221)	-	4.4 g/l	2.2 g
Sucrose	-	20 g/l	10 g
Glucose		10 g/l	5 g
Casein hydrolysate	-	1 g/l	0.5 g
100X Vitamins BCI	100X	1X	5 ml
L-Cysteine	8 g/l (1000X)	800 mg/l (1X)	0.5 ml
Dicamba	2.5 mg/ml	5 ug/ml	1ml
Acetosyringone	1 M	250 μM	125 μl

Mix everything in a 250ml bottle, adjust pH to 5.8 with 1M KOH, bring volume to **250 ml**, filter sterilize.

Part III: Ras-Co

Warm up 2x gelrite and 2x ras-co at 50°C, then mix them together and pour into petri dishes. After the medium is solid place a sterile filter paper on top of it. This filter paper will avoid the diffusion of Agro in the medium and will force Agro to use plant tissue as substrate.

Preparation of stock solutions:

Stock solutions for BCI-related Media (December 2020)

100X Vitamin Stock for BCI

Component	Concentration in stock	Amount for 500 ml of stock	Final concentration in medium
Thiamine HCl	100 mg/l	0.05 g	1 mg/l
myo-inositol	35 g/l	17.5 g	350 mg /l
Proline	69 g/l	34.5 g	690 mg/l

Dissolve in ~400 ml, bring volume to 500 ml, filter-sterilize and store at 4°C.

1.25 mg/ml (5 mM) $CuSO_4 \cdot 5H_2O$

Dissolve 125 mg $CuSO_4 \cdot 5H_2O$ in 100 ml water. Filter sterilize and store at 4°C.

2.5 mg/ml Dicamba

For 12 ml: Dissolve 30 mg Dicamba in 10 ml water. Add some drops (measure) of 1M KOH if necessary to help dissolution. Bring volume to 12 ml. Filter-sterilize, divide in 1 ml aliquots and store at -20°C.

8 g/l L-cysteine (L-cysteine maximum solubility is 25 mg/ml)

For 50 ml: Dissolve 400 mg of L-cysteine in 50 m of water. Filter-sterilize onto a Falcon tube and store at 4°C.

100 mM Acetosyringone (3'5'dimethoxy-4'-hydroxy-acetophenone)

For 10 ml: Dissolve 196 mg of acetosyringone in a small amount of DMSO. Bring volume to 10 ml with additional DMSO. Filter-sterilize. Make 0.5-ml aliquots in Eppendorf tubes and store at -20°C.

Stocks with higher concentrations are also fine.

300 mg/ml Timentin

For a 10 g Timetin bottle (Duchefa), add 20 ml water, dissolve, bring volume to 33.3 ml. Filter-sterilize, divide in 1 ml aliquots and store at -20°C.

Gamborg B5 Vitamins

To prepare a 1000x stock solution dissolve 11.2g in 100ml of water. Filter sterilize, separate in aliquots and store at -20°C

Stock solutions for K4N Media - December 2020

25X Macronutrients

Component	Amount for 400 ml of stock (grams)	Final concentration in medium (mg/L)
NH_4NO_3	3.2	320
$CaCl_2 \cdot 2H_2O$	4.41	441
KH_2PO_4	3.4	340
$MgSO_4 \cdot 7H_2O$	2.46	246

Dissolve and bring volume to 400 ml. Filter-sterilize, keep at room temperature and aliquot in the hood when needed

1000X Micronutrients

Component	Amount for 1 litre of stock (grams)	Final concentration in medium (mg/L)
$MnSO_4 \cdot H_2O$	9.6	9.6
H_3BO_3	3.1	3.1
$ZnSO_4 \cdot 7H_2O$	7.2	7.2
$CuSO_4 \cdot 5H_2O$	1.25	1.25
KI	0.17	0.17
$Na_2MoO_4 \cdot 2H_2O$	0.12	0.12
$CoCl_2 \cdot 6H_2O$	0.024	0.024

Dissolve and bring volume to 1000 ml. Autoclave, keep at room temperature and aliquot in the hood when needed.

1000X FeNaEDTA (27.5 g/l)

For 100 ml: Dissolve 2.75 g in water and bring volume to 100 ml. Filter-sterilize, keep at room temperature **in the dark** and aliquot under the hood when needed.

1 mg/ml 6-BAP

Dissolve 12 mg in 9 ml water and a few drops (~300 µl) of 1M NaOH. Bring volume to 12 ml. Filter-sterilize. Store at -20°C in 1-ml aliquots. Pre-made commercial solution is also fine.

1 mg/ml 1-NAA

Dissolve 50mg of 1-NAA powder in 50ml EtOH, filter sterilize, store at 4°C in darkness.

References

Allers, T., & Lichten, M. (2001). Differential timing and control of noncrossover and crossover recombination during meiosis. *Cell*, *106*(1), 47–57. https://doi.org/10.1016/s0092-8674(01)00416-0

Armstrong, S. J., Caryl, A. P., Jones, G. H., & Franklin, F. C. (2002). Asy1, a protein required for meiotic chromosome synapsis, localizes to axis-associated chromatin in Arabidopsis and Brassica. *J Cell Sci*, *115*(Pt 18), 3645–3655. https://doi.org/10.1242/jcs.00048

Baez, M., Kuo, Y. T., Dias, Y., Souza, T., Boudichevskaia, A., Fuchs, J., Schubert, V., Vanzela, A. L. L., Pedrosa-Harand, A., & Houben, A. (2020). Analysis of the small chromosomal Prionium serratum (Cyperid) demonstrates the importance of reliable methods to differentiate between mono- and holocentricity. *Chromosoma*, *129*(3–4), 285–297. https://doi.org/10.1007/s00412-020-00745-6

Barakate, A., Higgins, J. D., Vivera, S., Stephens, J., Perry, R. M., Ramsay, L., Colas, I., Oakey, H., Waugh, R., Franklin, F. C., Armstrong, S. J., & Halpin, C. (2014). The synaptonemal complex protein ZYP1 is required for imposition of meiotic crossovers in barley. *Plant Cell*, *26*(2), 729–740. https://doi.org/10.1105/tpc.113.121269

Beadle, G. W. (1932). *A Possible Influence of the Spindle Fibre on Crossing-Over in Drosophila*. *18*(2), 160–165. https://doi.org/doi:10.1073/pnas.18.2.160

Berardini, T. Z., Reiser, L., Li, D., Mezheritsky, Y., Muller, R., Strait, E., & Huala, E. (2015). The arabidopsis information resource: Making and mining the "gold standard" annotated reference plant genome. *Genesis*, *53*(8), 474–485. https://doi.org/10.1002/dvg.22877

Birky, C. W. (1996). Heterozygosity, Heteromorphy, and Phylogenetic Trees in Asexual Eukaryotes. *Genetics*, *144*(1), 427–437. https://doi.org/10.1093/genetics/144.1.427

Blokhina, Y. P., Nguyen, A. D., Draper, B. W., & Burgess, S. M. (2019). The telomere bouquet is a hub where meiotic double-strand breaks, synapsis, and stable homolog juxtaposition are coordinated in the zebrafish, Danio rerio. *PLOS Genetics*, *15*(1), e1007730. https://doi.org/10.1371/journal.pgen.1007730

Bomblies, K. (2022). Learning to tango with four (or more): The molecular basis of adaptation to

polyploid meiosis. *Plant Reproduction*. https://doi.org/10.1007/s00497-022-00448-1

Braz, G. T., Yu, F., do Vale Martins, L., & Jiang, J. (2020). Fluorescent In Situ Hybridization Using

Oligonucleotide-Based Probes. In B. S. Nielsen & J. Jones (Eds.), *In Situ Hybridization*

Protocols (pp. 71–83). Springer US. https://doi.org/10.1007/978-1-0716-0623-0_4

Brazier, T., & Glémin, S. (2022). Diversity and determinants of recombination landscapes in flowering

plants. *PLOS Genetics*, *18*(8), e1010141. https://doi.org/10.1371/journal.pgen.1010141

Butlin, R. (2002). The costs and benefits of sex: New insights from old asexual lineages. *Nature*

Reviews Genetics, *3*(4), 311–317. https://doi.org/10.1038/nrg749

Cabral, G., Marques, A., Schubert, V., Pedrosa-Harand, A., & Schlögelhofer, P. (2014). Chiasmatic and

achiasmatic inverted meiosis of plants with holocentric chromosomes. *Nature*

Communications, *5*(1), 5070. https://doi.org/10.1038/ncomms6070

Campos-Martin, R., Schmickler, S., Goel, M., Schneeberger, K., & Tresch, A. (2023). Reliable

genotyping of recombinant genomes using a robust hidden Markov model. *Plant Physiology*,

kiad191. https://doi.org/10.1093/plphys/kiad191

Campoy, J. A., Sun, H., Goel, M., Jiao, W.-B., Folz-Donahue, K., Wang, N., Rubio, M., Liu, C., Kukat, C.,

Ruiz, D., Huettel, B., & Schneeberger, K. (2020). Gamete binning: Chromosome-level and

haplotype-resolved genome assembly enabled by high-throughput single-cell sequencing of

gamete genomes. *Genome Biology*, *21*(1), 306. https://doi.org/10.1186/s13059-020-02235-5

Capilla-Pérez, L., Durand, S., Hurel, A., Lian, Q., Chambon, A., Taochy, C., Solier, V., Grelon, M., &

Mercier, R. (2021). The synaptonemal complex imposes crossover interference and

heterochiasmy in Arabidopsis. *Proc Natl Acad Sci U S A*, *118*(12).

https://doi.org/10.1073/pnas.2023613118

Cardinale, B. J., Duffy, J. E., Gonzalez, A., Hooper, D. U., Perrings, C., Venail, P., Narwani, A., Mace, G.

M., Tilman, D., Wardle, D. A., Kinzig, A. P., Daily, G. C., Loreau, M., Grace, J. B., Larigauderie,

A., Srivastava, D. S., & Naeem, S. (2012). Biodiversity loss and its impact on humanity. *Nature*, *486*(7401), 59–67. https://doi.org/10.1038/nature11148

Castle, L. A., Wu, G., & McElroy, D. (2006). Agricultural input traits: Past, present and future. *Current Opinion in Biotechnology*, *17*(2), 105–112. https://doi.org/10.1016/j.copbio.2006.01.011

Ceplitis, A. (2003). Coalescence times and the Meselson effect in asexual eukaryotes. *Genet Res*, *82*(3), 183–190. https://doi.org/10.1017/s0016672303006487

Chelysheva, L., Grandont, L., Vrielynck, N., le Guin, S., Mercier, R., & Grelon, M. (2010). An Easy Protocol for Studying Chromatin and Recombination Protein Dynamics during *Arabidopsisthaliana* Meiosis: Immunodetection of Cohesins, Histones and MLH1. *Cytogenetic and Genome Research*, *129*(1–3), 143–153. https://doi.org/10.1159/000314096

Chelysheva, L., Vezon, D., Chambon, A., Gendrot, G., Pereira, L., Lemhemdi, A., Vrielynck, N., Le Guin, S., Novatchkova, M., & Grelon, M. (2012). The Arabidopsis HEI10 Is a New ZMM Protein Related to Zip3. *PLOS Genetics*, *8*(7), e1002799. https://doi.org/10.1371/journal.pgen.1002799

Cheng, H., Concepcion, G. T., Feng, X., Zhang, H., & Li, H. (2021). Haplotype-resolved de novo assembly using phased assembly graphs with hifiasm. *Nature Methods*, *18*(2), 170–175. https://doi.org/10.1038/s41592-020-01056-5

Choi, K., Zhao, X., Tock, A. J., Lambing, C., Underwood, C. J., Hardcastle, T. J., Serra, H., Kim, J., Cho, H. S., Kim, J., Ziolkowski, P. A., Yelina, N. E., Hwang, I., Martienssen, R. A., & Henderson, I. R. (2018). Nucleosomes and DNA methylation shape meiotic DSB frequency in Arabidopsis thaliana transposons and gene regulatory regions. *Genome Research*, *28*(4), 532–546. https://doi.org/10.1101/gr.225599.117

Da Ines, O., Degroote, F., Goubely, C., Amiard, S., Gallego, M. E., & White, C. I. (2013). Meiotic recombination in Arabidopsis is catalysed by DMC1, with RAD51 playing a supporting role. *PLoS Genetics*, *9*(9), e1003787. https://doi.org/10.1371/journal.pgen.1003787

Danecek, P., Bonfield, J. K., Liddle, J., Marshall, J., Ohan, V., Pollard, M. O., Whitwham, A., Keane, T., McCarthy, S. A., Davies, R. M., & Li, H. (2021). Twelve years of SAMtools and BCFtools. *GigaScience*, *10*(2), giab008. https://doi.org/10.1093/gigascience/giab008

Durand, S., Lian, Q., Jing, J., Ernst, M., Grelon, M., Zwicker, D., & Mercier, R. (2022). Joint control of meiotic crossover patterning by the synaptonemal complex and HEI10 dosage. *Nature Communications*, *13*(1), 5999. https://doi.org/10.1038/s41467-022-33472-w

Fozard, J. A., Morgan, C., & Howard, M. (2023). Coarsening dynamics can explain meiotic crossover patterning in both the presence and absence of the synaptonemal complex. *ELife*, *12*, e79408. https://doi.org/10.7554/eLife.79408

Garcia-Muse, T., & Boulton, S. J. (2007). Meiotic recombination in Caenorhabditis elegans. *Chromosome Research*, *15*(5), 607–621. https://doi.org/10.1007/s10577-007-1146-x

Ghurye, J., Rhie, A., Walenz, B. P., Schmitt, A., Selvaraj, S., Pop, M., Phillippy, A. M., & Koren, S. (2019). Integrating Hi-C links with assembly graphs for chromosome-scale assembly. *PLOS Computational Biology*, *15*(8), e1007273. https://doi.org/10.1371/journal.pcbi.1007273

Goel, M., & Schneeberger, K. (2022). plotsr: Visualizing structural similarities and rearrangements between multiple genomes. *Bioinformatics*, *38*(10), 2922–2926. https://doi.org/10.1093/bioinformatics/btac196

Guindon, S., Dufayard, J.-F., Lefort, V., Anisimova, M., Hordijk, W., & Gascuel, O. (2010). New Algorithms and Methods to Estimate Maximum-Likelihood Phylogenies: Assessing the Performance of PhyML 3.0. *Systematic Biology*, *59*(3), 307–321. https://doi.org/10.1093/sysbio/syq010

Guiraldelli, M. F., Felberg, A., Almeida, L. P., Parikh, A., de Castro, R. O., & Pezza, R. J. (2018). SHOC1 is a ERCC4-(HhH)2-like protein, integral to the formation of crossover recombination intermediates during mammalian meiosis. *PLoS Genetics*, *14*(5), e1007381. https://doi.org/10.1371/journal.pgen.1007381

Haenel, Q., Laurentino, T. G., Roesti, M., & Berner, D. (2018). *Meta-analysis of chromosome-scale crossover rate variation in eukaryotes and its significance to evolutionary genomics*. *27*(11), 2477–2497. https://doi.org/10.1111/mec.14699

Heckmann, S., Schubert, V., & Houben, A. (2014). Holocentric plant meiosis: First sisters, then homologues. *Cell Cycle*, *13*(23), 3623–3624. https://doi.org/10.4161/15384101.2014.986628

Higgins, J. D., Sanchez-Moran, E., Armstrong, S. J., Jones, G. H., & Franklin, F. C. (2005). The Arabidopsis synaptonemal complex protein ZYP1 is required for chromosome synapsis and normal fidelity of crossing over. *Genes Dev*, *19*(20), 2488–2500. https://doi.org/10.1101/gad.354705

Hofstatter, P. G., Thangavel, G., Castellani, M., & Marques, A. (2021). Meiosis Progression and Recombination in Holocentric Plants: What Is Known? *Front Plant Sci*, *12*, 658296. https://doi.org/10.3389/fpls.2021.658296

Hofstatter, P. G., Thangavel, G., Lux, T., Neumann, P., Vondrak, T., Novak, P., Zhang, M., Costa, L., Castellani, M., Scott, A., Toegelová, H., Fuchs, J., Mata-Sucre, Y., Dias, Y., Vanzela, A. L. L., Huettel, B., Almeida, C. C. S., Šimková, H., Souza, G., … Marques, A. (2022). Repeat-based holocentromeres influence genome architecture and karyotype evolution. *Cell*. https://doi.org/10.1016/j.cell.2022.06.045

Indrajeet Patil. (2021). Visualizations with statistical details: The 'ggstatsplot' approach. *Journal of Open Source Software*, *6*(61), 3167. https://doi.org/10.21105

John, A., Vinayan, K., & Varghese, J. (2016). Achiasmy: Male Fruit Flies Are Not Ready to Mix. *Frontiers in Cell and Developmental Biology*, *4*. https://doi.org/10.3389/fcell.2016.00075

Katoh, K., & Standley, D. M. (2013). MAFFT Multiple Sequence Alignment Software Version 7: Improvements in Performance and Usability. *Molecular Biology and Evolution*, *30*(4), 772–780. https://doi.org/10.1093/molbev/mst010

Keeney, S. (2008). Spo11 and the Formation of DNA Double-Strand Breaks in Meiosis. *Genome Dyn Stab*, *2*, 81–123. https://doi.org/10.1007/7050_2007_026

Keeney, S., Giroux, C. N., & Kleckner, N. (1997). Meiosis-specific DNA double-strand breaks are catalyzed by Spo11, a member of a widely conserved protein family. *Cell*, *88*(3), 375–384. https://doi.org/10.1016/s0092-8674(00)81876-0

Kim, D., Paggi, J. M., Park, C., Bennett, C., & Salzberg, S. L. (2019). Graph-based genome alignment and genotyping with HISAT2 and HISAT-genotype. *Nature Biotechnology*, *37*(8), 907–915. https://doi.org/10.1038/s41587-019-0201-4

Krueger, F., & Andrews, S. R. (2011). Bismark: A flexible aligner and methylation caller for Bisulfite-Seq applications. *Bioinformatics*, *27*(11), 1571–1572. https://doi.org/10.1093/bioinformatics/btr167

Kruskal, W. H., & Wallis, W. A. (1952). Use of ranks in one-criterion variance analysis. *Journal of the American Statistical Association*, *47*, 583–621. https://doi.org/10.2307/2280779

Kursel, L. E., & Malik, H. S. (2016). Centromeres. *Current Biology*, *26*(12), R487–R490. https://doi.org/10.1016/j.cub.2016.05.031

Kuttig, V., Sims, J., Hamamura, Y., Komaki, S., Köhler, M., Stolze, S. C., De Jaeger-Braet, J., Tuncay Elbasy, H., Nakagami, H., Failla, A. V., Schlögelhofer, P., & Schnittger, A. (2022). The cohesin subunit RAD21.2 functions as a recombination silencer of ribosomal DNA arrays. *BioRxiv*, 2022.06.20.496767. https://doi.org/10.1101/2022.06.20.496767

Lambie, E. J., & Roeder, G. S. (1986). Repression of meiotic crossing over by a centromere (CEN3) in Saccharomyces cerevisiae. *Genetics*, *114*(3), 769–789. https://doi.org/10.1093/genetics/114.3.769

Lambing, C., Franklin, F. C. H., & Wang, C.-J. R. (2017). Understanding and Manipulating Meiotic Recombination in Plants. *Plant Physiology*, *173*(3), 1530–1542. https://doi.org/10.1104/pp.16.01530 %J Plant Physiology

Lambing, C., Kuo, P. C., Tock, A. J., Topp, S. D., & Henderson, I. R. (2020). *ASY1 acts as a dosage-dependent antagonist of telomere-led recombination and mediates crossover interference in* Arabidopsis. *117*(24), 13647–13658. https://doi.org/doi:10.1073/pnas.1921055117

Lambing, C., Tock, A. J., Topp, S. D., Choi, K., Kuo, P. C., Zhao, X., Osman, K., Higgins, J. D., Franklin, F. C. H., & Henderson, I. R. (2020). Interacting Genomic Landscapes of REC8-Cohesin, Chromatin, and Meiotic Recombination in Arabidopsis[CC-BY]. *Plant Cell*, *32*(4), 1218–1239. https://doi.org/10.1105/tpc.19.00866 %J The Plant Cell

Langmead, B., & Salzberg, S. L. (2012). Fast gapped-read alignment with Bowtie 2. *Nature Methods*, *9*(4), 357–359. https://doi.org/10.1038/nmeth.1923

Lenormand, T., & Dutheil, J. (2005). Recombination Difference between Sexes: A Role for Haploid Selection. *PLOS Biology*, *3*(3), e63. https://doi.org/10.1371/journal.pbio.0030063

Lhuissier, F. G. P., Offenberg, H. H., Wittich, P. E., Vischer, N. O. E., & Heyting, C. (2007). The Mismatch Repair Protein MLH1 Marks a Subset of Strongly Interfering Crossovers in Tomato. *Plant Cell*, *19*(3), 862–876. https://doi.org/10.1105/tpc.106.049106 %J The Plant Cell

Lian, Q., Solier, V., Walkemeier, B., Durand, S., Huettel, B., Schneeberger, K., & Mercier, R. (2022). The megabase-scale crossover landscape is largely independent of sequence divergence. *Nature Communications*, *13*(1), 3828. https://doi.org/10.1038/s41467-022-31509-8

Liu, D. (2019). Algorithms for efficiently collapsing reads with Unique Molecular Identifiers. *PeerJ*, *7*, e8275. https://doi.org/10.7717/peerj.8275

Lopez-Delisle, L., Rabbani, L., Wolff, J., Bhardwaj, V., Backofen, R., Grüning, B., Ramírez, F., & Manke, T. (2021). pyGenomeTracks: Reproducible plots for multivariate genomic datasets. *Bioinformatics*, *37*(3), 422–423. https://doi.org/10.1093/bioinformatics/btaa692

Loureiro, J., Rodriguez, E., Dolezel, J., & Santos, C. (2007). Two new nuclear isolation buffers for plant DNA flow cytometry: A test with 37 species. *Annals of Botany*, *100*(4), 875–888. https://doi.org/10.1093/aob/mcm152

Macaisne, N., Novatchkova, M., Peirera, L., Vezon, D., Jolivet, S., Froger, N., Chelysheva, L., Grelon, M., & Mercier, R. (2008). SHOC1, an XPF endonuclease-related protein, is essential for the formation of class I meiotic crossovers. *Current Biology : CB*, *18*(18), 1432–1437. https://doi.org/10.1016/j.cub.2008.08.041

Mann, H. B., & Whitney, D. R. (1947). On a test of whether one of two random variables is stochastically larger than the other. *Annals of Mathematical Statistics*, *18*, 50–60. https://doi.org/10.1214/aoms/1177730491

Marcial Escudero, J. Ignacio Márquez-Corro, & Andrew L. Hipp. (2016). The Phylogenetic Origins and Evolutionary History of Holocentric Chromosomes. *Systematic Botany*, *41*(3), 580–585. https://doi.org/10.1600/036364416X692442

Mark Welch, D. B., & Meselson, M. (2000). Evidence for the Evolution of Bdelloid Rotifers Without Sexual Reproduction or Genetic Exchange. *Science*, *288*(5469), 1211–1215. https://doi.org/10.1126/science.288.5469.1211

Marques, A., & Pedrosa-Harand, A. (2016). Holocentromere identity: From the typical mitotic linear structure to the great plasticity of meiotic holocentromeres. *Chromosoma*, *125*(4), 669–681. https://doi.org/10.1007/s00412-016-0612-7

Marques, A., Ribeiro, T., Neumann, P., Macas, J., Novák, P., Schubert, V., Pellino, M., Fuchs, J., Ma, W., Kuhlmann, M., Brandt, R., Vanzela, A. L. L., Beseda, T., Šimková, H., Pedrosa-Harand, A., & Houben, A. (2015). *Holocentromeres in* Rhynchospora *are associated with genome-wide centromere-specific repeat arrays interspersed among euchromatin*. *112*(44), 13633–13638. https://doi.org/doi:10.1073/pnas.1512255112

Marques, A., Schubert, V., Houben, A., & Pedrosa-Harand, A. (2016a). Restructuring of Holocentric Centromeres During Meiosis in the Plant Rhynchospora pubera. *Genetics*, *204*(2), 555–568. https://doi.org/10.1534/genetics.116.191213

Marques, A., Schubert, V., Houben, A., & Pedrosa-Harand, A. (2016b). Restructuring of Holocentric Centromeres During Meiosis in the Plant Rhynchospora pubera. *Genetics*, *204*(2), 555–568. https://doi.org/10.1534/genetics.116.191213

Martin, M. (2011). Cutadapt removes adapter sequences from high-throughput sequencing reads. *EMBnet.Journal*, *17*(1), 10. https://doi.org/10.14806/ej.17.1.200

McKee, B. D., Yan, R., & Tsai, J.-H. (2012). Meiosis in male Drosophila. *Spermatogenesis*, *2*(3), 167–184. https://doi.org/10.4161/spmg.21800

Melamed-Bessudo, C., Shilo, S., & Levy, A. A. (2016). Meiotic recombination and genome evolution in plants. *Current Opinion in Plant Biology*, *30*, 82–87. https://doi.org/10.1016/j.pbi.2016.02.003

Melters, D. P., Paliulis, L. V., Korf, I. F., & Chan, S. W. (2012). Holocentric chromosomes: Convergent evolution, meiotic adaptations, and genomic analysis. *Chromosome Res*, *20*(5), 579–593. https://doi.org/10.1007/s10577-012-9292-1

Mercier, R., Mézard, C., Jenczewski, E., Macaisne, N., & Grelon, M. (2015). The molecular biology of meiosis in plants. *Annu Rev Plant Biol*, *66*, 297–327. https://doi.org/10.1146/annurev-arplant-050213-035923

Mézard, C., Tagliaro Jahns, M., & Grelon, M. (2015). Where to cross? New insights into the location of meiotic crossovers. *Trends in Genetics*, *31*(7), 393–401. https://doi.org/10.1016/j.tig.2015.03.008

Morgan, C., Fozard, J. A., Hartley, M., Henderson, I. R., Bomblies, K., & Howard, M. (2021). Diffusion-mediated HEI10 coarsening can explain meiotic crossover positioning in Arabidopsis. *Nature Communications*, *12*(1), 4674. https://doi.org/10.1038/s41467-021-24827-w

Naish, M., Alonge, M., Wlodzimierz, P., Tock, A. J., Abramson, B. W., Schmücker, A., Mandáková, T., Jamge, B., Lambing, C., Kuo, P., Yelina, N., Hartwick, N., Colt, K., Smith, L. M., Ton, J., Kakutani, T., Martienssen, R. A., Schneeberger, K., Lysak, M. A., … Henderson, I. R. (2021). The genetic and epigenetic landscape of the *Arabidopsis* centromeres. *Science*, *374*(6569), eabi7489. https://doi.org/10.1126/science.abi7489

Neumann, P., Novák, P., Hoštáková, N., & Macas, J. (2019). Systematic survey of plant LTR-retrotransposons elucidates phylogenetic relationships of their polyprotein domains and provides a reference for element classification. *Mobile DNA*, *10*(1), 1. https://doi.org/10.1186/s13100-018-0144-1

Niwa, O., Shimanuki, M., & Miki, F. (2000). Telomere-led bouquet formation facilitates homologous chromosome pairing and restricts ectopic interaction in fission yeast meiosis. *Embo j*, *19*(14), 3831–3840. https://doi.org/10.1093/emboj/19.14.3831

Novák, P., Neumann, P., & Macas, J. (2020). Global analysis of repetitive DNA from unassembled sequence reads using RepeatExplorer2. *Nature Protocols*, *15*(11), 3745–3776. https://doi.org/10.1038/s41596-020-0400-y

Pingali, P. L. (2012). *Green Revolution: Impacts, limits, and the path ahead*. *109*(31), 12302–12308. https://doi.org/doi:10.1073/pnas.0912953109

Prosekov, A. Y., & Ivanova, S. A. (2018). Food security: The challenge of the present. *Geoforum*, *91*, 73–77. https://doi.org/10.1016/j.geoforum.2018.02.030

Quinlan, A. R., & Hall, I. M. (2010). BEDTools: A flexible suite of utilities for comparing genomic features. *Bioinformatics*, *26*(6), 841–842. https://doi.org/10.1093/bioinformatics/btq033

R Core Team. (2022). R: A Language and Environment for Statistical Computing. *R Foundation for Statistical Computing*. https://www.R-project.org/

Ramírez, F., Ryan, D. P., Grüning, B., Bhardwaj, V., Kilpert, F., Richter, A. S., Heyne, S., Dündar, F., & Manke, T. (2016). deepTools2: A next generation web server for deep-sequencing data analysis. *Nucleic Acids Research*, *44*(W1), W160–W165. https://doi.org/10.1093/nar/gkw257

Rockman, M. V., & Kruglyak, L. (2009). Recombinational Landscape and Population Genomics of Caenorhabditis elegans. *PLOS Genetics*, *5*(3), e1000419. https://doi.org/10.1371/journal.pgen.1000419

Rockmill, B., & Roeder, G. S. (1998). Telomere-mediated chromosome pairing during meiosis in budding yeast. *Genes & Development*, *12*(16), 2574–2586. https://doi.org/10.1101/gad.12.16.2574

Rowan, B. A., Patel, V., Weigel, D., & Schneeberger, K. (2015). Rapid and Inexpensive Whole-Genome Genotyping-by-Sequencing for Crossover Localization and Fine-Scale Genetic Mapping. *G3 Genes|Genomes|Genetics*, *5*(3), 385–398. https://doi.org/10.1534/g3.114.016501

Ruban, A., Fuchs, J., Marques, A., Schubert, V., Soloviev, A., Raskina, O., Badaeva, E., & Houben, A. (2014). B Chromosomes of Aegilops speltoides Are Enriched in Organelle Genome-Derived Sequences. *PLOS ONE*, *9*(2), e90214. https://doi.org/10.1371/journal.pone.0090214

Saini, R., Singh, A. K., Hyde, G. J., & Baskar, R. (2020). Levels of Heterochiasmy During Arabidopsis Development as Reported by Fluorescent Tagged Lines. *G3 Genes|Genomes|Genetics*, *10*(6), 2103–2110. https://doi.org/10.1534/g3.120.401296 %J G3 Genes|Genomes|Genetics

Saito, T. T., & Colaiácovo, M. P. (2017). Regulation of Crossover Frequency and Distribution during Meiotic Recombination. *Cold Spring Harb Symp Quant Biol*, *82*, 223–234. https://doi.org/10.1101/sqb.2017.82.034132

Schneeberger, K., Ossowski, S., Lanz, C., Juul, T., Petersen, A. H., Nielsen, K. L., Jørgensen, J.-E., Weigel, D., & Andersen, S. U. (2009). SHOREmap: Simultaneous mapping and mutation identification by deep sequencing. *Nature Methods*, *6*(8), 550–551. https://doi.org/10.1038/nmeth0809-550

Schubert, V., Neumann, P., Marques, A., Heckmann, S., Macas, J., Pedrosa-Harand, A., Schubert, I., Jang, T. S., & Houben, A. (2020). Super-Resolution Microscopy Reveals Diversity of Plant Centromere Architecture. *Int J Mol Sci*, *21*(10). https://doi.org/10.3390/ijms21103488

Senaratne, A. P., Muller, H., Fryer, K. A., Kawamoto, M., Katsuma, S., & Drinnenberg, I. A. (2021). Formation of the CenH3-Deficient Holocentromere in Lepidoptera Avoids Active Chromatin. *Curr Biol*, *31*(1), 173-181.e7. https://doi.org/10.1016/j.cub.2020.09.078

Serra, H., Lambing, C., Griffin, C. H., Topp, S. D., Nageswaran, D. C., Underwood, C. J., Ziolkowski, P. A., Séguéla-Arnaud, M., Fernandes, J. B., Mercier, R., & Henderson, I. R. (2018). *Massive crossover elevation via combination of* HEI10 *and* recq4a recq4b *during* Arabidopsis *meiosis*. *115*(10), 2437–2442. https://doi.org/doi:10.1073/pnas.1713071115

Sims, J., Copenhaver, G. P., & Schlögelhofer, P. (2019). Meiotic DNA Repair in the Nucleolus Employs a Nonhomologous End-Joining Mechanism. *Plant Cell*, *31*(9), 2259–2275. https://doi.org/10.1105/tpc.19.00367

Spalink, D., Drew, B. T., Pace, M. C., Zaborsky, J. G., Starr, J. R., Cameron, K. M., Givnish, T. J., & Sytsma, K. J. (2016). Biogeography of the cosmopolitan sedges (Cyperaceae) and the area-richness correlation in plants. *Journal of Biogeography*, *43*(10), 1893–1904. https://doi.org/10.1111/jbi.12802

Stapley, J., Feulner, P. G. D., Johnston, S. E., Santure, A. W., & Smadja, C. M. (2017). Variation in recombination frequency and distribution across eukaryotes: Patterns and processes. *Philosophical Transactions of the Royal Society of London. Series B, Biological Sciences*, *372*(1736). https://doi.org/10.1098/rstb.2016.0455

Stauffer, W., Zhang, L., & Dernburg, A. (2019). *Diffusion through a liquid crystalline compartment regulates meiotic recombination* (Vol. 10888). SPIE.

Steiner, F. A., & Henikoff, S. (2014). Holocentromeres are dispersed point centromeres localized at transcription factor hotspots. *ELife*, *3*, e02025. https://doi.org/10.7554/eLife.02025

Talbert, P. B., & Henikoff, S. (2010). Centromeres Convert but Don't Cross. *PLOS Biology*, *8*(3), e1000326. https://doi.org/10.1371/journal.pbio.1000326

Topp, C. N., & Dawe, R. K. (2006). Reinterpreting pericentromeric heterochromatin. *Current Opinion in Plant Biology*, *9*(6), 647–653. https://doi.org/10.1016/j.pbi.2006.09.008

Underwood, C. J., & Mercier, R. (2022). Engineering Apomixis: Clonal Seeds Approaching the Fields. *Annual Review of Plant Biology*, *73*(1), 201–225. https://doi.org/10.1146/annurev-arplant-102720-013958

Van de Peer, Y., Mizrachi, E., & Marchal, K. (2017). The evolutionary significance of polyploidy. *Nature Reviews Genetics*, *18*(7), 411–424. https://doi.org/10.1038/nrg.2017.26

Vanzela, A.L.L., G., M. ,. Luceno, M. (1996). Rhynchospora tenuis Link (Cyperaceae), a species with the lowest number of holocentric chromosomes. *Cytobios*, *88*(355), 219–228. AGRIS.

Veller, C., Muralidhar, P., Constable, G. W. A., & Nowak, M. A. (2017). Drift-Induced Selection Between Male and Female Heterogamety. *Genetics*, *207*(2), 711–727. https://doi.org/10.1534/genetics.117.300151 %J Genetics

Wang, K., Wang, M., Tang, D., Shen, Y., Miao, C., Hu, Q., Lu, T., & Cheng, Z. (2012). The Role of Rice HEI10 in the Formation of Meiotic Crossovers. *PLOS Genetics*, *8*(7), e1002809. https://doi.org/10.1371/journal.pgen.1002809

Wang, M., Wang, K., Tang, D., Wei, C., Li, M., Shen, Y., Chi, Z., Gu, M., & Cheng, Z. (2010). The central element protein ZEP1 of the synaptonemal complex regulates the number of crossovers during meiosis in rice. *Plant Cell*, *22*(2), 417–430. https://doi.org/10.1105/tpc.109.070789

Weir, W., Capewell, P., Foth, B., Clucas, C., Pountain, A., Steketee, P., Veitch, N., Koffi, M., De Meeûs, T., Kaboré, J., Camara, M., Cooper, A., Tait, A., Jamonneau, V., Bucheton, B., Berriman, M., & MacLeod, A. (2016). Population genomics reveals the origin and asexual evolution of human infective trypanosomes. *ELife*, *5*, e11473. https://doi.org/10.7554/eLife.11473

Wiebe, K., Robinson, S., & Cattaneo, A. (2019). Chapter 4—Climate Change, Agriculture and Food Security: Impacts and the Potential for Adaptation and Mitigation. In C. Campanhola & S. Pandey (Eds.), *Sustainable Food and Agriculture* (pp. 55–74). Academic Press.

Wyatt, H. D., & West, S. C. (2014). Holliday junction resolvases. *Cold Spring Harb Perspect Biol*, *6*(9), a023192. https://doi.org/10.1101/cshperspect.a023192

Yelina, N., Diaz, P., Lambing, C., & Henderson, I. R. (2015). Epigenetic control of meiotic recombination in plants. *Science China Life Sciences*, *58*(3), 223–231. https://doi.org/10.1007/s11427-015-4811-x

Zelkowski, M., Olson, M. A., Wang, M., & Pawlowski, W. (2019). Diversity and Determinants of Meiotic Recombination Landscapes. *Trends in Genetics*, *35*(5), 359–370. https://doi.org/10.1016/j.tig.2019.02.002

Zhang, L., Liang, Z., Hutchinson, J., & Kleckner, N. (2014). Crossover Patterning by the Beam-Film Model: Analysis and Implications. *PLoS Genetics*, *10*(1), e1004042. https://doi.org/10.1371/journal.pgen.1004042

Zhang, L., Stauffer, W., Zwicker, D., & Dernburg, A. F. (2021). *Crossover patterning through kinase-regulated condensation and coarsening of recombination nodules*. 2021.08.26.457865. https://doi.org/10.1101/2021.08.26.457865 %J bioRxiv

Zhang, Y., Liu, T., Meyer, C. A., Eeckhoute, J., Johnson, D. S., Bernstein, B. E., Nusbaum, C., Myers, R. M., Brown, M., Li, W., & Liu, X. S. (2008). Model-based Analysis of ChIP-Seq (MACS). *Genome Biology*, *9*(9), R137. https://doi.org/10.1186/gb-2008-9-9-r137

Zickler, D., & Kleckner, N. (2015). Recombination, Pairing, and Synapsis of Homologs during Meiosis. *Cold Spring Harbor Perspectives in Biology*, *7*(6). https://doi.org/10.1101/cshperspect.a016626

Final Acknowledgements

I dedicate this work to all the people that supported me and inspired me during this journey. It has been a long and challenging path, with a lot of satisfactions, but also dark moments. Yet, I succeeded with my own strength and with the support of many. First and foremost, I thank André for being an amazing supervisor, a great colleague and a good friend. Then I acknowledge my PhD colleagues for inspiring me to be a better scientist every day, and especially Meng for her contribution to this work. My journey would have never been this great if it wasn´t for all the members of my group, department and the great people from the rest of the institute that created a nourishing and exiting environment. Thanks to my family for being so loving and teaching me how to be a good man, and thanks to all my friends abroad for making me feel at home even when divided by great distance. Thanks to the amazing people I met in this stimulating city, and finally, thanks to my past self for enduring the challenge, and thanks to my future self for being the better version of myself that I want to be. Now it´s time to turn the page, and on to the next chapter.